

P
2 min

NASA TECHNICAL
MEMORANDUM

NASA TM X-62,197

NASA TM X-62,197

(NASA-TM-X-62197) WIND TUNNEL
INVESTIGATION OF A LARGE-SCALE 25 DEG
SWEPT-WING JET TRANSPORT MODEL WITH AN
EXTERNAL BLOWING TRIPLE-SLOTTED FLAP

N74-13721

(NASA) -59 p HC \$5 00
100

CSCL 01C

G3/2 26032

Unclass

WIND-TUNNEL INVESTIGATION OF A LARGE-SCALE 25° SWEPT-WING
JET TRANSPORT MODEL WITH AN EXTERNAL BLOWING
TRIPLE-SLOTTED FLAP

Kiyoshi Aoyagi, Michael D. Falarski, and David G. Koenig

Ames Research Center
and
U.S. Army Air Mobility R&D Laboratory
Moffett Field, Calif. 94035

November 1973



PRECEDING PAGE BLANK NOT FILMED
SYMBOLS

b	wing span, m (ft)
c	wing chord measured parallel to the plane of symmetry, m (ft)
c_t	horizontal tail chord measured parallel to the plane of symmetry, m (ft)
c_v	vertical tail chord measured parallel to the plane of symmetry, m (ft)
\bar{c}	mean aerodynamic chord of the wing, $\frac{2}{S} \int_0^{b/2} c^2 dy$, m (ft)
C_D	drag coefficient about the wind axis, $\frac{\text{drag}}{q_\infty S}$
C_{DRAM}	ram drag coefficient about the wind axis, $\frac{Wv}{g q_\infty S}$
C_L	lift coefficient about the wind axis, $\frac{\text{lift}}{q_\infty S}$
C_T	gross thrust coefficient, $\frac{F_g}{q_\infty S}$
C_λ	rolling-moment coefficient about the stability axis, $\frac{\text{rolling moment}}{q_\infty S b}$
C_m	pitching-moment coefficient about the wind axis at 0.40 \bar{c} , $\frac{\text{pitching moment}}{q_\infty S \bar{c}}$
C_n	yawing-moment coefficient about the stability axis, $\frac{\text{yawing moment}}{q_\infty S b}$
C_y	side-force coefficient about the stability axis, $\frac{\text{side force}}{q_\infty S}$
EBF	externally blown flap
F_A	static (wind off) incremental axial force due to flap deflection with power on, N (lb)
F_g	gross engine thrust, N (lb) (obtained statically)
F_N	static (wind off) incremental normal force due to flap deflection with power on, N (lb)
F_R	resultant force, $\sqrt{F_A^2 + F_N^2}$, N (lb)
g	acceleration of gravity, 9.81 m/sec ² (32.2 ft/sec ²)

i_t	horizontal tail incidence, deg
N_1	engine fan rotational speed, RPM
p_s	free-stream static pressure, N/m ² (lb/sq ft)
P_∞	free-stream total pressure, N/m ² (lb/sq ft)
P_T	total pressure, N/m ² (lb/sq ft)
q_∞	free-stream dynamic pressure, N/m ² (lb/sq ft)
R	Reynolds number
S	wing area, m ² (sq ft)
T	free-stream absolute temperature, °K
T_0	standard absolute temperature, 288.16°K
v	free-stream air velocity, m/sec (ft/sec)
W	engine inlet weight rate of flow, kg/sec (lb/sec)
WCP	wing chord plane
x	chordwise distance from the wing or horizontal tail leading edge parallel to the model plane of symmetry, m (ft)
y	spanwise distance perpendicular to the plane of symmetry, m (ft)
z	perpendicular distance from wing or horizontal tail reference plane, m (ft). (Positive direction above reference plane.)
α	angle of attack, deg
δ_{ail}	aileron deflection, deg
δ_e	horizontal tail elevator deflection, deg
δ_{f1}	trailing-edge first flap deflection measured parallel to the plane of symmetry, deg
δ_{f2}	trailing-edge second flap deflection measured parallel to the plane of symmetry, deg
δ_{f3}	trailing-edge third flap deflection measured parallel to the plane of symmetry, deg
δ_j	jet exhaust turning angle (wind off), $\tan^{-1} \frac{F_N}{F_A}$, deg

δ_s leading-edge slat deflection measured parallel to the plane of symmetry, deg
 δ_{sp} spoiler deflection measured parallel to the plane of symmetry, deg
 η wing semispan station, $\frac{y}{b/2}$
 η_f flap system static turning efficiency, $\frac{F_R}{F_g}$
 θ relative absolute temperature, $\frac{T}{T_0}$
 $()_u$ uncorrected

WIND-TUNNEL INVESTIGATION OF A LARGE-SCALE 25° SWEPT-WING JET
TRANSPORT MODEL WITH AN EXTERNAL BLOWING TRIPLE-SLOTTED FLAP

Kiyoshi Aoyagi, Michael D. Falarski, and David G. Koenig
Ames Research Center

SUMMARY

An investigation has been conducted to determine the aerodynamic characteristics of a large-scale subsonic jet transport model with an externally blown triple-slotted flap. The lift of the model was augmented by the turbofan engine exhaust impingement on the flap surface. The model had a 25° swept wing of aspect ratio 7.28 and four turbofan engines.

The model was tested with two flap extents. One extended from 0.11 to 1.00 of the wing semispan, and the other extended from 0.11 to 0.75 of the wing semispan with a single-slotted aileron from 0.75 to 1.00 of the wing semispan. The results were obtained for several flap deflections with and without the horizontal tail at gross thrust coefficients from 0 to 4.0.

Longitudinal and lateral data are presented with three and four engines operating.

INTRODUCTION

The principle of augmenting lift by directing the jet engine exhaust toward the trailing-edge flap surface has been investigated extensively. This principle is commonly referred to as the externally blown flap concept (EBF). Wind-tunnel investigations of a large-scale model using this concept have been reported in references 1 and 2. Other investigations are reported in references 3 and 4. Because of the possibility of incorporating EBF in future transport designs, a growing interest has been expressed in the noise

characteristics and flap loads, in addition to the aerodynamic characteristics, of this concept using higher bypass-ratio turbofan engines.

An investigation was therefore undertaken using a large-scale EBF transport model to measure the aerodynamic and noise characteristics as well as surface pressures in the Ames 40-by-80-Foot Wind Tunnel. The model had a 25° swept wing and four turbofan engines. This report presents only the aerodynamic characteristics of the model. The noise characteristics and loads data will be reported separately. Results were obtained with several flap deflections at two spanwise extents and at gross thrust coefficients from 0 to 4.0. The data were obtained at Reynolds numbers from 1.5×10^6 to 3.8×10^6 , based on a mean aerodynamic chord of 1.69 m (5.56 ft) and dynamic pressures of 143.6 to 861.8 N/m² (3.0 to 18.0 psf).

MODEL AND APPARATUS

Figure 1 is a photograph of the model in the Ames 40-by-80-Foot Wind Tunnel. Pertinent dimensions of the model are given in fig. 2(a). The wing, fuselage, and tail geometries are the same as reported in reference 5. The model was equipped with four JT15D-1 turbofan engines.

Wing

The wing had a quarter-chord sweep of 25°, an aspect ratio of 7.28, and an incidence of 0°. The airfoil had an NACA 63₂A214 section at the root and an NACA 63₂A211 section at the tip. The wing tapered linearly in thickness between these two sections. The ordinates of these sections are given in Table I.

Leading-Edge Slats

Full span leading-edge slats were installed on the wing as shown in fig. 2(b). The slats were installed throughout the investigation.

Trailing-Edge Flap System

The flap system had three segments with fixed pivots as shown in fig. 2(c). Each flap segment was deflected either full span ($\eta = .11$ to 1.0) or part-span ($\eta = .11$ to .75) during the investigation.

A .10c plain spoiler hinged at .725c formed part of the flap lip when undeflected, and extended from $\eta = .11$ to .75 with a break at .50 η . The spoiler was deflected 30° and 60° above the wing surface during the investigation.

Aileron

A single-slotted aileron extended from $\eta = .75$ to 1.0 when the part-span trailing-edge flap was investigated as shown in fig. 2(d). The aileron is the same one reported in reference 5.

Propulsion

The JT15D-1 engines were housed in nacelles as shown in fig. 2(e). The engines have a bypass ratio of 3 and a normal maximum gross thrust rating of 2200 pounds. Each nacelle centerline was coincident with the engine centerline and was parallel to the wing chord plane and model plane of symmetry. The nacelle contours are defined in fig. 2(f).

Tail

The geometry of the horizontal and vertical tails is described in fig. 2(a). These tails are the same ones used in reference 5. The horizontal tail detail is shown in fig. 2(g). The vertical tail remained installed throughout the investigation.

TESTING AND PROCEDURE

In most cases, forces and moments were measured through an angle-of-attack range of -8° to 26° . Tests were conducted at Reynolds numbers from 1.5×10^6 to 3.8×10^6 , based on a mean aerodynamic chord of 1.69 m (5.56 ft) and dynamic pressures of 143.6 to 861.8 N/m² (3.0 to 18.0 psf).

Tests to measure jet turning (δ_j) and turning efficiency (η_f) were obtained in the wind tunnel with zero airspeed. The measurements were recorded with two engines operating simultaneously on the same side of the wing and at the same power setting before air recirculation could be generated in the test section. An exception to this procedure was at a flap setting of $\delta_{f_1}/\delta_{f_2}/\delta_{f_3} = 15^\circ/35^\circ/55^\circ$ where four engines were operating.

All wind-on tests were conducted by varying either angle of attack ($\alpha_y = -8^\circ$ to 26°) at 0° sideslip or sideslip ($\beta = 4^\circ$ to -20°) at constant angle of attack while maintaining constant engine gross thrust setting on each engine. The thrust values were obtained by maintaining a corrected engine fan rotational speed ($N_1/\sqrt{\theta}$) which corresponded to the desired static thrust. The static thrust variation with fan speed was obtained for each engine with the flaps up at zero airspeed. Except where Reynolds number was varied, most of the tests were conducted at C_T values of 0, .5, 1.0, 2.0, 3.0,

4.0 and a dynamic pressure of 287.3 N/m² (6.0 psf).

Model configuration variables included flap deflection, spanwise flap extent, horizontal tail on or off, aileron deflection, elevator deflection, spoiler deflection, and outboard engine out. Table II may be used as an index to the tests.

CORRECTIONS

The data were corrected for wind-tunnel wall constraints. These corrections were determined by considering only the aerodynamic lift of the model (C'_L) that resulted after the jet reaction components had been subtracted from the data as follows:

$$C'_L = C_L - n_f C_T [\sin (\delta_j + \alpha_u)]$$

$$\alpha = \alpha_u + .4175 C'_L$$

$$C_D = C_{D_u} + .0073 C'^2_L$$

$$C_m = C_{m_u} + .025 C'_L \quad (\text{horizontal-tail-on tests only})$$

The engine thrust values used to define C_T were based on the calibrations of the engine static thrust variation with engine fan rotational speed. These calibrations were obtained from wind-tunnel scale measurements with the flaps undeflected. The δ_j and n_f values obtained from static tests with flaps deflected are shown in fig. 3.

The data are presented in this report for specified gross thrust coefficients (C_T). For reference the ram drag values are given in fig. 4.

RESULTS

The static turning angles (δ_j) and static turning efficiencies (η_f) for the flap deflections investigated are shown in fig. 3. Figure 4 shows the variation of C_{DRAM} with C_T . The jet exhaust total pressure distributions at the engine centerline for several power settings are shown in fig. 5. The jet exhaust total pressure distributions for several values of α at the maximum power setting used during the investigation are shown in fig. 6.

The basic aerodynamic data obtained from this investigation are presented in figs. 6 through 38. An index to these data is given in Table II.

REFERENCES

1. Aoyagi, Kiyoshi; and Hall, Leo P.: Wind-Tunnel Investigation of a Large 35° Swept-Wing Jet Transport Model with an External-Flow Jet-Augmented Double-Slotted Flap. NASA TN D-6482, August, 1971.
2. Aoyagi, Kiyoshi; Hall, Leo P.; and Falarski, Michael D.: Wind-Tunnel Investigation of a Large-Scale 35° Swept-Wing Jet Transport Model with an External Blowing Triple-Slotted Flap. NASA TMX-2600, July, 1972.
3. Parlett, Lysle P.; Greer, Douglas H.; and Henderson, Robert L.: Wind-Tunnel Investigation of an External-Flow Jet-Flap Transport Configuration Having Full-Span Triple-Slotted Flap. NASA TN D-6391, August, 1971.
4. Parlett, Lysle P.; and Smith, Charles C., Jr.: Wind-Tunnel Investigation of Effects of Variations in Reynolds Number and Leading-Edge Treatment on the Aerodynamic Characteristics of an Externally Blown Jet-Flap Configuration. NASA TN D-7194, Aug. 1973.

5. Aoyagi, Kiyoshi; Falarski, Michael D.; and Koenig, David G.: Wind Tunnel Investigation of a Large-Scale Upper Surface Blown-Flap Transport Model Having Two Engines. NASA TMX 62,296, August, 1973.

TABLE I
WING SECTION CONTOURS OF ROOT AND TIP SECTIONS

x, % c	z, % c			
	Section at model centerline		Section at wing tip	
	Upper	Lower	Upper	Lower
0	0	0	0	0
0.55	1.356	-	1.060	-
0.88	-	-1.275	-	-0.998
1.00	1.748	-1.358	1.379	-1.061
3.00	2.957	-2.324	2.363	-1.785
5.00	3.802	-2.962	3.055	-2.259
8.00	4.774	-3.662	3.852	-2.776
10.00	5.304	-4.032	4.288	-3.065
12.50	5.873	-4.419	4.757	-3.329
15.00	6.357	-4.741	5.157	-3.562
20.00	7.127	-5.232	5.796	-3.915
25.00	7.680	-5.558	6.258	-4.143
30.00	8.045	-5.740	6.566	-4.265
35.00	8.220	-5.772	6.721	-4.273
40.00	8.217	-5.662	6.730	-4.174
45.00	8.046	-5.422	6.604	-3.978
50.00	7.730	-5.071	6.358	-3.699
55.00	7.288	-4.633	6.010	-3.357
60.00	6.738	-4.137	5.572	-2.999
65.00	6.091	-3.643	5.053	-2.643
70.00	5.363	-3.149	4.465	-2.286
75.00	4.574	-2.655	3.824	-1.929
80.00	3.742	-2.161	3.138	-1.573
85.00	2.839	-1.667	2.382	-1.204
90.00	1.912	-1.173	1.605	-0.859
95.00	0.971	-0.679	0.814	-0.503
100.00	0	-0.185	0	-0.146

TABLE II. — LIST OF BASIC DATA FIGURES

Run	Figure	$\delta_{f_1}/\delta_{f_2}/\delta_{f_3}$	Flap span n	α_u , deg	β , deg	q		R $\times 10^{-6}$	C _T	δ_{ail}		δ_{sp}		Horiz. tail		Remarks	
						N/m ²	psf			Left	Rt.	Left	Rt.	Span	i _t , deg	δ_e , deg	
192	7	0/0/0	-	-4 to 16	0	289.7	6.05	2.3	3.96	None	None	0	0	-	off	-	Plain wing
193				-4 to 20		287.8	6.01	2.2	2.99								
194				-4 to 18		289.2	6.04		2.31								
195				-4 to 16		290.1	6.06		.99								
196				-4 to 16		288.7	6.03		0								
181	8	0/20/40	.11 to 1.0	-4 to 26		290.1	6.06		3.95								Take off flap configuration
182						289.2	6.04		2.97								
183						287.8	6.01		2.32								
184						289.2	6.04		1.00								
185						287.3	6.00		0								
56	9	15/35/55		-8 to 26		283.4	5.92		4.05								Landing flap configuration
60						287.3	6.00		2.99								
58						281.1	5.87		2.38								
57						286.3	5.98		1.00								
54						↓	+		0								
185	10(a)	0/20/40		-4 to 24		287.3	6.00		0								Reynolds number effects
190						574.6	11.94		3.1								
186						861.8	18.06		3.8								
184	10(b)			-4 to 26		287.3	6.04		2.2	1.00							
188				-4 to 24		660.7	13.87		3.3								
189				↓		861.8	18.03		3.8								
183	10(c)			-4 to 24		287.3	6.01		2.2	2.32							
187				↓		574.6	12.03		3.1	+							
53	11(a)	15/35/55		-4 to 20		143.6	3.00		1.5	0							
54						287.3	5.98		2.2								
55						574.6	11.97		3.1								

TABLE II. — LIST OF BASIC DATA FIGURES — Continued

Run	Figure	$\delta_{f_1}/\delta_{f_2}/\delta_{f_3}$	Flap span η	α_u , deg	β , deg	q		R $\times 10^{-6}$	C_T	δ_{ail}		δ_{sp}			Horiz. tail		Remarks
						N/m ²	psf			Left	Rt.	Left	Rt.	Span	i_t , deg	δ_e , deg	
59						143.6	2.95	1.5	2.37	None	None	0	0	-	off		
58	11(b)	15/35/55	.11 to 1.0	-4 to 26 ↓	0	282.5	5.87	2.2	↓								
61						574.6	11.87	3.1	↓								
4						284.9	5.95	2.3	4.03						0	-25	
5						287.3	6.00	2.2	3.05								
6	12					285.8	5.97	+	2.34								
8						293.5	6.13	2.3	.99								
12						293.0	6.12	+	0								
41						143.6	3.06	1.5	0								
12	13(a)					293.0	6.12	2.3									
42						574.6	11.97	3.1									
48						861.8	18.12	3.9	↓								
52						143.6	3.00	1.5	1.16								
45	13(b)					287.3	6.01	2.2									
44						574.6	12.05	3.1									
51						861.8	18.01	3.8	↓								
6	13(c)					287.3	5.97	2.2	2.34								
49						574.6	11.96	3.1	+								
17						282.5	5.90	2.2	4.06			20	20	.11			Symmetric spoiler deflections
18						284.4	5.94		3.02								
15	14(a)					286.8	5.99		2.33								
14						289.7	6.05		.99								
16						287.8	6.01	↓	0								
34	14(b)					287.3	6.00	2.3	3.99			30	30				
35						288.2	6.02	2.2	2.32			↓	↓				

TABLE II. — LIST OF BASIC DATA FIGURES — Continued

Run	Figure	$\delta_{f_1}/\delta_{f_2}/\delta_{f_3}$	Flap span η	α_u , deg	β , deg	q		$R \times 10^{-6}$	C_T	δ_{ail}		δ_{sp}		Horiz. tail		Remarks	
						N/m ²	psf			Left	Rt.	Left	Rt.	Span	i_t , deg	δ_e , deg	
19	14(c)	15/35/55	.11 to 1.0	-8 to 26 ↓ -4 to 26	0	287.3	6.00	2.3	3.99	None	None	40	40	.11 to .75	0	-25	Tail incidence changes
20						288.2	6.02	+	2.98								
21						288.7	6.03	2.2	2.32								
22						288.2	6.02	+	.99								
23						288.7	6.03	2.3	0								
24				-4 to 26 ↓ 0 to 26		287.8	6.01	2.2	3.99			60	60				
25						287.3	6.00	↓	2.33								
26						287.8	6.01	↓	0								
31	15(a)	15/35/55	.11 to 1.0	-4 to 26 ↓ 0 to 26		288.2	6.02	2.3	3.98			30	30	.11 to .50			
32						289.2	6.04	2.2	2.31								
33						290.6	6.07	2.3	0								
27	15(b)	15/35/55	.11 to 1.0	-8 to 26 ↓ -8 to 24		288.0	6.02	2.2	3.98			60	60				Tail incidence changes
29						288.7	6.03	↓	2.32								
30						289.7	6.05	↓	0								
28						289.2	6.04	↓	0			0	0	-	7		
40	16(a)	15/35/55	.11 to 1.0	-8 to 26 -8 to 24 -8 to 16		288.7	6.03	↓	2.32								Tail incidence changes
37						289.2	6.04	↓	3.97								
36						288.7	6.03	↓	3.97								
39	16(b)	15/35/55	.11 to 1.0	-8 to 26 ↓ -8 to 20		289.2	6.04	↓	0						-5		Tail incidence changes
38						288.7	6.03	2.1	2.32								
47						286.3	5.98	2.2	4.01								
175	17(a)	0/20/30	.11 to .75	-8 to 26		285.4	5.96	2.3	4.02	5	5			off	-	Symmetric aileron deflec-	
176						280.1	5.85	↓	2.39								tions
177						285.4	5.96	↓	0								
178	17(b)	0/20/30	.11 to .75	-8 to 26		286.3	5.98	2.4	4.01	20	20						Tail incidence changes
179						286.3	5.98	↓	2.34								
180						287.3	6.00	↓	0								

TABLE II. — LIST OF BASIC DATA FIGURES — Continued

Run	Figure	$\delta_{f_1}/\delta_{f_2}/\delta_{f_3}$	Flap span η	α_u , deg	β , deg	q		R $\times 10^{-6}$	C_T	δ_{ail}		δ_{sp}		Horiz. tail		Remarks	
						N/m ²	psf			Left	Rt.	Left	Rt.	Span	i_t , deg	δ_e , deg	
171	18(a)	0/20/20	.11	-8 to 26	0	287.8	6.01	2.2	3.99	5	5	0	0	-	0	-25	
172			to .75	+ -4 to 24		288.7	6.03	↓	2.32								
173						↓	↓	2.3	0								
163	18(b)	0/20/30	.	-8 to 26		286.8	5.99	↓	4.00								
164						286.3	5.98	2.2	3.00								
165						↓	↓	↓	2.34								
166						287.3	6.00	↓	1.00								
169						↓	↓	0									
69	19(a)	15/35/55	.	-4 to 26		286.3	5.98	2.3	4.01						off	-	
70						287.3	6.00	↓	2.33								
71						289.2	6.04	0									
63	19(b)		.	-8 to 26		287.3	5.99	2.2	4.00	20	20						
66						↓	5.98	2.3	3.00								
67						↓	6.02	2.2	2.32								
64						574.6	11.90	3.0	2.35								
68						287.3	6.02	2.2	.99								
65						↓	5.98	↓	0								
72	19(c)		.	-8 to 26		286.8	5.99	2.3	4.00	35	35						
73						288.2	6.02	2.2	2.32	↓	↓						
74						289.2	6.04	0		↓	↓						
78	20(a)		.			288.2	6.02	↓	3.98	20	20	30	30	.11			
79						288.7	6.03	↓	2.32	↓	↓	↓	↓				
80						289.2	6.04	2.3	0	↓	↓	↓	↓	.75			
75	20(b)		↓	0 to 26	↓	287.3	6.00	2.2	3.99	35	35	↓	↓	↓			
76						288.2	6.02	↓	2.32	0	↓	↓	↓				
77						289.7	6.05	↓	0	↓	↓	↓	↓				

Symmetric
spoiler and
aileron deflec-
tions

TABLE II. — LIST OF BASIC DATA FIGURES — Continued

Run	Figure	$\delta_{f_1}/\delta_{f_2}/\delta_{f_3}$	Flap span η	α_u , deg	β , deg	q		$R \times 10^{-6}$	C_T	δ_{ail}		δ_{sp}		Horiz. tail		Remarks	
						N/m ²	psf			Left	Rt.	Left	Rt.	Span	i_t , deg	δ_e , deg	
143	21(a)	15/35/55	.11 to .75	-8 to 26	0	286.3	5.98	2.2	4.01	23	23	0	0	.11 to .75	0	-25	Third flap deflections
144						↓	+	3.00									
145						287.3	6.00		2.33								
146						288.2	6.02		.99								
150						↓	+	0									
81	21(b)	15/35/55				286.8	5.99	2.3	4.00	20	20	30	30				Asymmetric aileron effects
82						289.2	6.04		2.97								
83						288.2	6.02		2.32								
84						289.7	6.05		.99								
93						283.9	5.93		0								
154	22(a)	15/35/45				286.3	5.98		4.01	23	23	0	0				Asymmetric aileron effects
155						286.8	5.99		2.33								
156						↓	+	0									
151	22(b)	15/35/65				282.5	5.90		4.06								Asymmetric spoiler effects
152						↓	+	2.2	2.37								
153						283.9	5.93	2.3	0								
117	23(a)	15/35/55				287.3	6.00		3.99	20	35			-			Asymmetric aileron effects
118						286.8	5.99		2.33								
119						286.3	5.98		0								
117	23(b)					287.3	6.00		3.99								Asymmetric spoiler effects
118						286.8	5.99		2.33								
119						286.3	5.98		0								
120	24(a)					284.9	5.95	2.2	4.03			20	30		.11 to .75		Asymmetric spoiler effects
121						↓	+	2.35									
122						286.3	5.98	↓	0								

TABLE II. — LIST OF BASIC DATA FIGURES — Continued

TABLE II. — LIST OF BASIC DATA FIGURES — Continued

Run	Figure	$\delta_{f_1}/\delta_{f_2}/\delta_{f_3}$	Flap span η	α_u , deg	β , deg	q		R $\times 10^{-6}$	C_T	δ_{ail}		δ_{sp}		Horiz. tail		Remarks				
						N/m ²	psf			Left	Rt.	Left	Rt.	Span	i_t , deg	δ_e , deg				
94	29(a)	15/35/55	.11 to .75	-8 to 26	0	286.8	5.99	2.3	3.00	20	20	30	30	.11 to .75	0	-25	Right hand inboard engine out effects			
95						283.9	5.93	2.2	1.77											
94	29(b)					286.8	5.99	2.3	3.00											
95						283.9	5.93	2.2	1.77	↓	↓	↓	↓							
135	30(a)				↓	285.8	5.97		3.01	5	35	60	0				Asymmetric aileron and spoiler effects with an engine out			
136					-4 to 26	287.8	6.01	↓	1.74											
130						285.4	5.96	2.3	0											
135	30(b)				-8 to 26	285.8	5.97		3.01											
136					↓	287.8	6.01		1.74											
130					-4 to 26	285.4	5.96		0	↓	↓	↓								
9	31(a)	.11 to 1.0	.11 to 1.0	-8 to 26	293.0	6.12		2.94	None	None	0						Left hand outboard engine out effects			
10					294.0	6.14		2.19												
11					294.0	+		1.71												
9	31(b)				↓	293.0	6.12		2.94											
10					↓	294.0	6.14		2.19											
11					↓	294.0	+	1.71		↓	↓									
147	32(a)				0	285.8	5.97	2.2	2.34	23	23						Sideslip effects			
148					4 to 8	285.4	5.96	↓												
149					16	286.8	5.99	↓												
125	32(b)				0	286.8	5.99	2.3				60								
126					8	287.3	6.00													
127					16	↓	↓													
105	33(a)				0	283.0	5.91		0	20	20	20	20							
106					8	286.3	5.98			↓	↓	↓	↓							
107					16	↓	↓			↓	↓	↓	↓							

TABLE II. — LIST OF BASIC DATA FIGURES — Continued

Run	Figure	$\delta_{f_1}/\delta_{f_2}/\delta_{f_3}$	Flap span n	α_u , deg	β , deg	q		R $\times 10^{-6}$	C_T	δ_{ail}		δ_{sp}		Horiz. tail		Remarks	
						N/m ²	psf			Left	Rt.	Left	Rt.	Span	i_t , deg	δ_e , deg	
88	33(b)	15/35/55		.11	0	4	284.9	5.95	2.4	2.34	20	20	20	20	.11	0	-25
89				to .75	8	to -20	286.3	5.98	2.3	↓					to .75		
90					16		+	+	↓	↓							
85	33(c)				0		286.8	5.99	2.2	4.00							
86					8		+	+	↓	↓							
87					16		285.8	5.97	↓	↓							
132	34				0		286.8	5.99	2.3	2.33							
133					8		287.3	6.00	↓	↓	5	35	60	0			
134					16		+	+	↓	↓							
140	35(a)				0		288.2	6.02	2.2	1.74							
141					8		287.8	6.01	↓	↓							
142					16		287.3	6.00	↓	↓							
137	35(b)				0		287.3	6.00	2.3	2.99							
138					8		287.8	6.01	↓	↓							
139					16		289.2	6.04	↓	↓							
114	36(a)				0		288.7	6.03	2.2	0	20	5	30	30			
115					8		285.9	5.95	↓	↓							
116					16		285.8	5.97	↓	↓							
111	36(b)				0		289.2	6.04	↓	2.31							
112					8		288.7	6.03	↓	↓							
113					16		291.1	6.08	↓	↓							
108	36(c)				0		285.8	5.97	2.3	3.99							
109					8		287.8	6.01	↓	↓							
110					16		287.3	6.00	2.2	↓							

L

TABLE II. — LIST OF BASIC DATA FIGURES — Concluded

Run	Figure	$\delta_{f_1}/\delta_{f_2}/\delta_{f_3}$	Flap span n	α_u , deg	β , deg	q		R $\times 10^{-6}$	C_T	δ_{ail}		δ_{sp}		Horiz. tail		Remarks		
						N/m ²	psf			Left	Rt.	Left	Rt.	Span	i_t , deg	δ_e , deg		
102	37(a)	15/35/55		.11	0	4	288.2	6.02	2.2	1.74	20	20	30	30	.11	0	-25	
103				to	8	to	288.7	6.03	↓									
104				.75	16	-20	283.9	5.93	2.3	↓					.75			
99					0		289.2	6.04	2.2	2.99								
100	37(b)				8		287.3	6.00	↓		↓	↓	↓	↓				
101					16	↓	↓	↓	↓									
43				.11	-8	0	287.8	6.01	↓	2.32	None	None	0	0	-	0	-10	Elevator effectiveness
				to	0					↓		↓	↓	↓			to	
				1.0	8	↓				↓							-35	
					16	↓											↓	

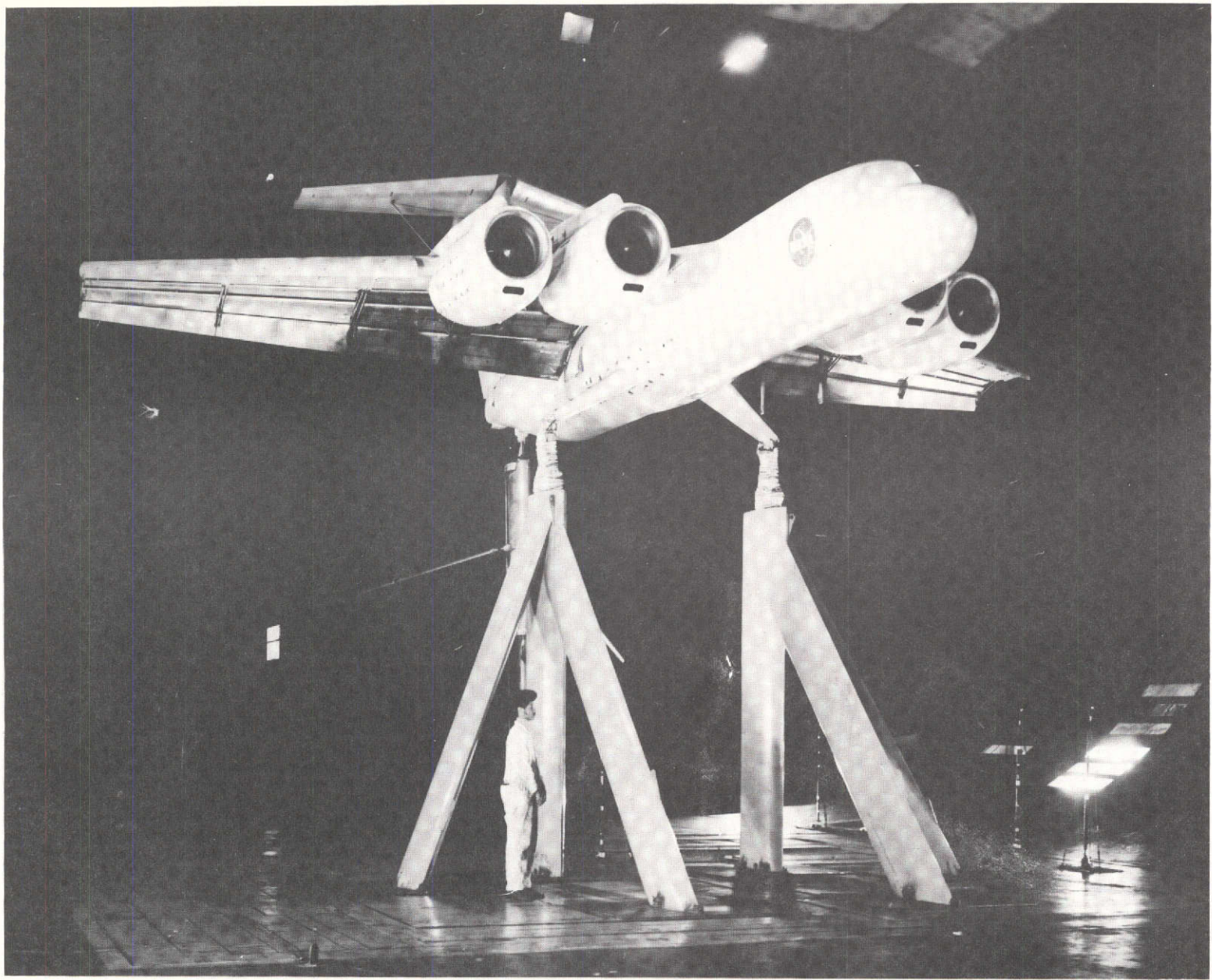
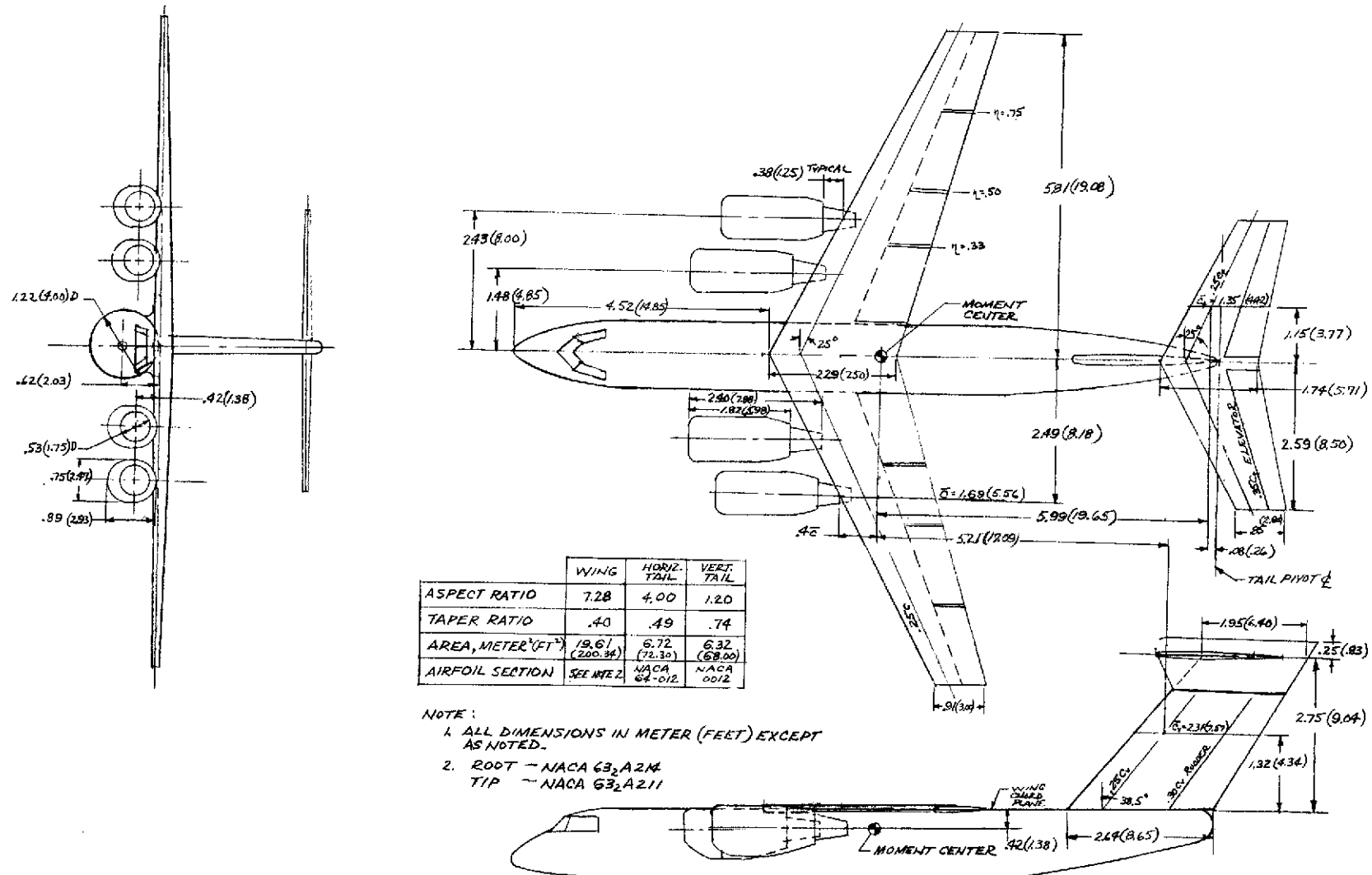


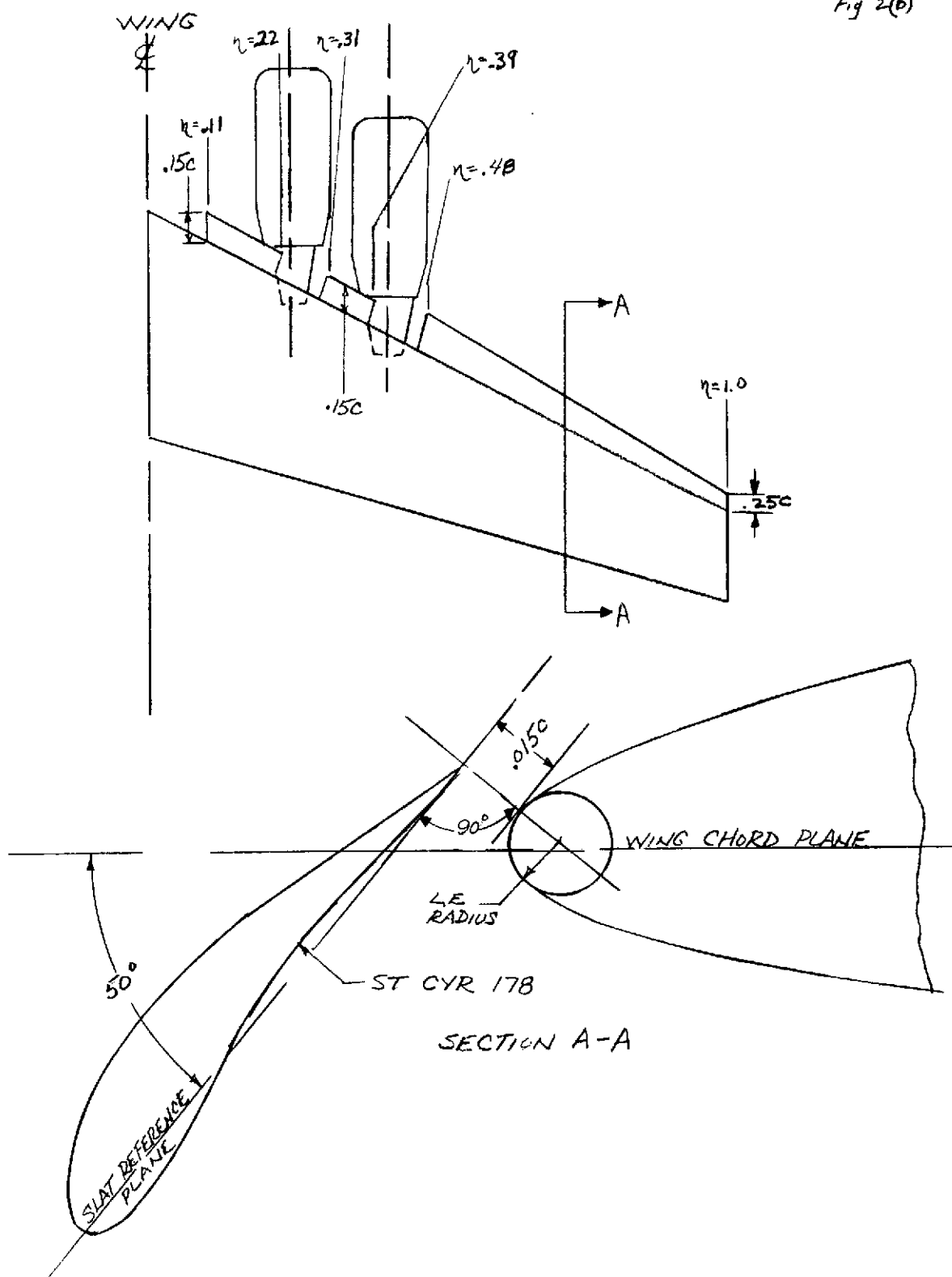
Figure 1.—Photograph of the model as mounted in the Ames 40- by 80-Foot Wind Tunnel.



(a) General arrangement of the model.

Figure 2.—Geometric details of the model.

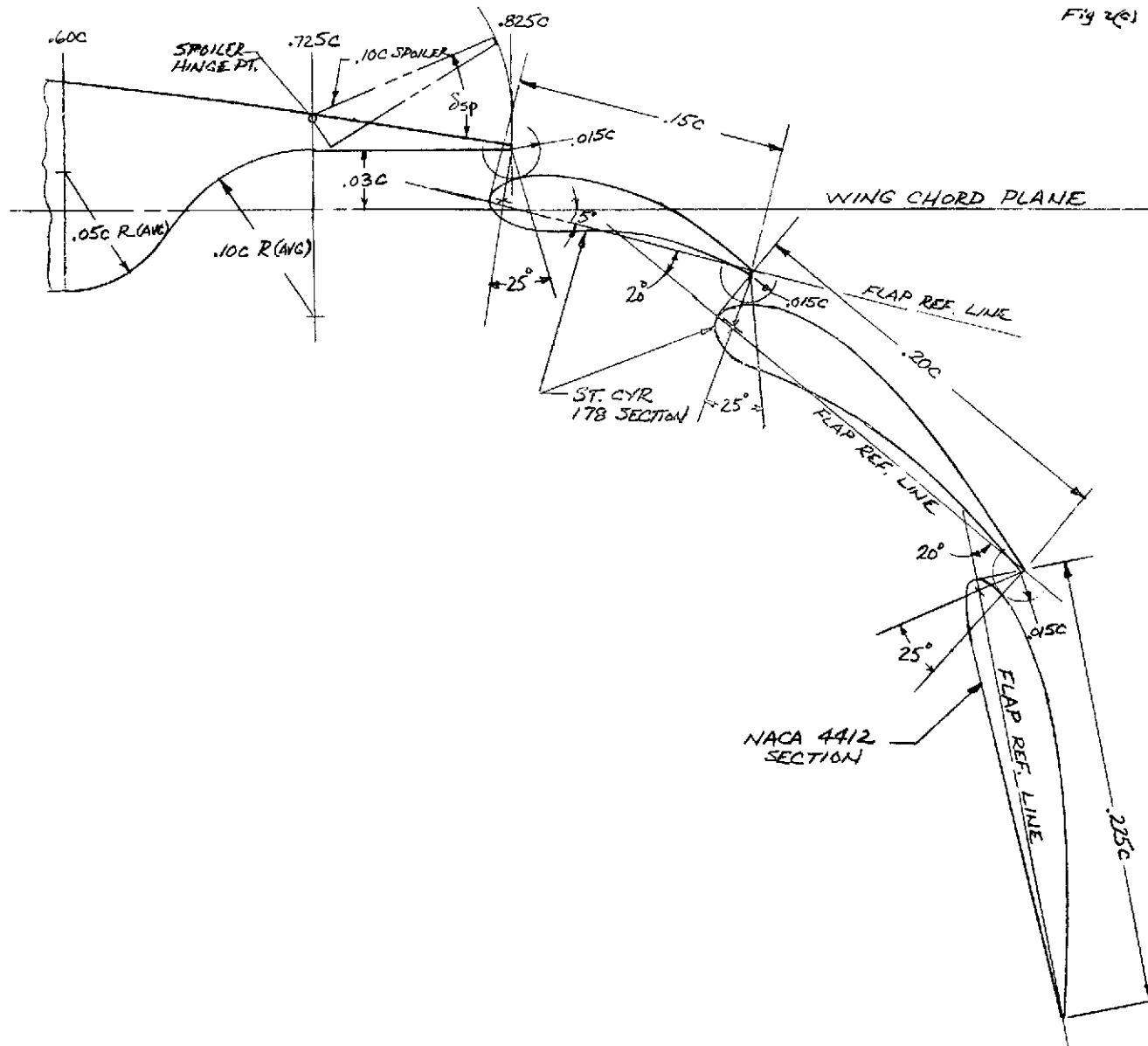
Fig 2(b)



(b) Leading-edge slat arrangement.

Figure 2.—Continued.

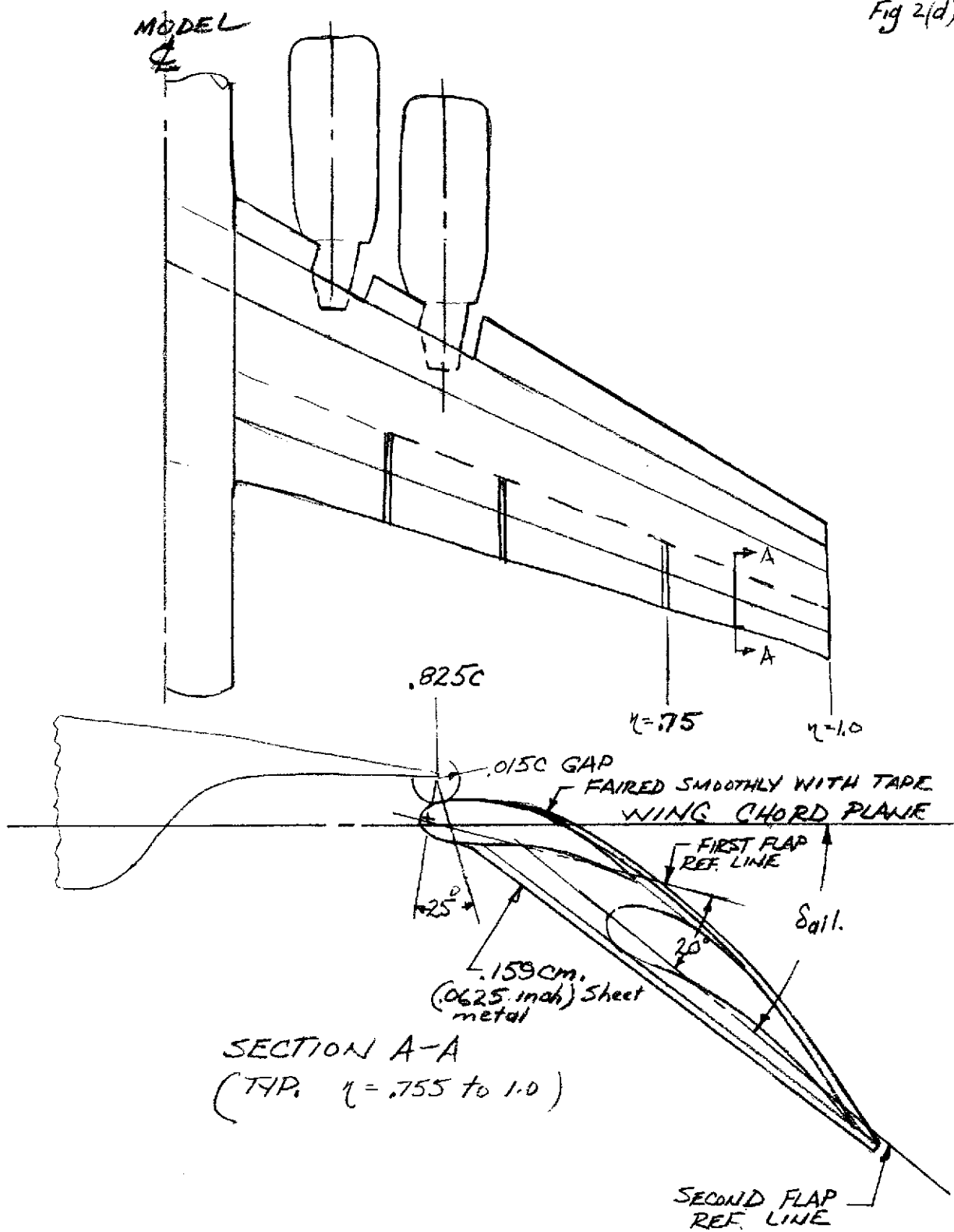
Fig 2(c)



(c) Trailing-edge flap section (streamwise).

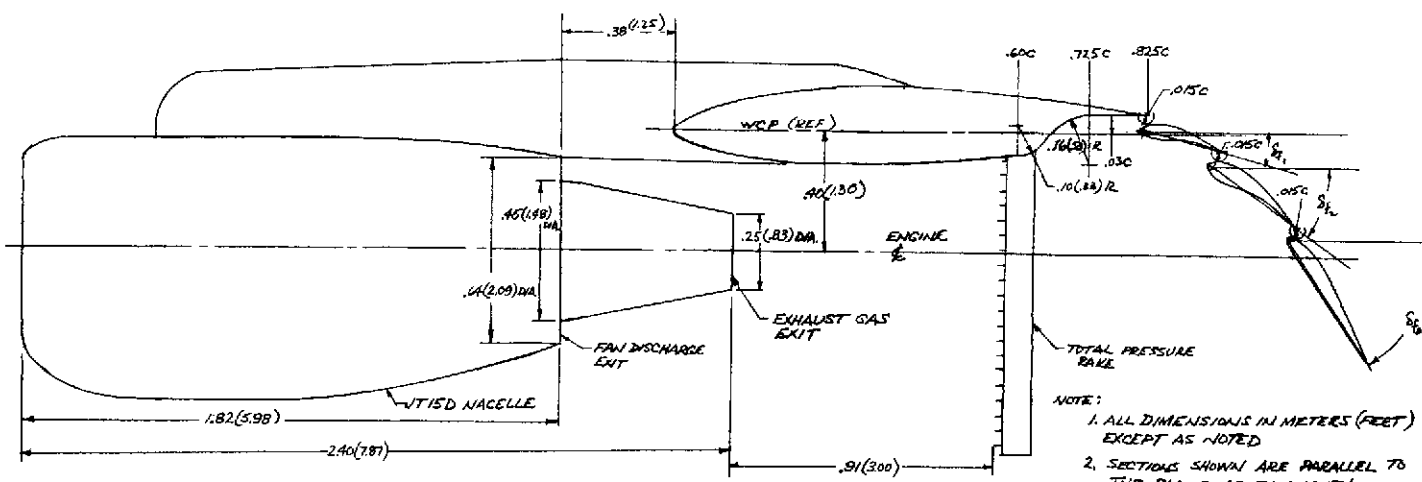
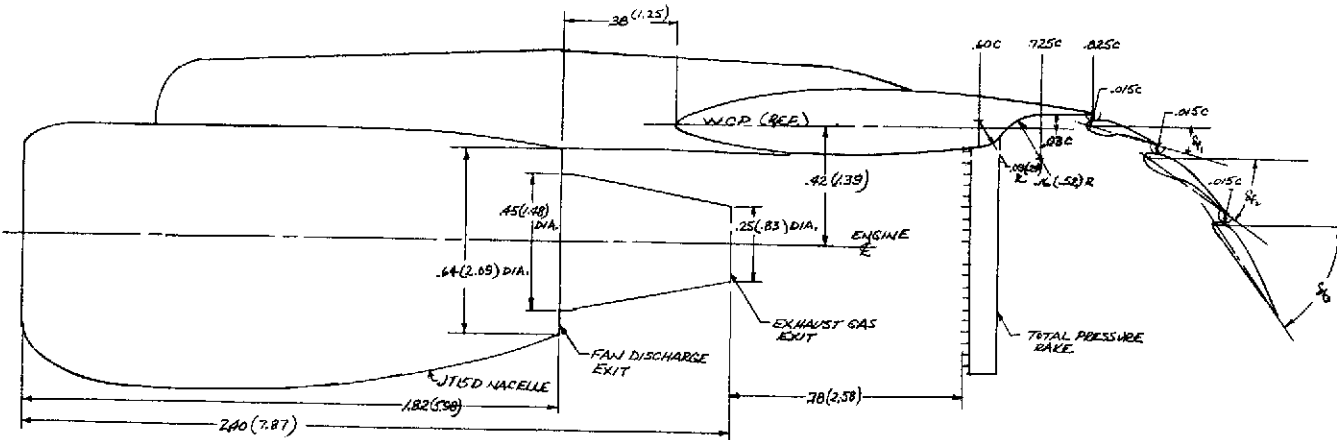
Figure 2.—Continued.

Fig 2(d)



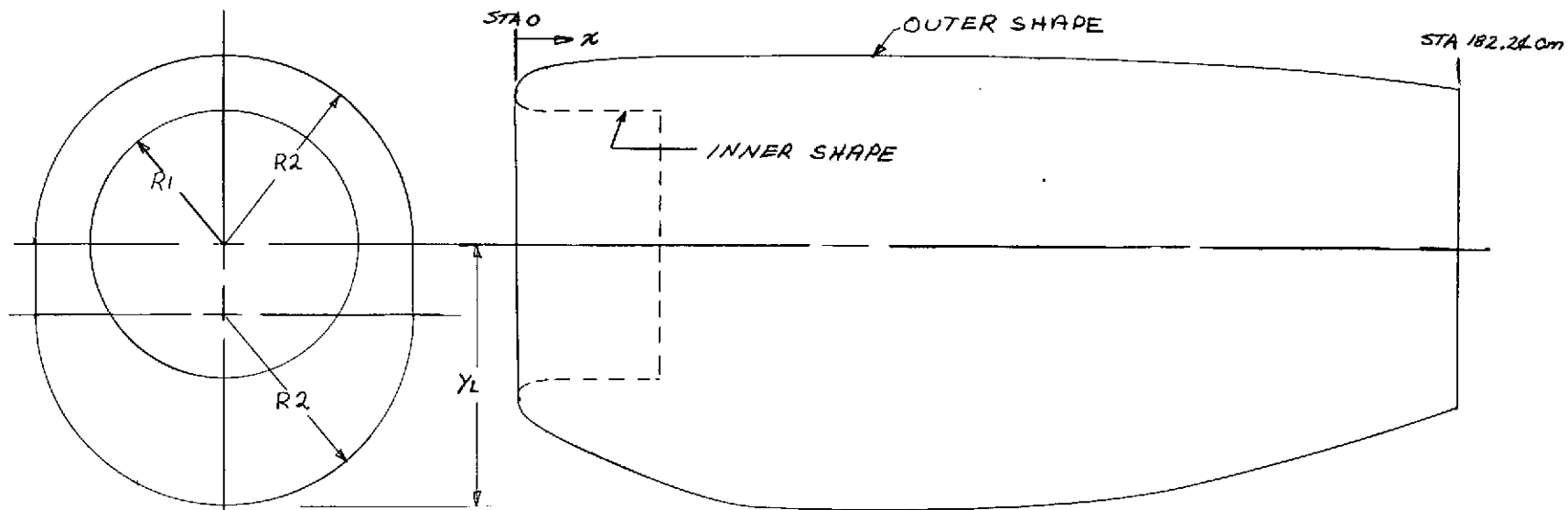
(d) Aileron arrangement.

Figure 2.—Continued.



(e) Engine and nacelle arrangement with the wing.

Figure 2.—Continued.



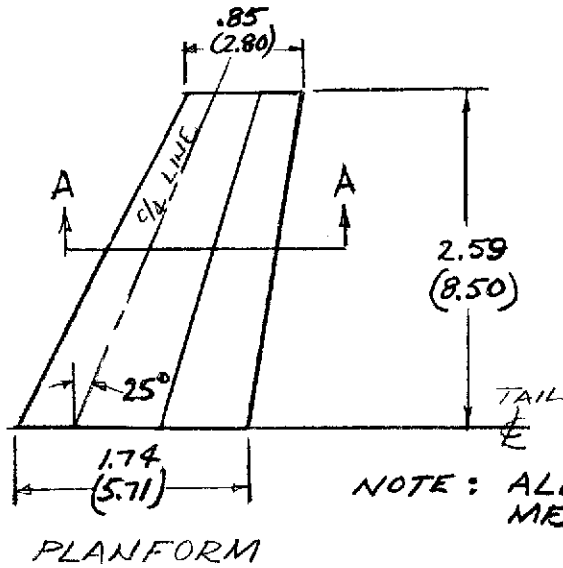
<i>X</i> cm	OUTER SHAPE <i>R</i> ₂ cm	INNER SHAPE <i>R</i> ₁ cm
	<i>Y</i> _L cm	
0.0	29.58	29.58
.63		27.85
1.27	31.89	27.19
2.54	32.78	26.46
3.81		26.01
5.08	33.86	25.77
5.99		25.72
7.62	34.71	40.74
10.16	35.30	42.24
15.24	36.01	44.63
17.78		45.57
20.32		46.40
20.95	36.26	
25.40		47.67
30.48		48.60
35.56		49.26
45.72		49.75
57.88		49.75
105.02		48.38
122.68	36.26	45.93
138.43	35.77	42.99
154.17	34.54	39.20
169.92	32.58	34.66
182.24	30.79	30.79

Fig 2(f)

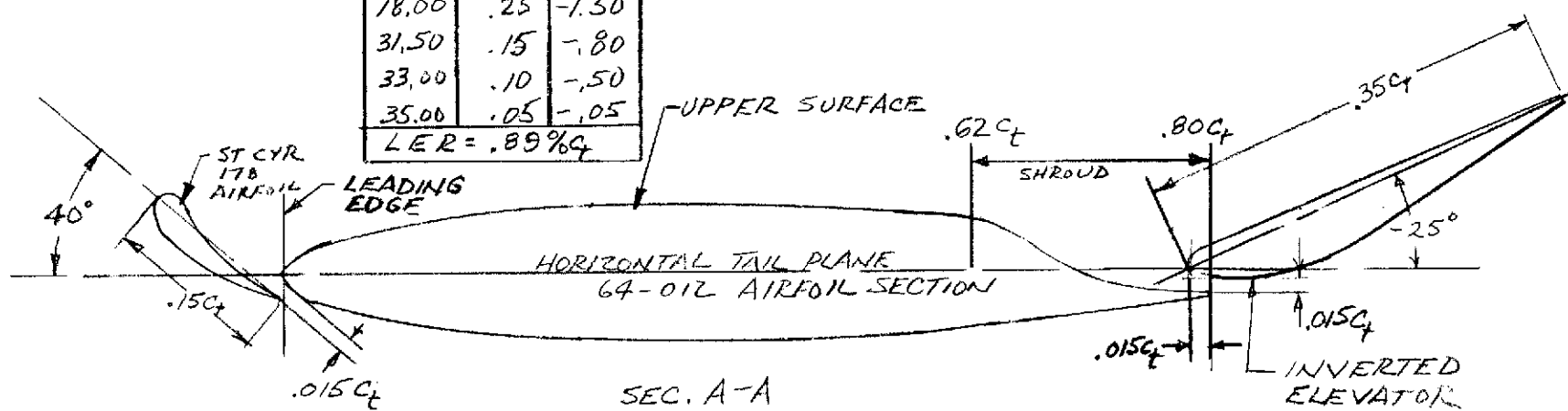
(f) Nacelle contour.

Figure 2.—Continued.

SH. %C _t	DUD COORDINATES		ELEVATOR COORDINATES		
	Z %C _t	X %C _t	Z %C _t	X %C _t	Z %C _t
X, %C _t	UPPER LOWER	X, %C _t	UPPER LOWER	X, %C _t	UPPER LOWER
62.00	3.98	-4.28	0	0	0
64.00	2.75	-4.06	.44	.57	-.98
65.00	1.93	-3.95	.87	.78	-1.36
66.00	1.22	-3.84	1.75	.98	-1.89
68.00	.14	-3.61	2.63	.97	-2.20
70.00	-.67	-3.39	3.50	.95	-2.63
72.00	-1.28	-3.17	5.26	.90	-3.16
74.00	-1.68	-2.95	7.00	.85	-3.52
75.00	-1.84	-2.84	8.75	.80	-3.77
76.00	-1.98	-2.73	10.50	.75	-3.90
78.00	-2.14	-2.50	14.00	.65	-3.92
80.00	-2.19	-2.28	17.50	.55	-3.40
			21.00	.45	-2.90
			24.50	.35	-2.20
			18.00	.25	-1.50
			31.50	.15	-.80
			33.00	.10	-.50
			35.00	.05	-.05
			LER = .89% _{C_t}		



NOTE: ALL DIMENSIONS IN METERS(FEET)



(g) Horizontal tail detail.

Figure 2.—Concluded.

Fig 3

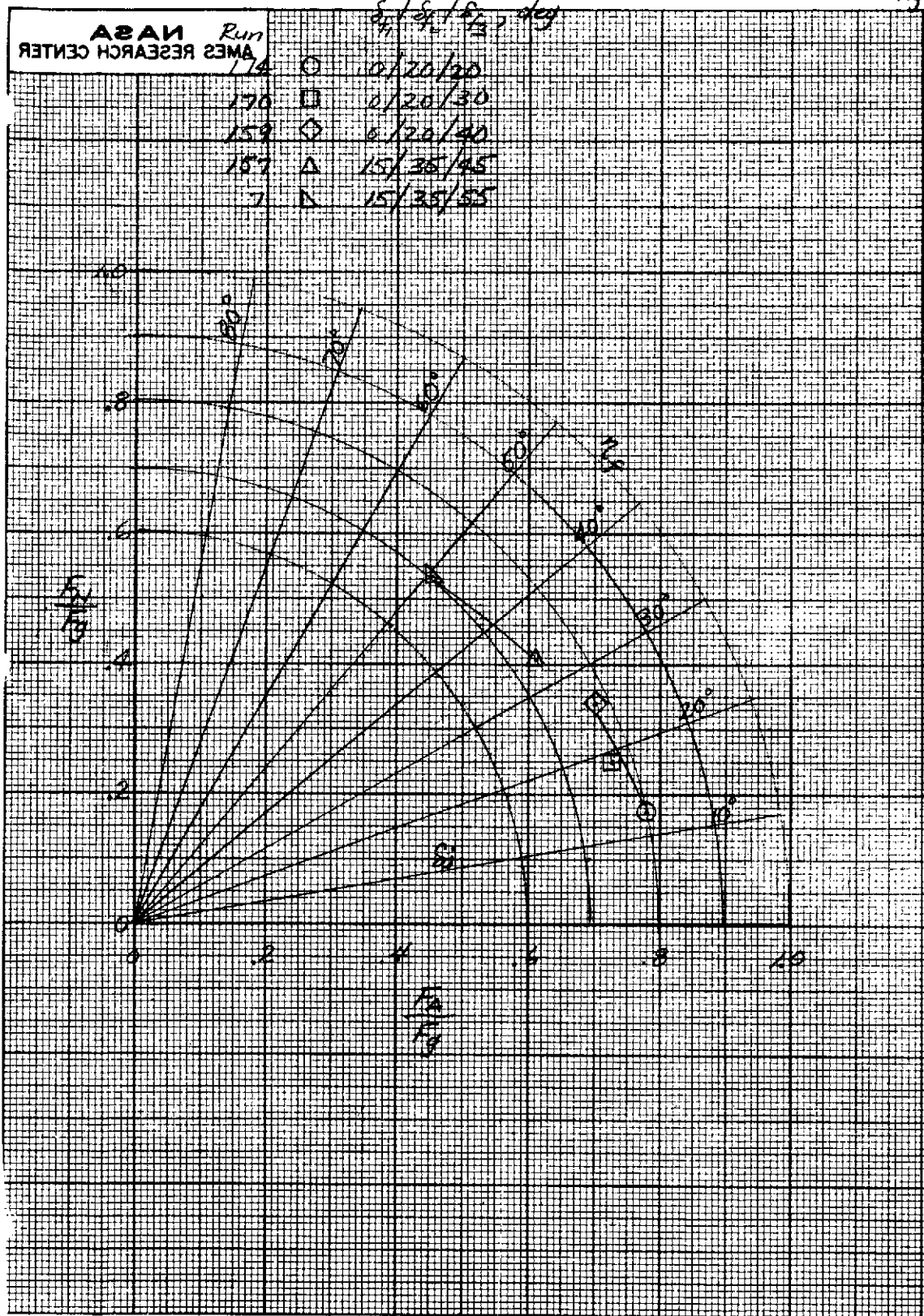


Figure 3.—Trailing-edge flap static turning angle and turning efficiency.

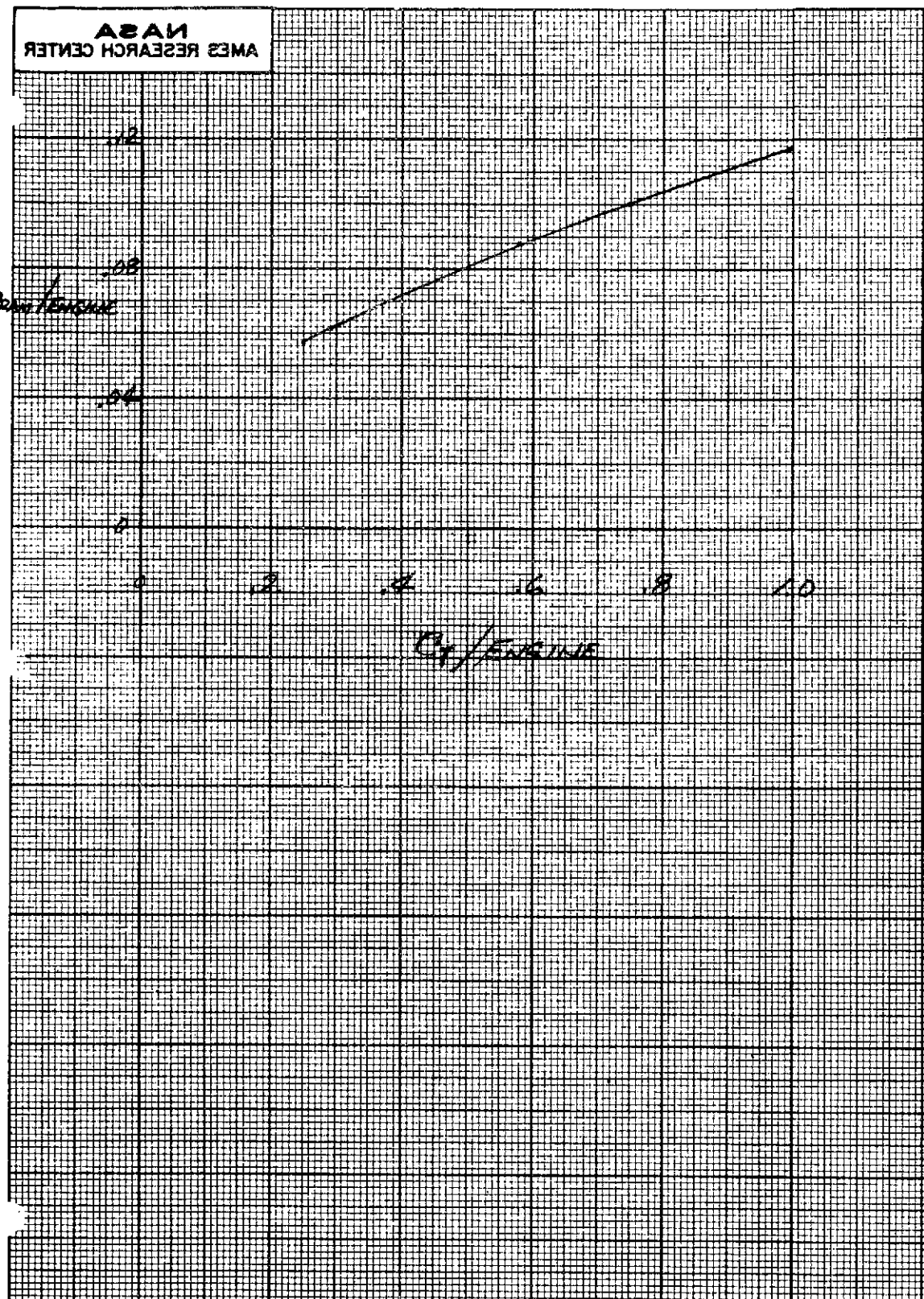
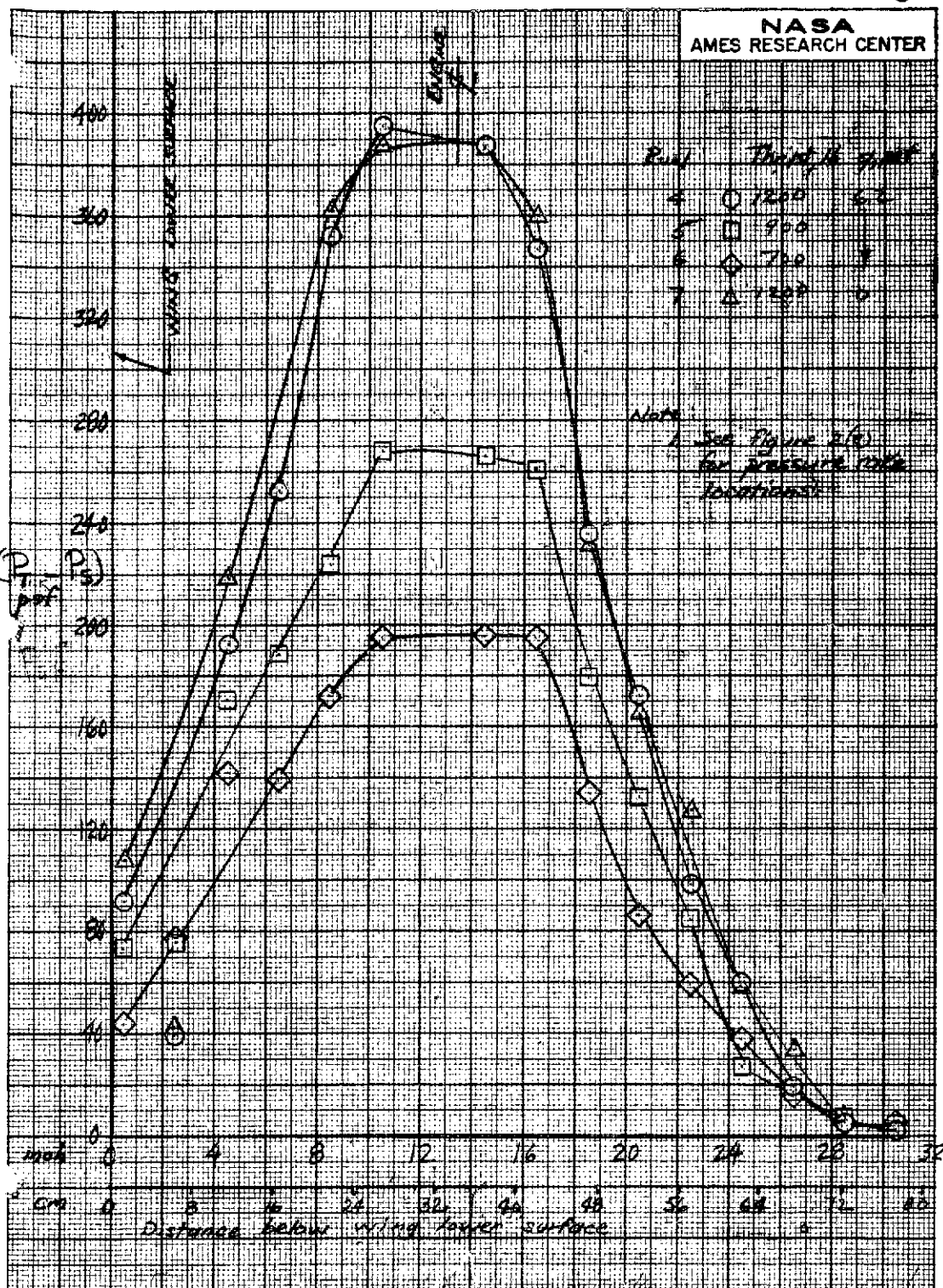


Fig. 4

Figure 4.—Variation of estimated C_{DRAM} with C_T per engine.

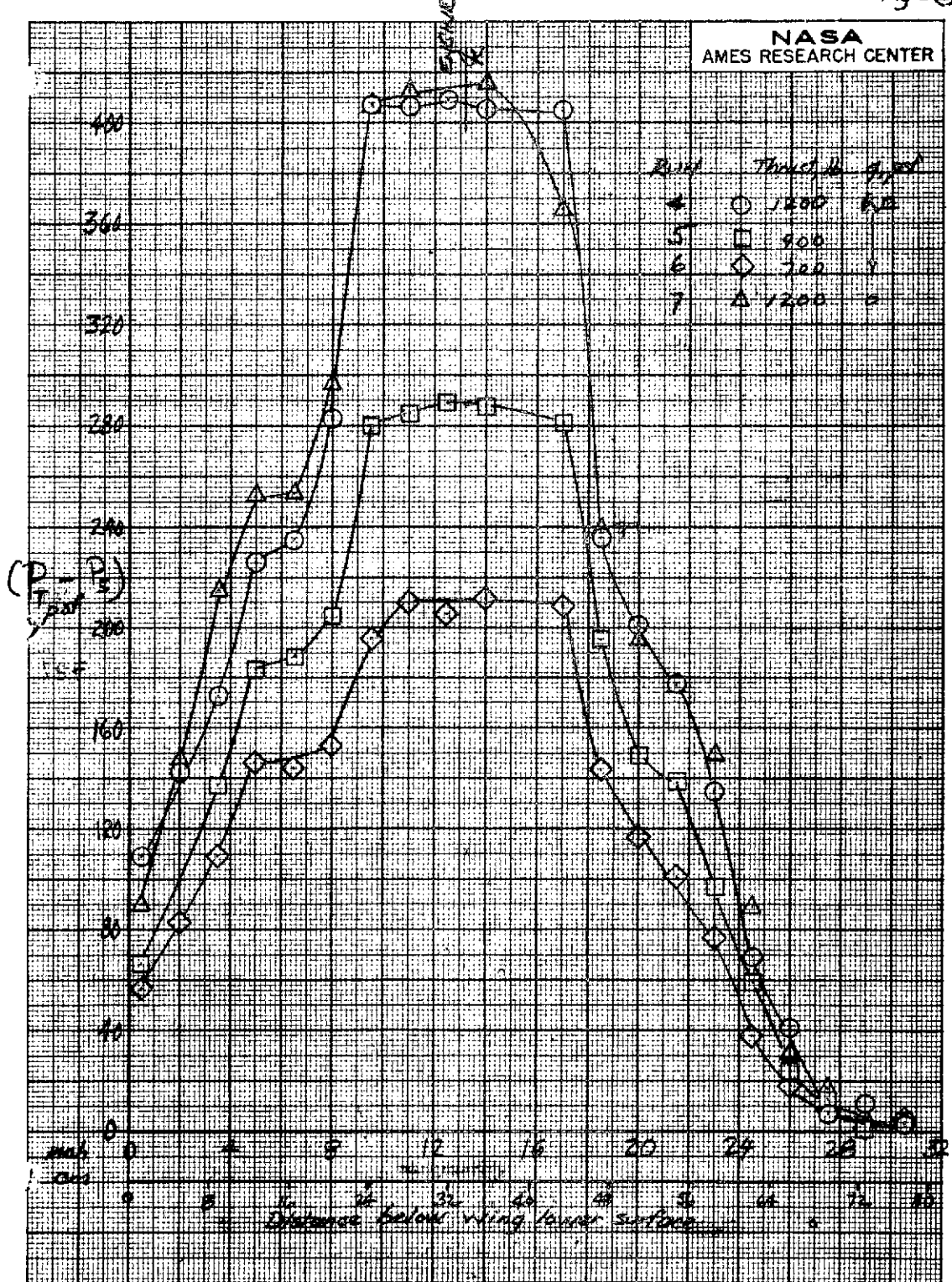
Fig 5(e)



(a) Left inboard engine centerline.

Figure 5.—Jet exhaust total pressure distribution at several power settings;
 $\delta_{f_1}/\delta_{f_2}/\delta_{f_3} = 15^\circ/35^\circ/55^\circ$, $\alpha_u = 0^\circ$.

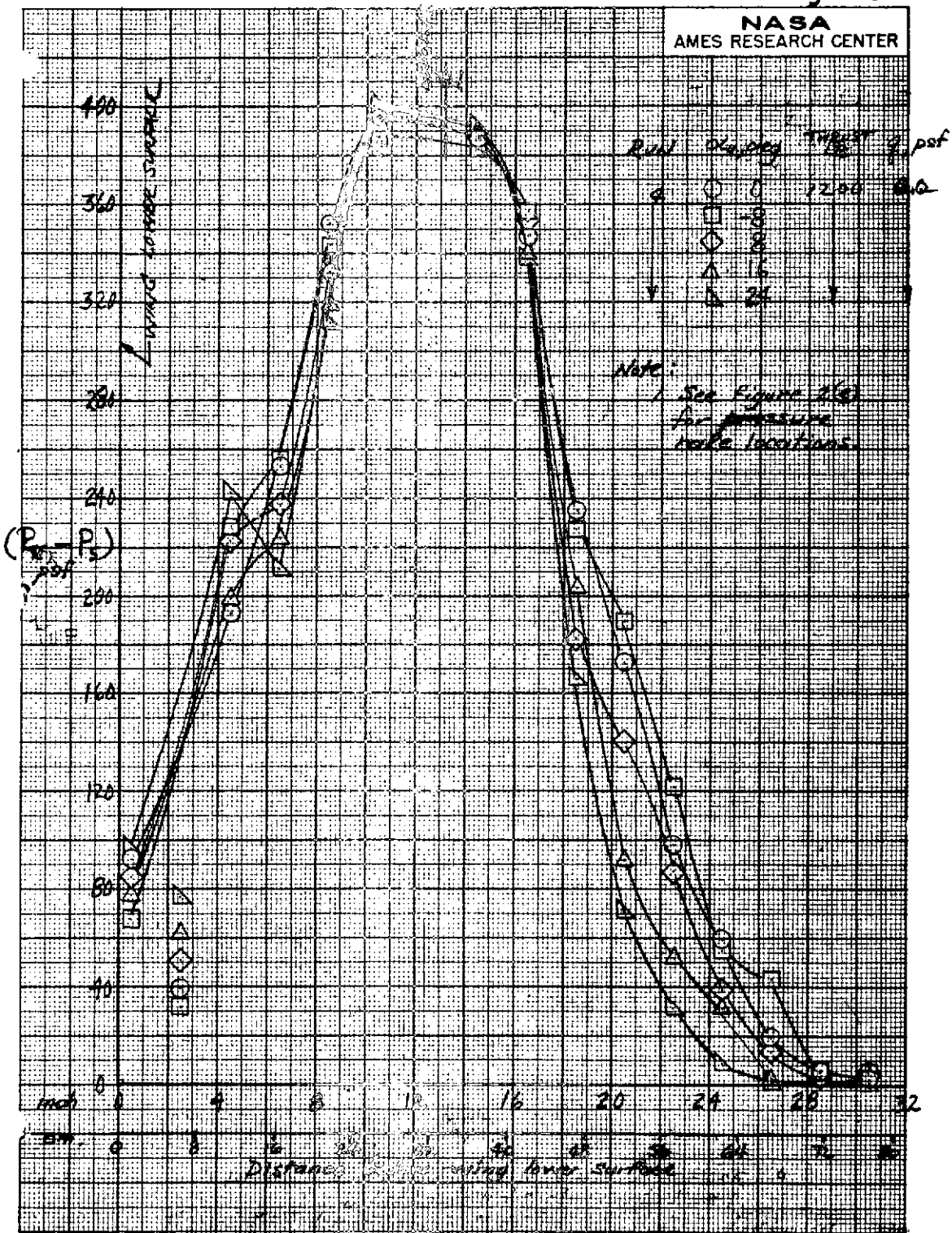
Fig 5(b)



(b) Left outboard engine centerline.

Figure 5.--Concluded.

Fig. 6(a)

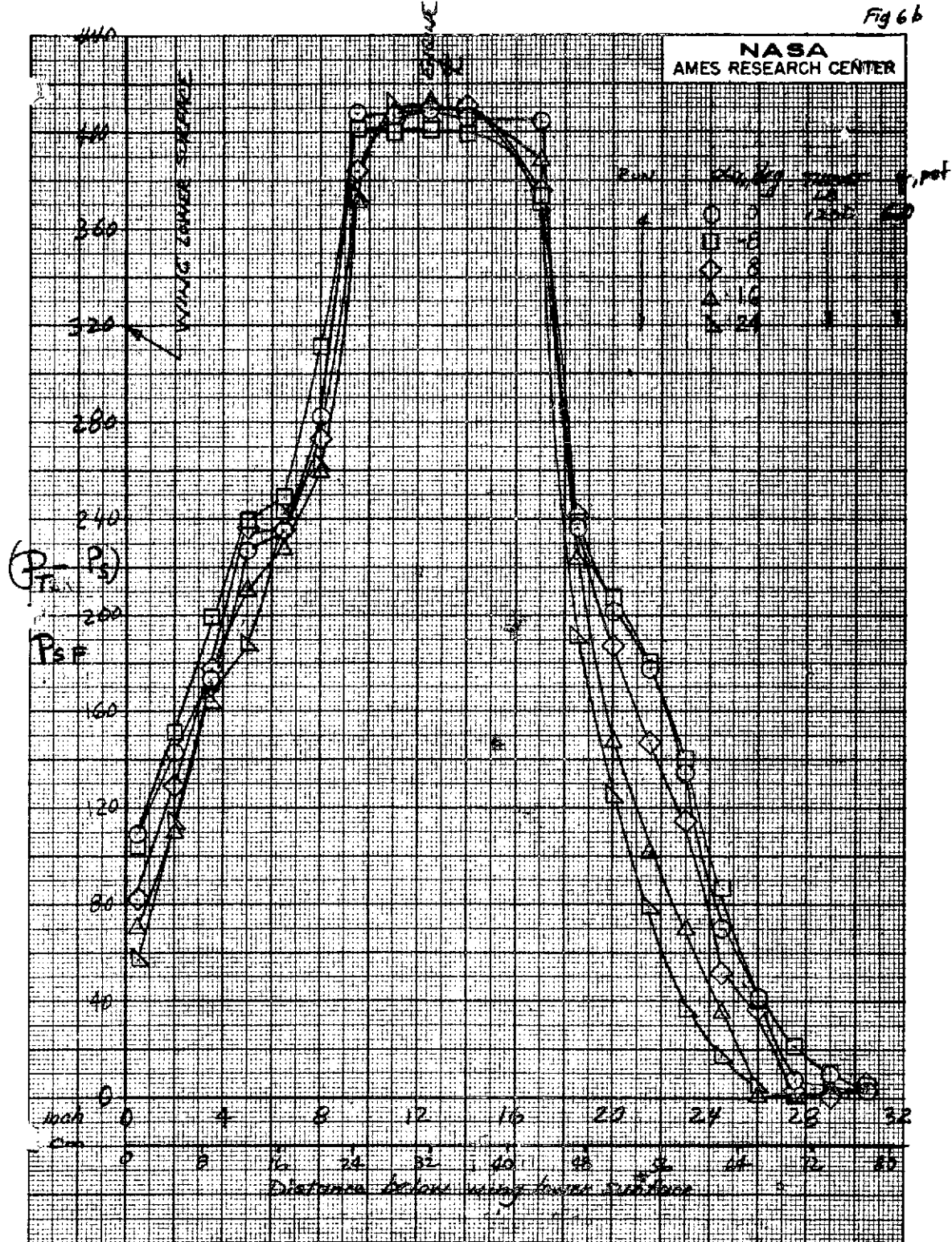


(a) Left inboard engine centerline.

Figure 6.—Jet exhaust total pressure distribution at several α values;
 $\delta_{f_1} / \delta_{f_2} / \delta_{f_3} = 15^\circ / 35^\circ / 55^\circ$.

Fig 6b

NASA
AMES RESEARCH CENTER



(b) Left outboard engine centerline.

Figure 6.--Concluded.

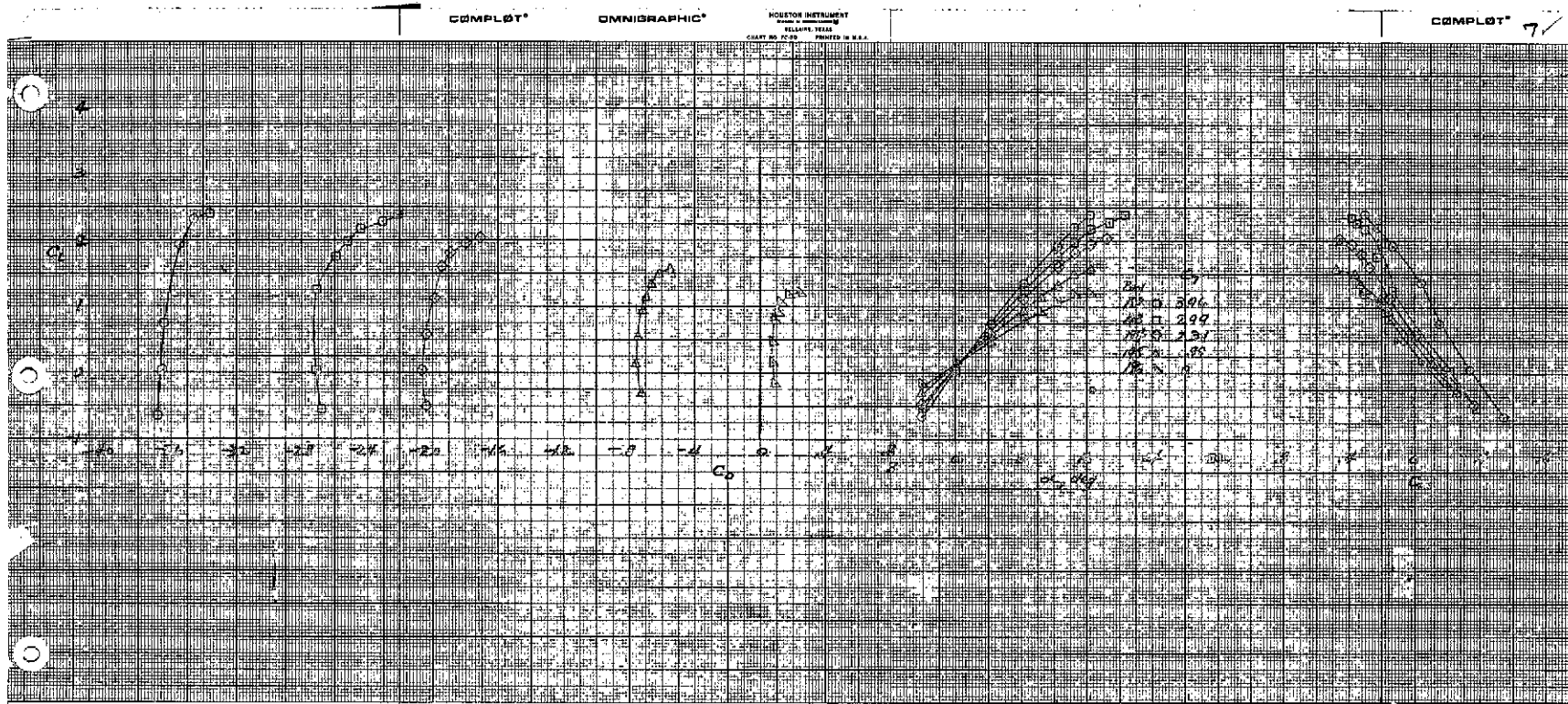


Figure 7.—Longitudinal characteristics of the model with the plain wing, tail off.

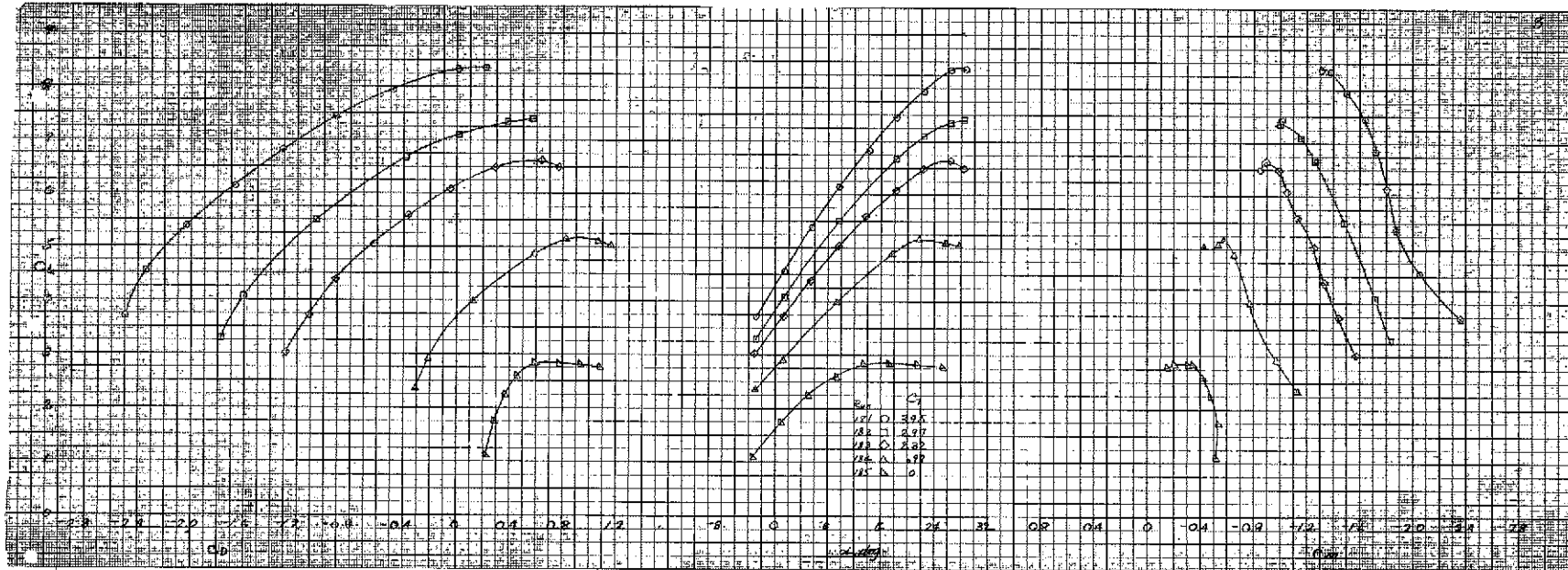


Figure 8.—Longitudinal characteristics of the model with full span flaps deflected;
 $\delta_{f_1}/\delta_{f_2}/\delta_{f_3} = 0^\circ/20^\circ/40^\circ$, tail off.

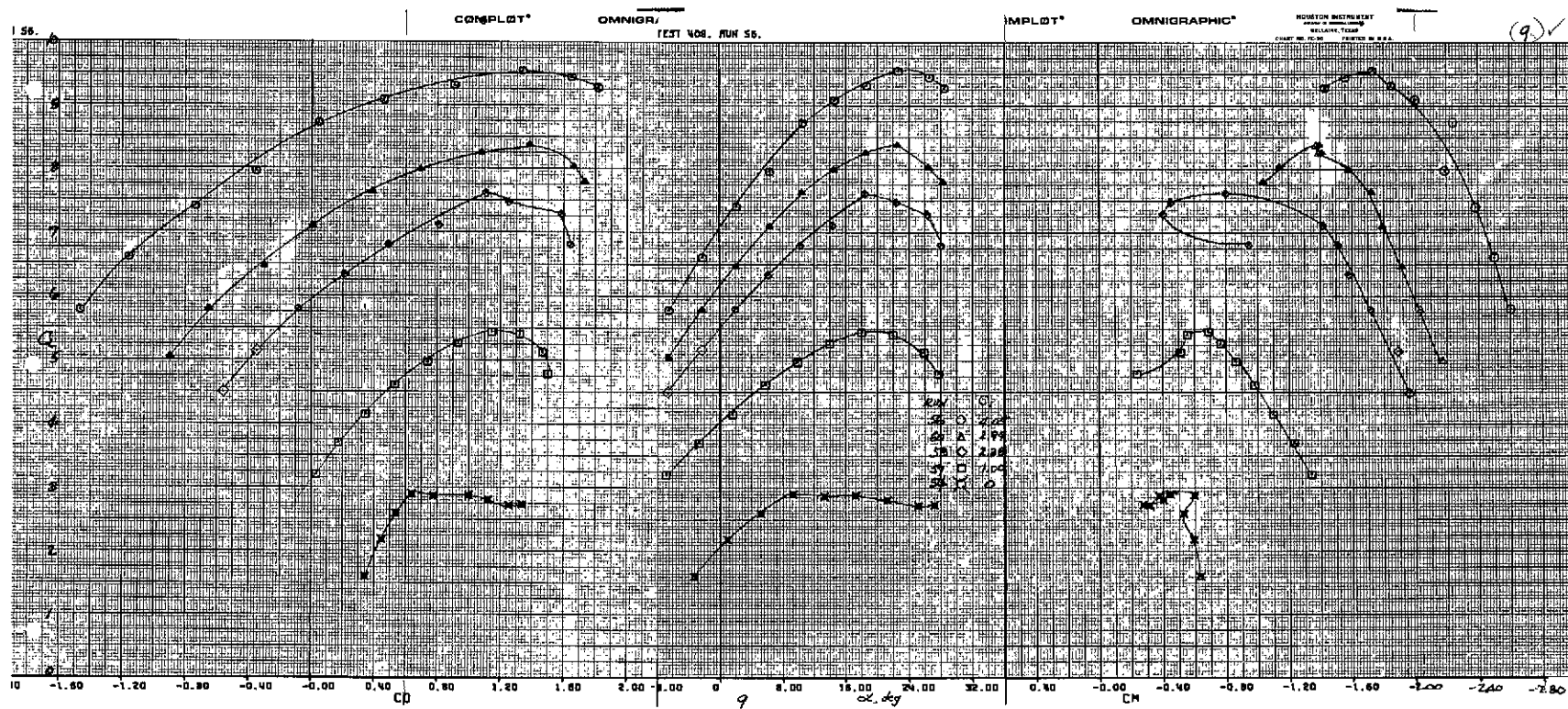
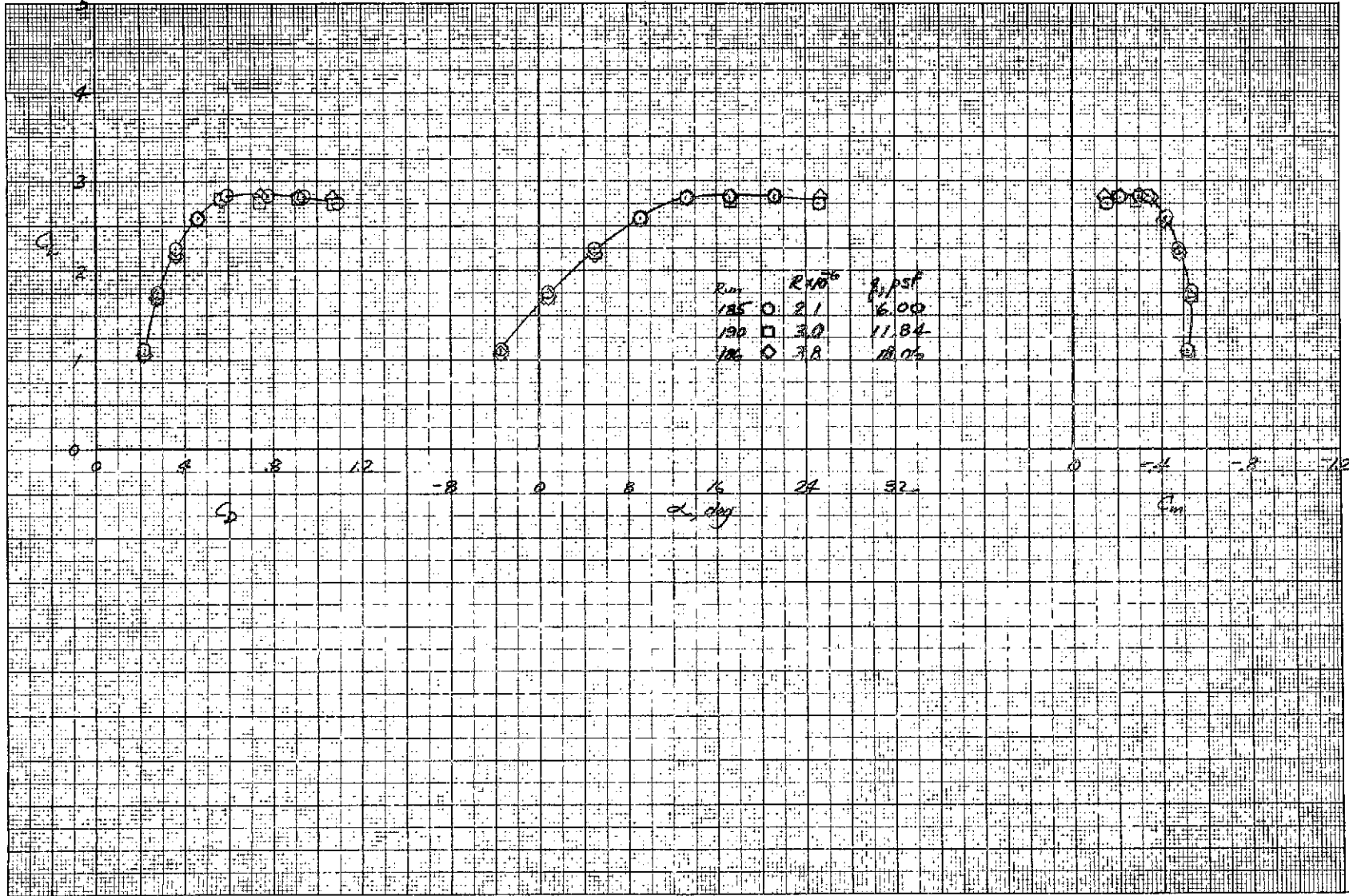


Figure 9.—Longitudinal characteristics of the model with full span flaps deflected;
 $\delta_{f_1}/\delta_{f_2}/\delta_{f_3} = 15^\circ/35^\circ/55^\circ$, tail off.



(a) $C_T = 0$.

Figure 10.—Effect of Reynolds number on the longitudinal characteristics of the model with full span flaps deflected; $\delta_{f_1}/\delta_{f_2}/\delta_{f_3} = 0^\circ/20^\circ/40^\circ$, tail off.

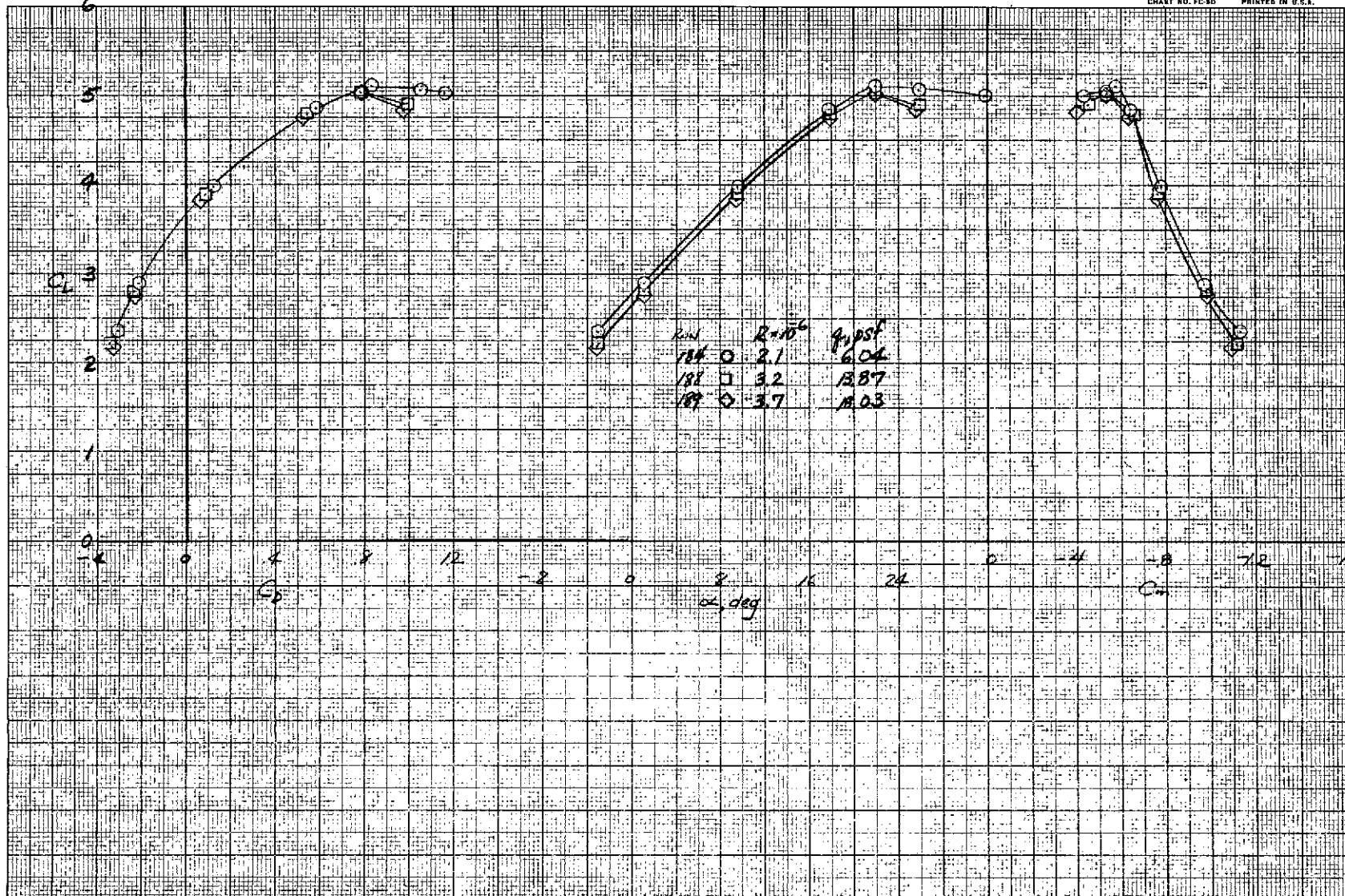
COMPLÖT®

OMNIGRAPHIC®

HOUSTON INSTRUMENT
DIVISION OF OMNIGRAPHIC CORP.
BELLMIRE, TEXAS

CHART NO. PC-500 PRINTED IN U.S.A.

10b



72

(b) $C_T = 1.00$.

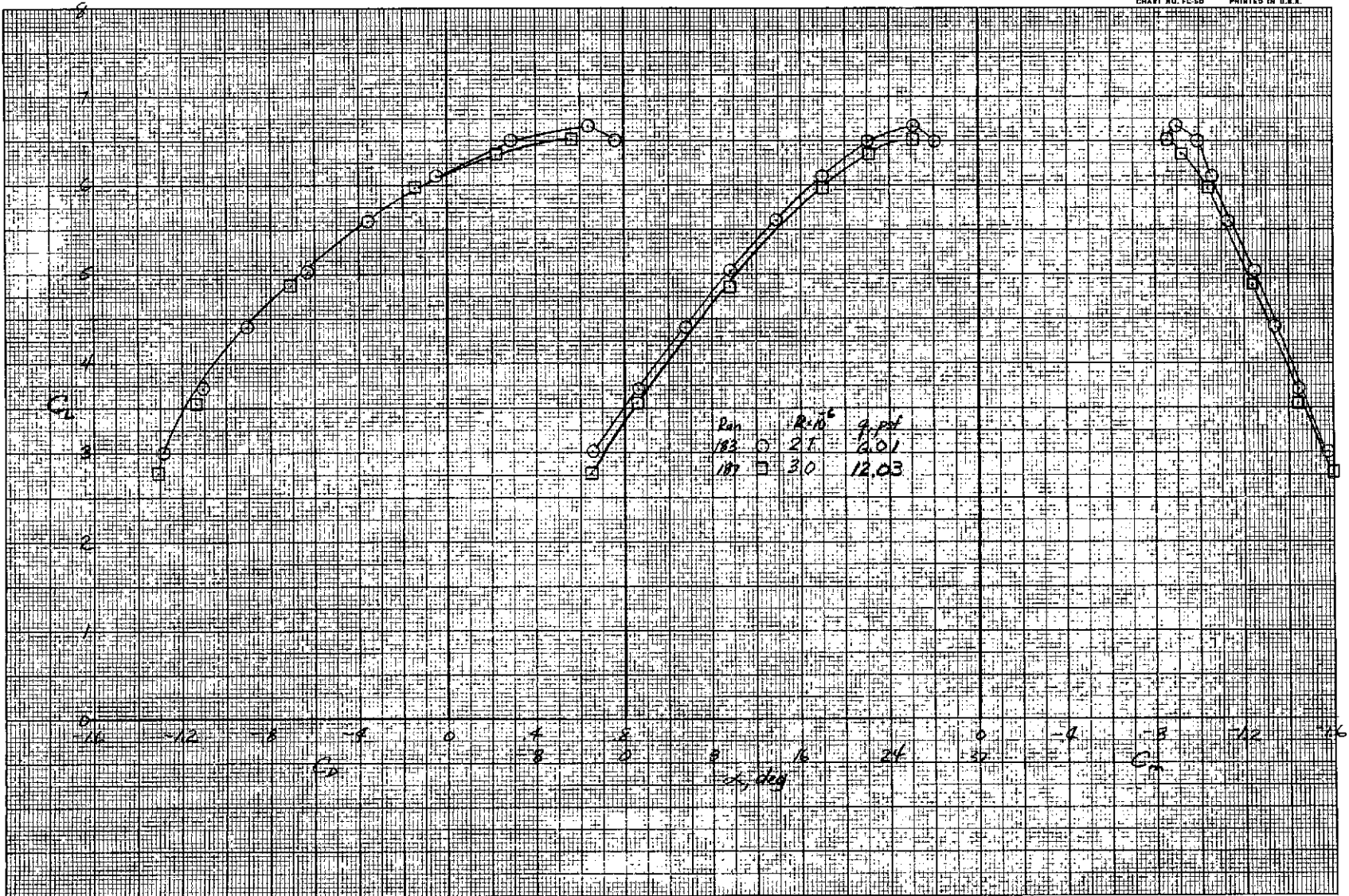
Figure 10.—Continued.

COMPLOT®

OMNIGRAPHIC®

HOUSTON INSTRUMENT
Division of Omnitronics®
Bellaire, Texas
PRINTED IN U.S.A.

CHART NO. FC-50



75

$$(c) C_T = 2.32.$$

Figure 10.—Concluded.

COMPLÖT®

OMNIGRAPHIC®

HOUSTON INSTRUMENT
DIVISION OF MARSH & LAMSON®

BELLMEIR, TEXAS

CHART NO. FC-50 PRINTED IN U.S.A.

11(1)

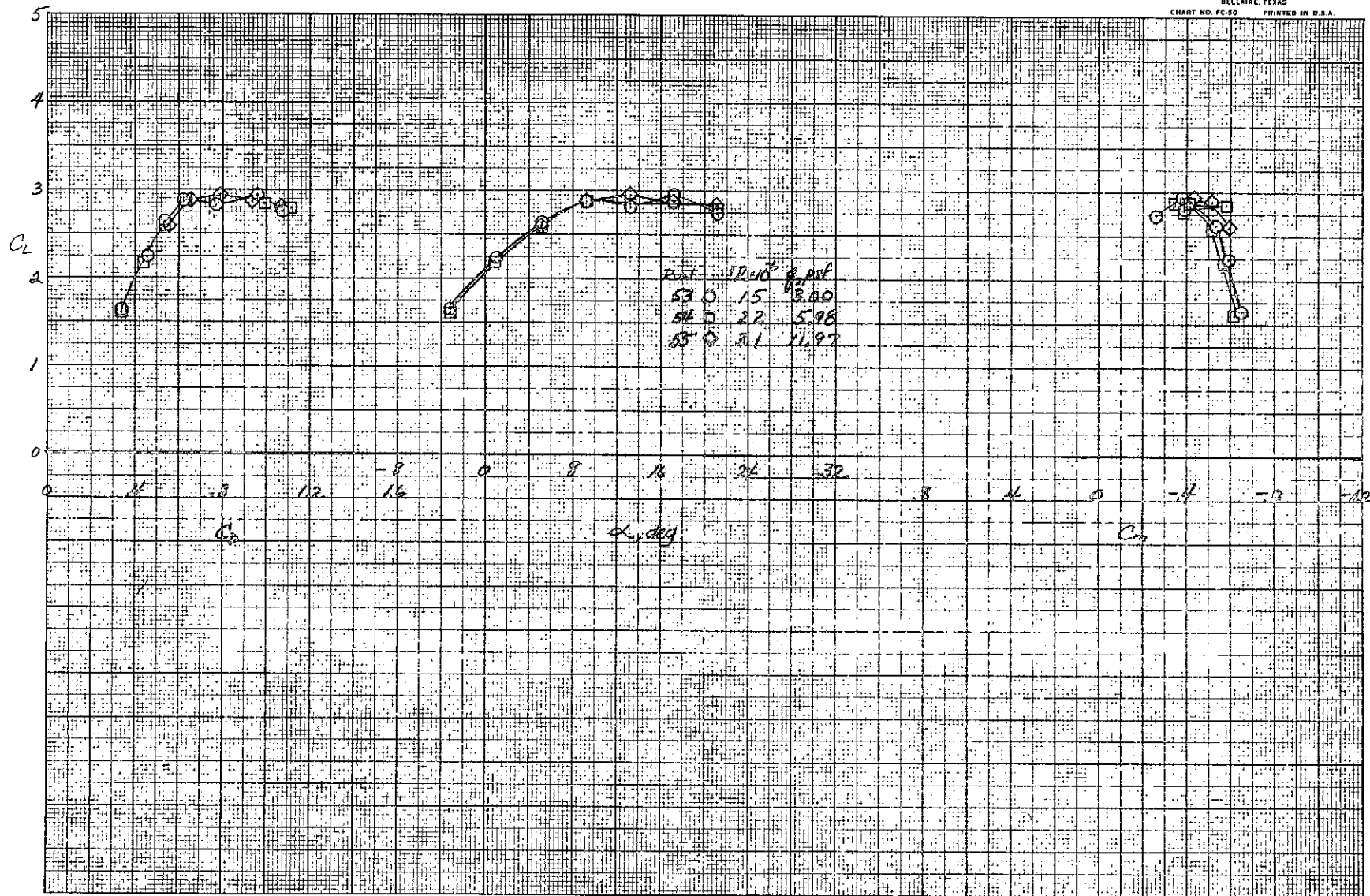
(a) $C_T = 0$.

Figure 11.—Effect of Reynolds number on the longitudinal characteristics of the model with full span flaps deflected; $\delta_{f_1}/\delta_{f_2}/\delta_{f_3} = 15^\circ/35^\circ/55^\circ$, tail off.

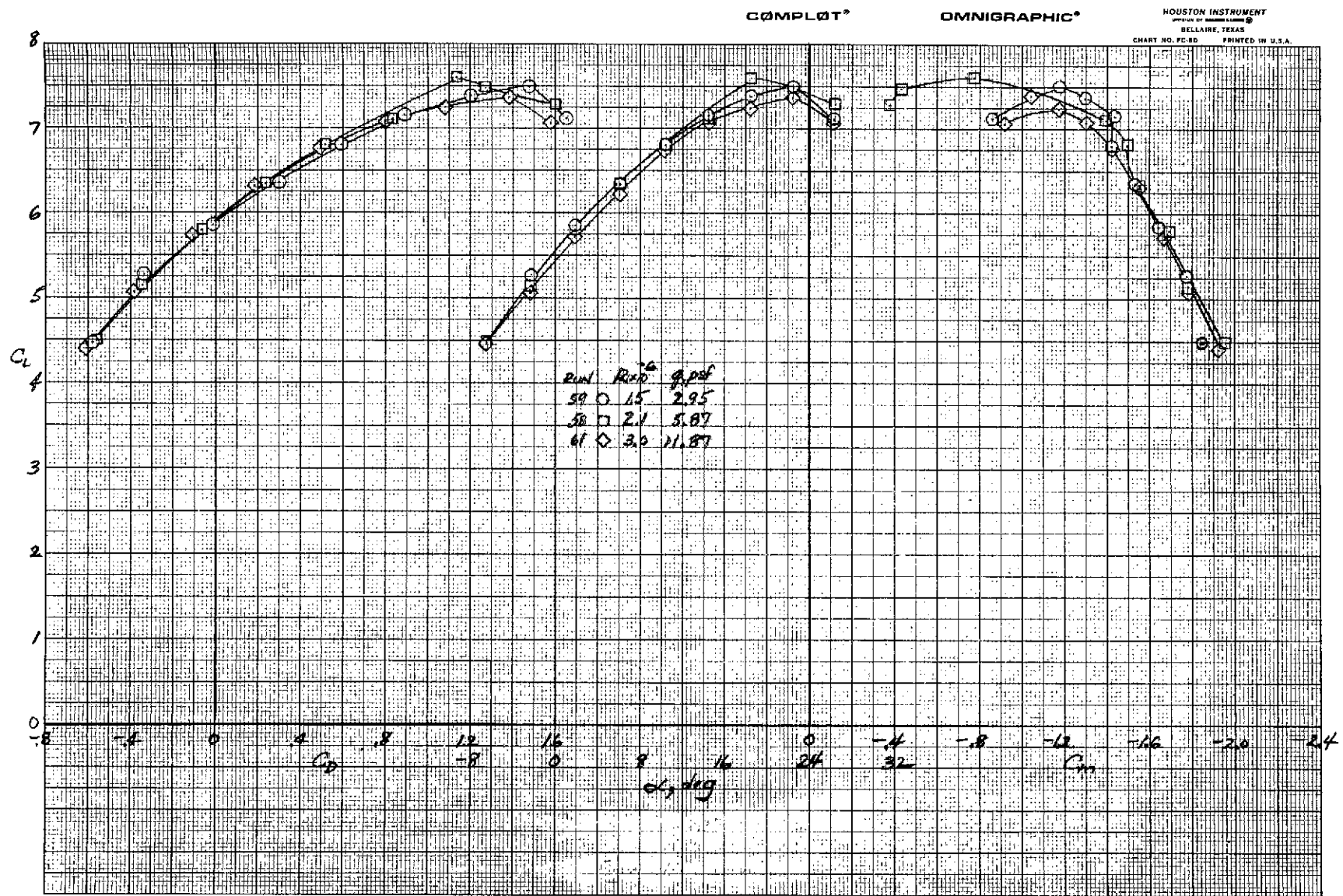


Figure 11.—Concluded.

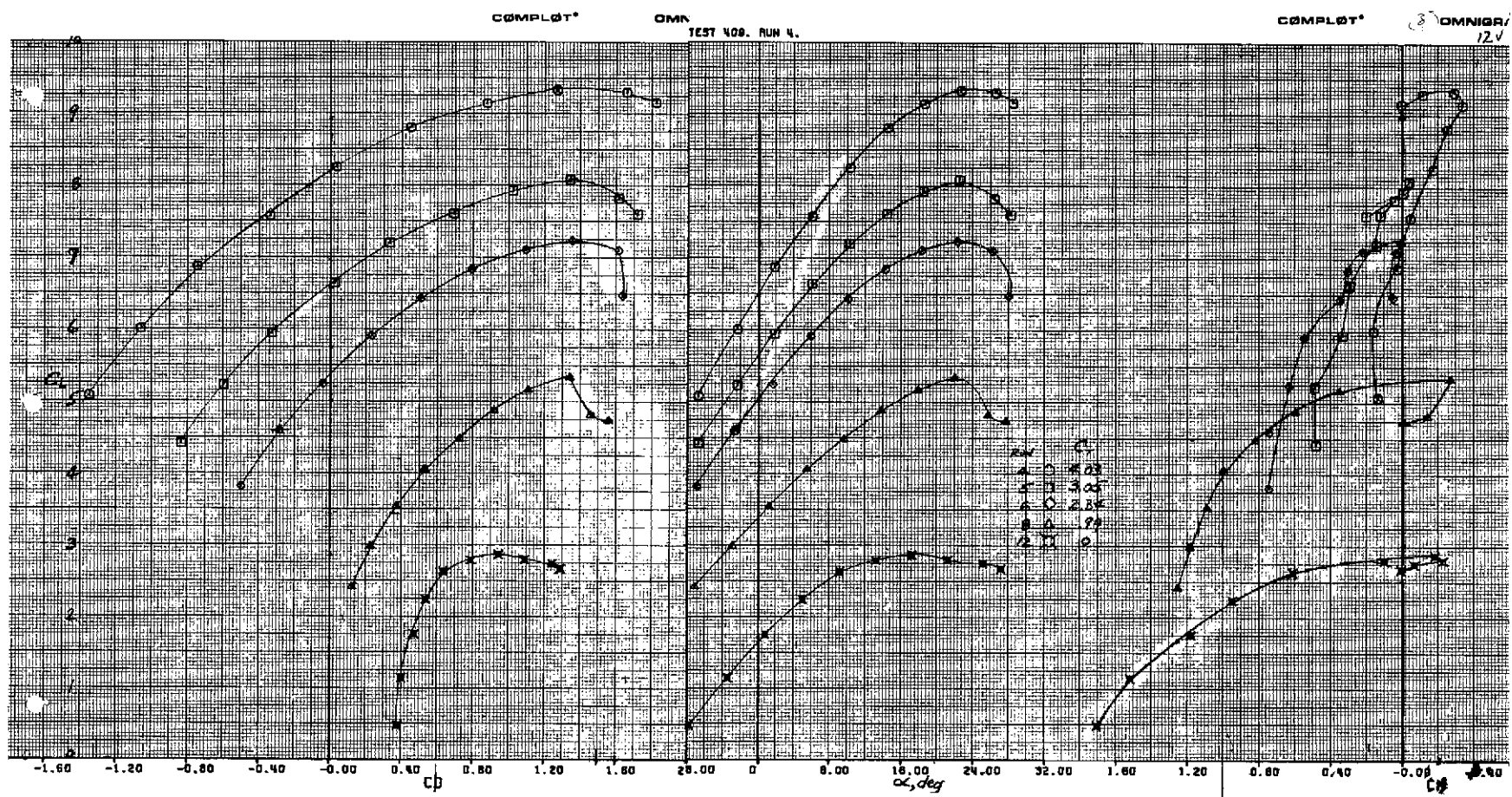


Figure 12.—Longitudinal characteristics of the model with full span flaps deflected;
 $\delta_{f_1}/\delta_{f_2}/\delta_{f_3} = 15^\circ/35^\circ/55^\circ$, tail on, $i_t = 0^\circ$, $\delta_e = -25^\circ$.

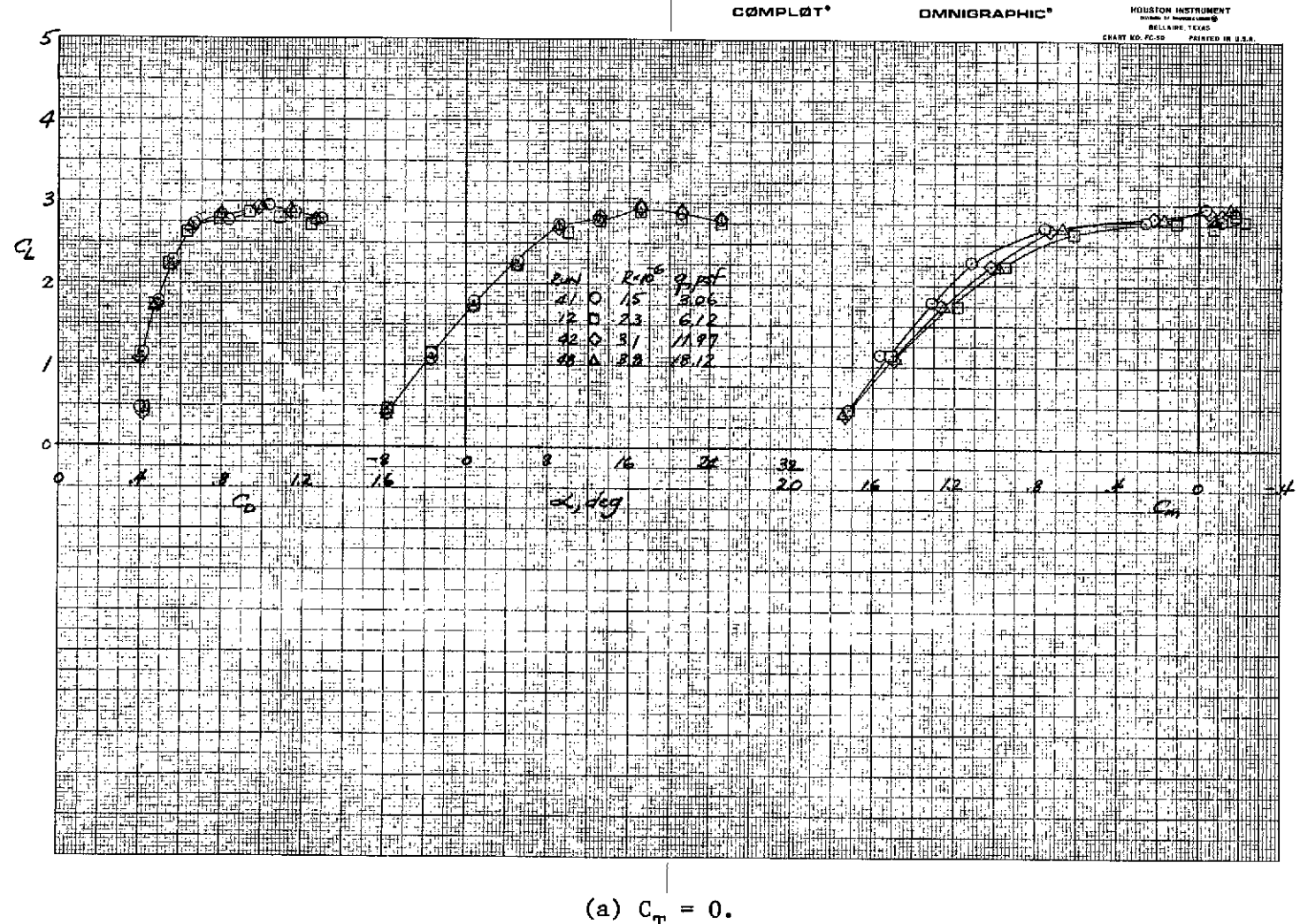
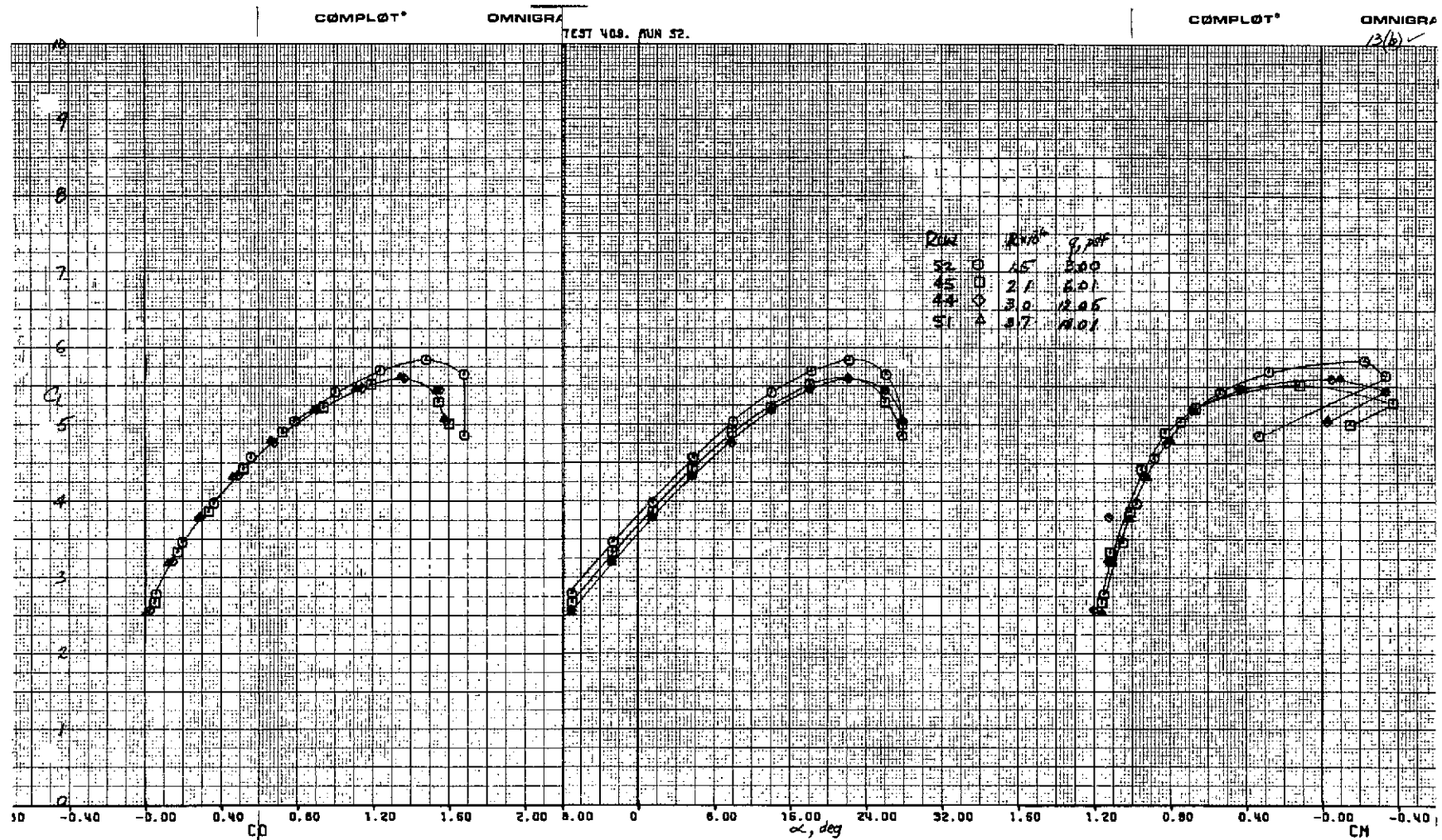
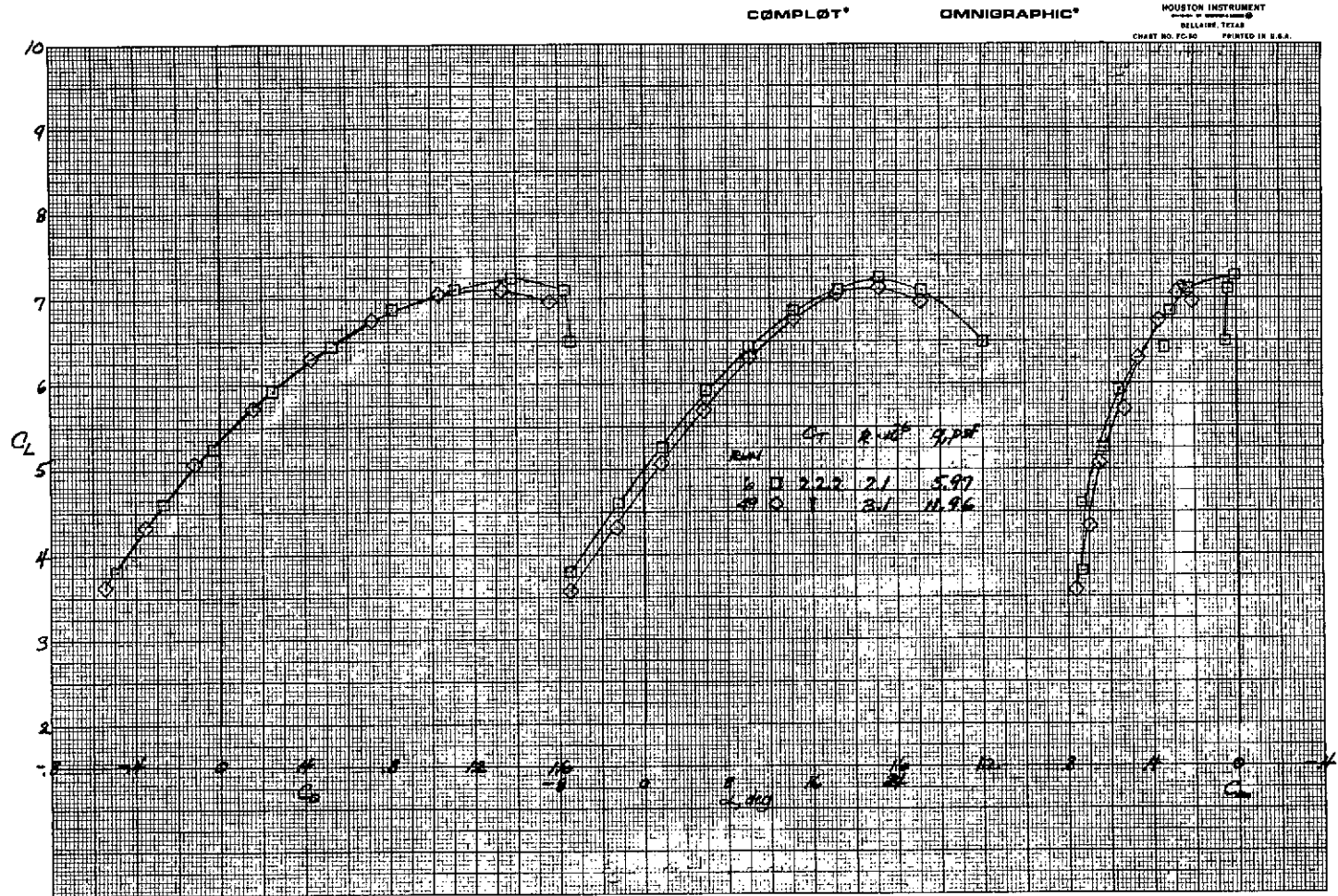


Figure 13.—Effect of Reynolds number on the longitudinal characteristics of the model with full span flaps deflected; $\delta_{f_1}/\delta_{f_2}/\delta_{f_3} = 15^\circ/35^\circ/55^\circ$, tail on, $i_t = 0^\circ$, $\delta_e = -25^\circ$.



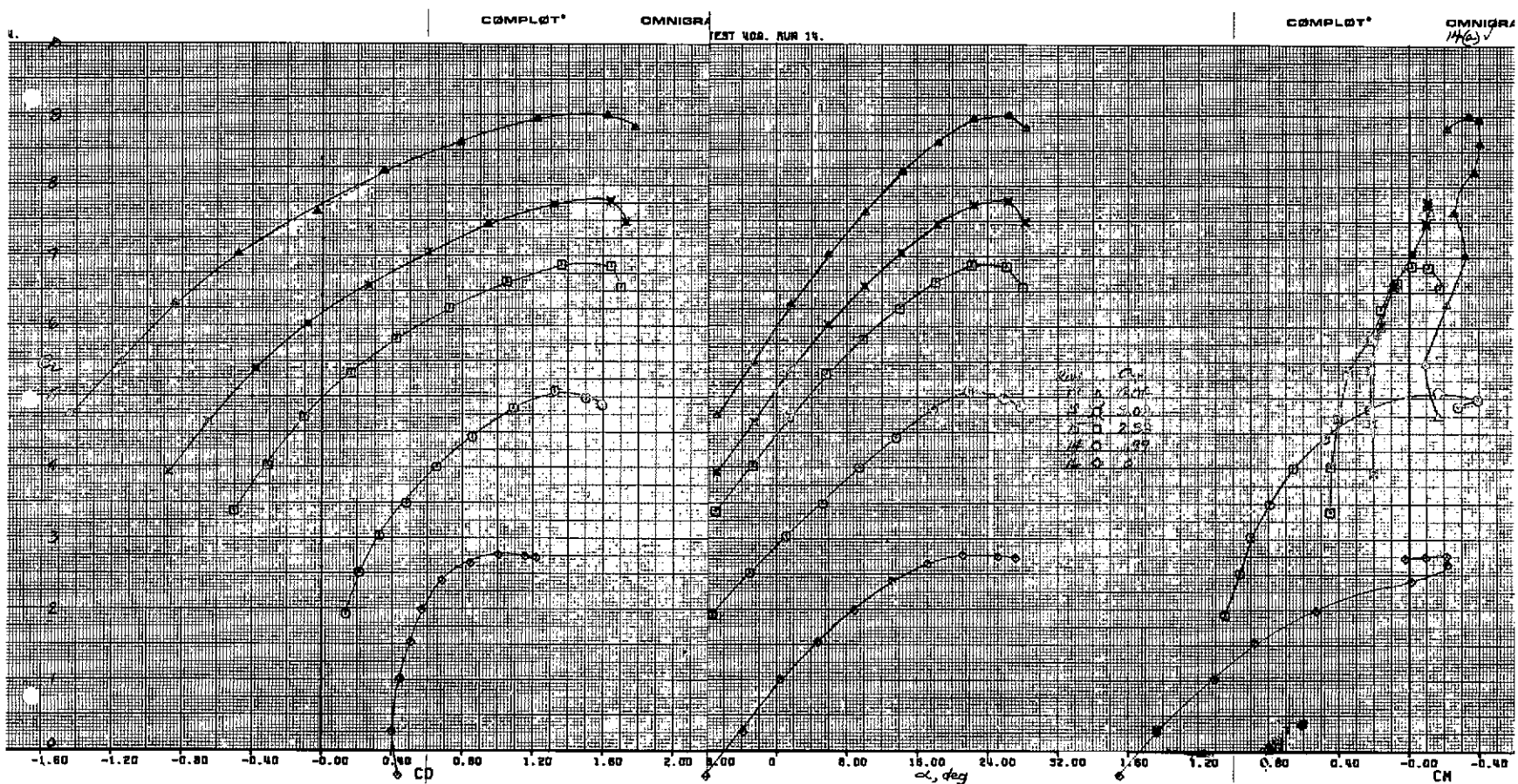
(b) $C_T = 1.16$.

Figure 13.—Continued.



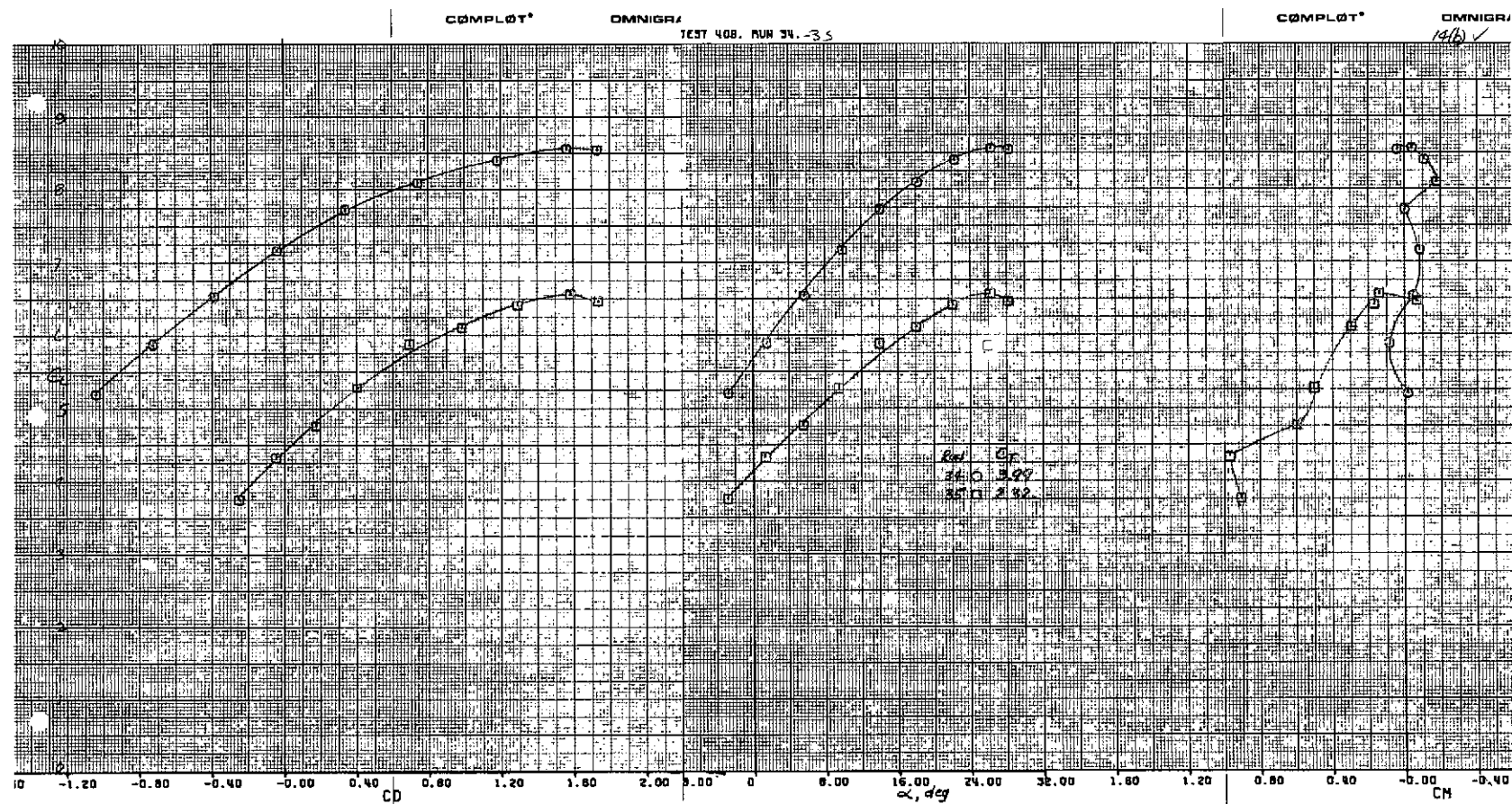
(c) $C_T = 2.34$.

Figure 13.—Concluded.



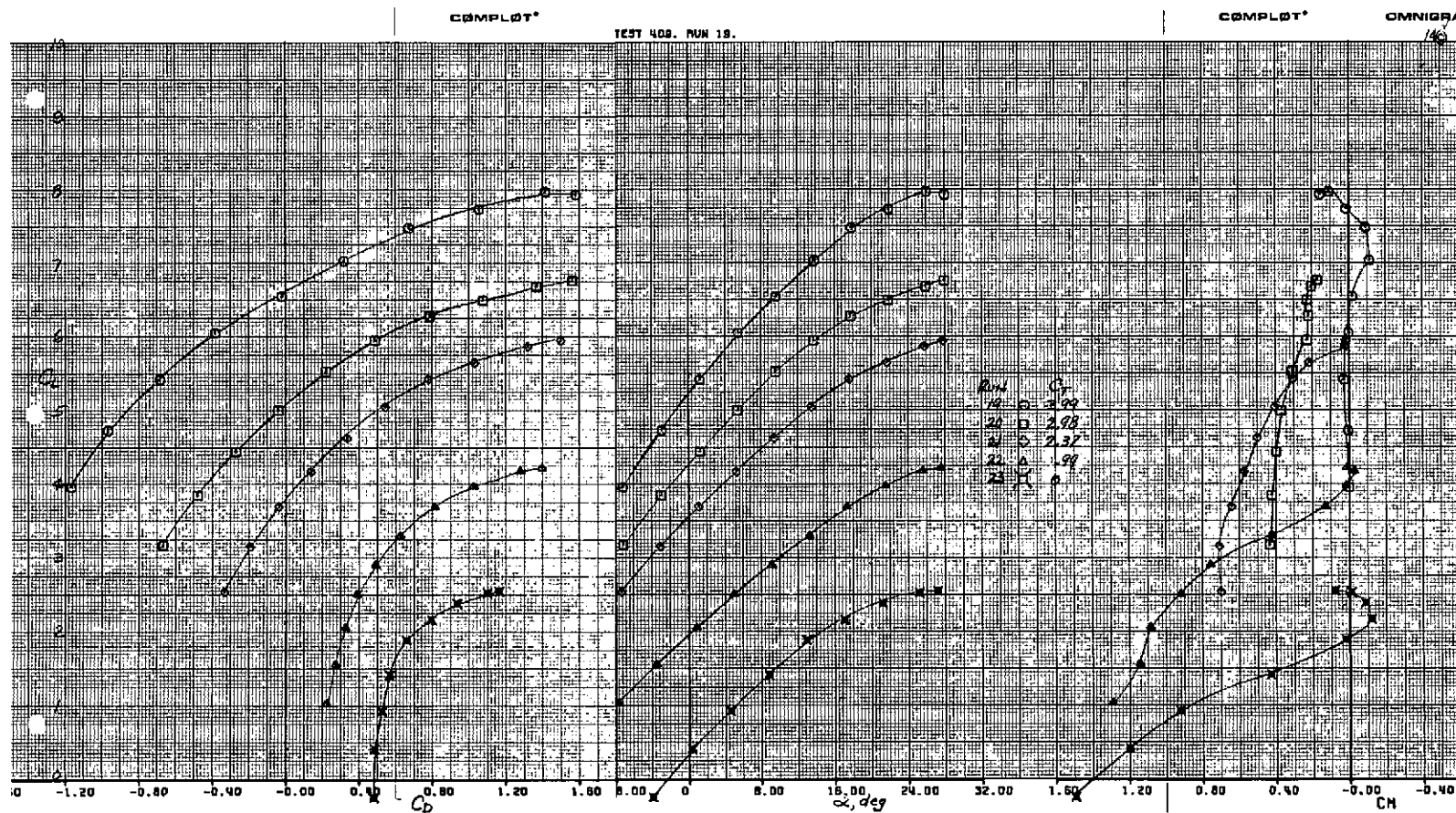
(a) $\delta_{sp} = 20^\circ$ ($n = .11$ to $.75$).

Figure 14.—Longitudinal characteristics of the model with full span flaps deflected and spoilers symmetrically deflected; $\delta_{f_1}/\delta_{f_2}/\delta_{f_3} = 15^\circ/35^\circ/55^\circ$, tail on, $i_t = 0^\circ$, $\delta_e = -25^\circ$.



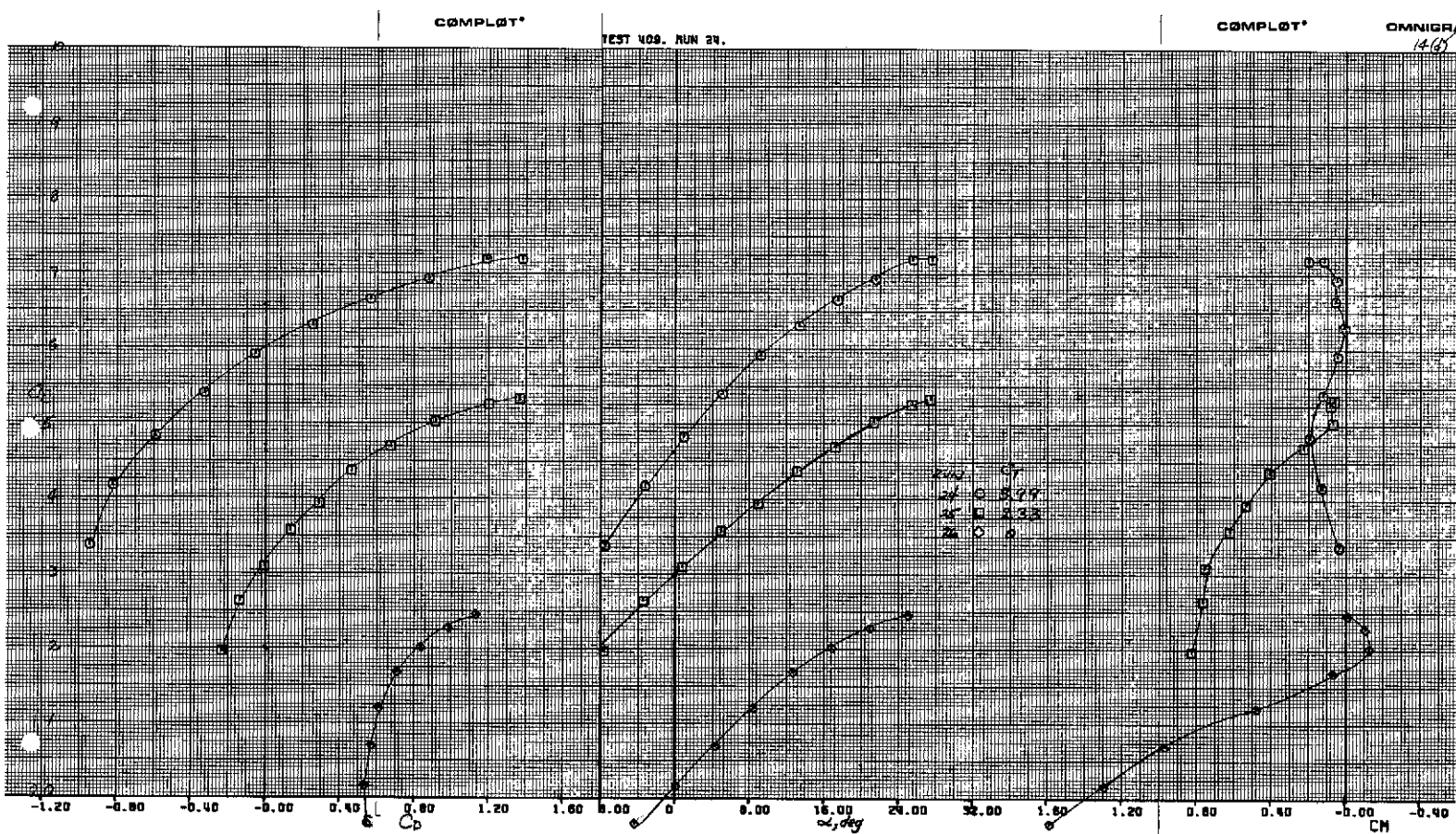
(b) $\delta_{sp} = 30^\circ$ ($\eta = .11$ to $.75$).

Figure 14.—Continued.



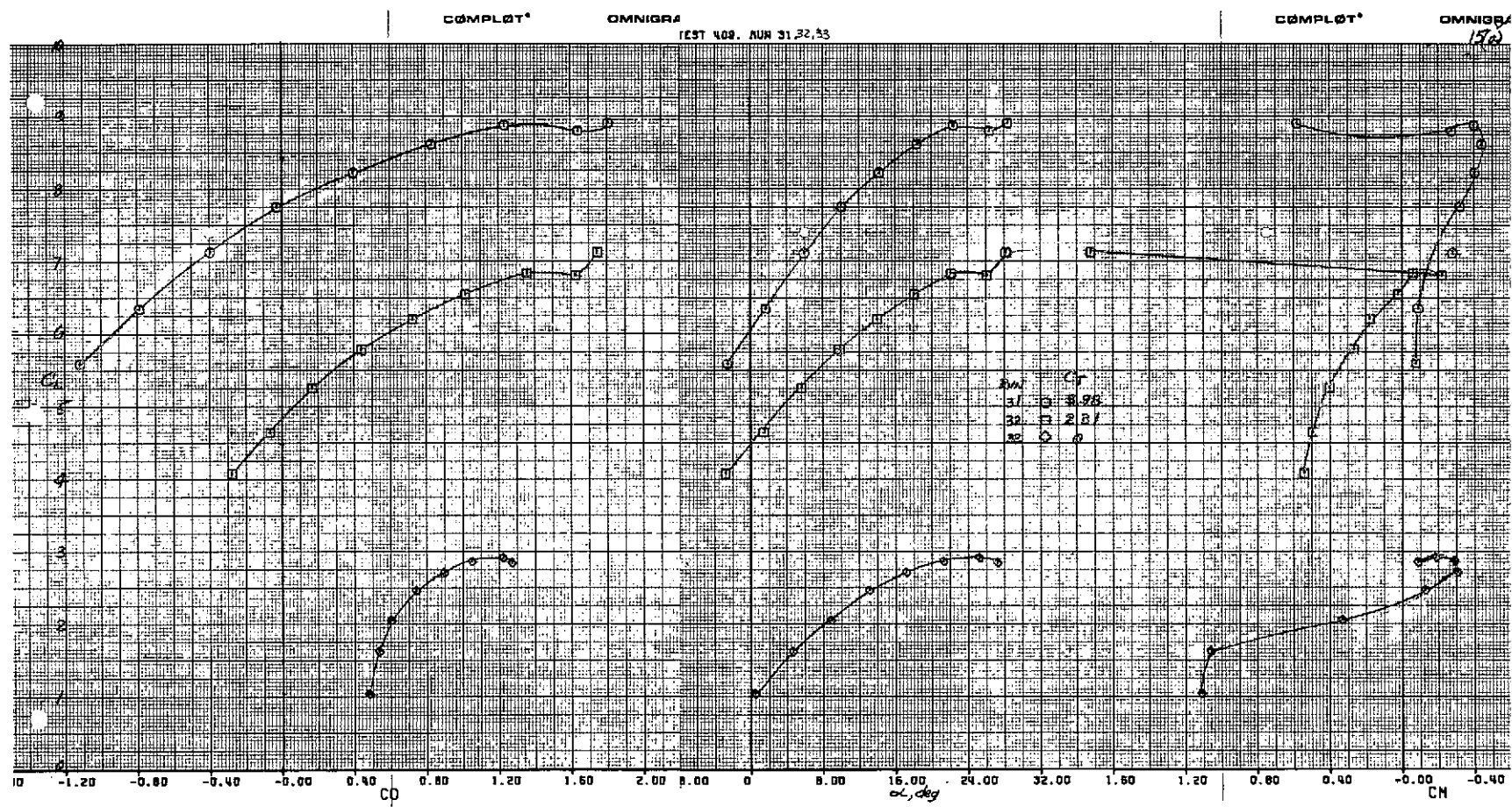
(c) $\delta_{sp} = 40^\circ$ ($n = .11$ to $.75$).

Figure 14.—Continued.



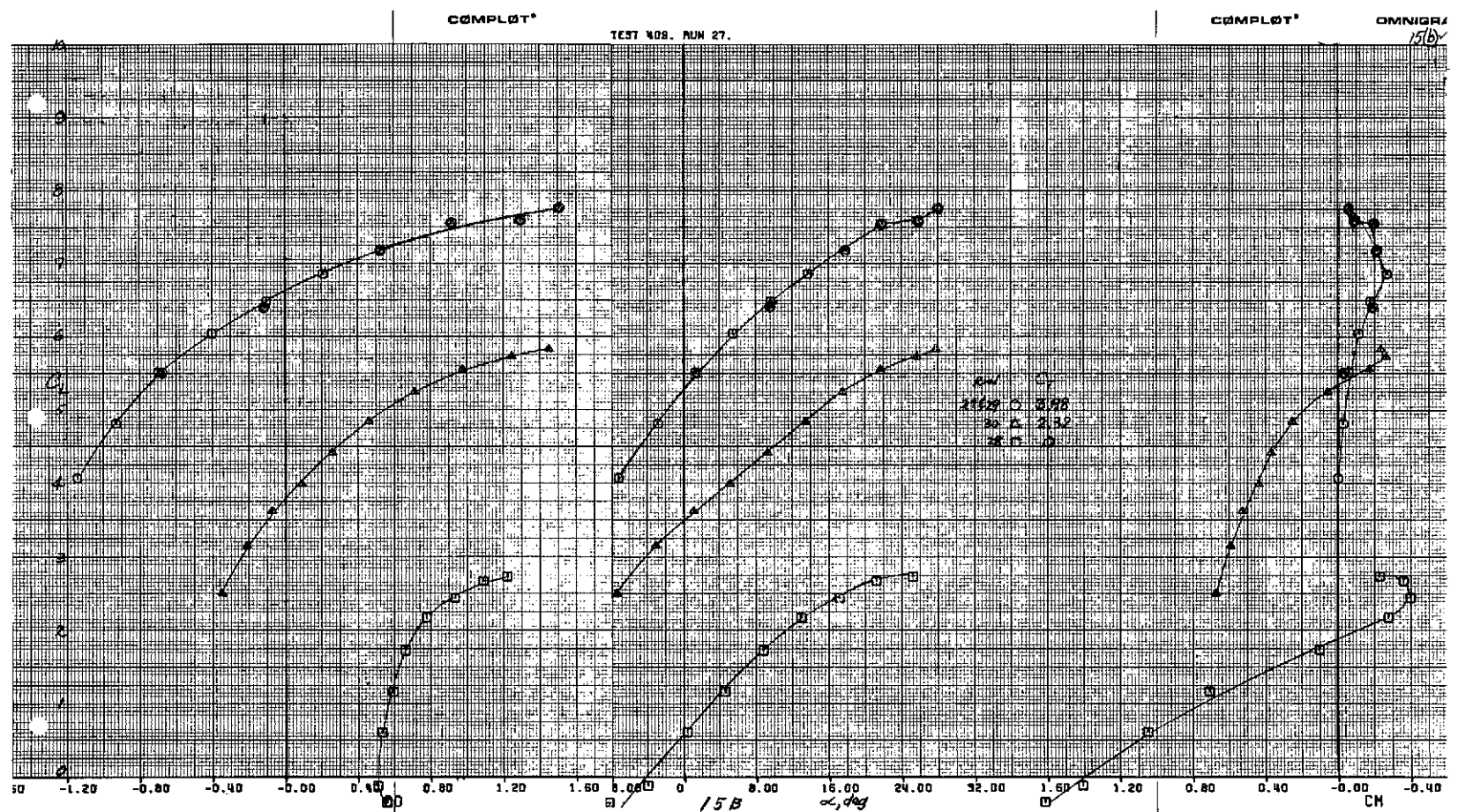
(d) $\delta_{sp} = 60^\circ$ ($\eta = .11$ to $.75$).

Figure 14.—Concluded.



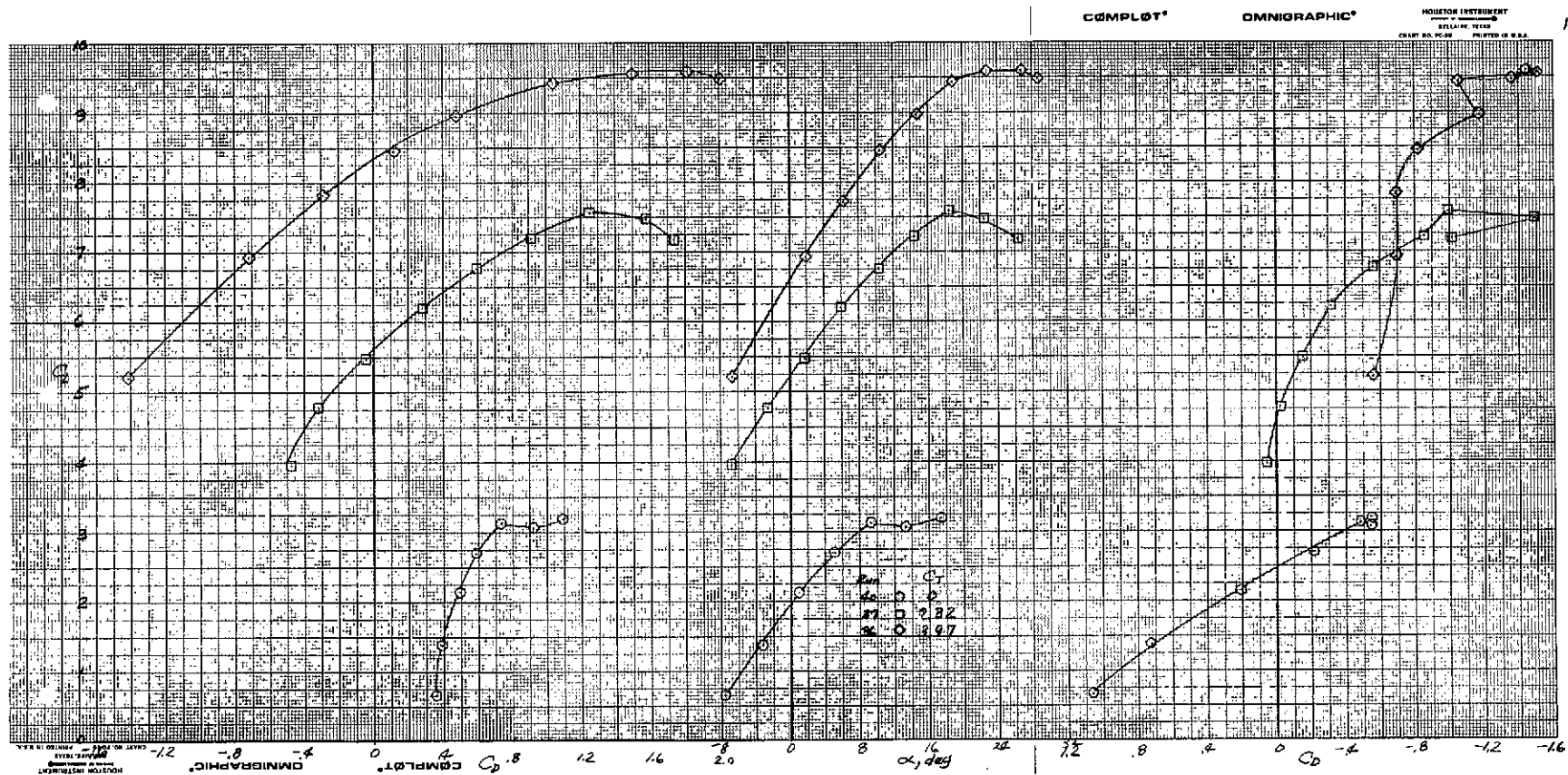
(a) $\delta_{sp} = 30^\circ$ ($\eta = .11$ to $.50$).

Figure 15.—Longitudinal characteristics of the model with full span flaps deflected and part span spoilers symmetrically deflected; $\delta_{f_1}/\delta_{f_2}/\delta_{f_3} = 15^\circ/35^\circ/55^\circ$, tail on, $i_t = 0^\circ$, $\delta_e = -25^\circ$.



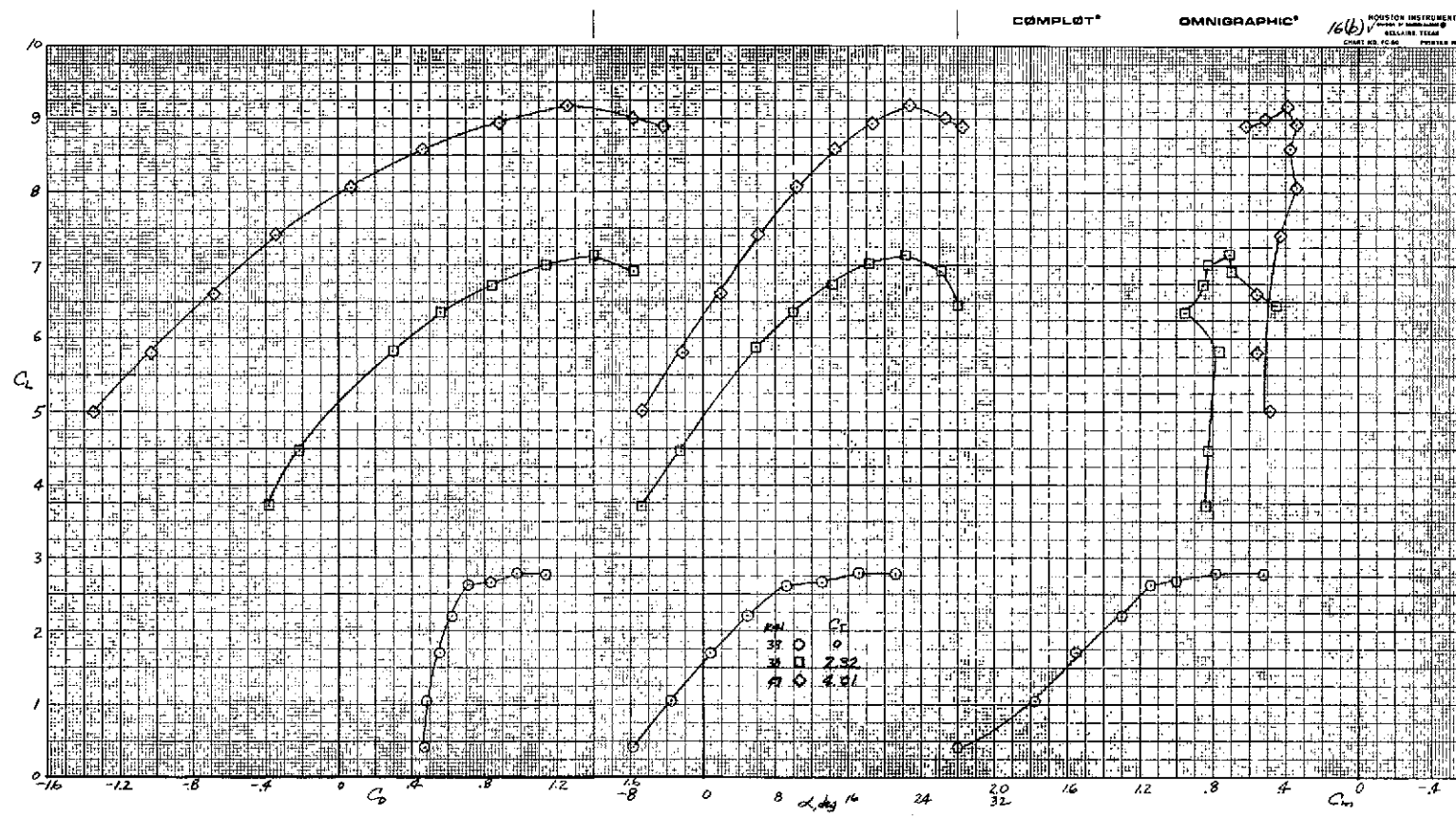
(b) $\delta_{sp} = 60^\circ$ ($\eta = .11$ to $.50$).

Figure 15.—Concluded.



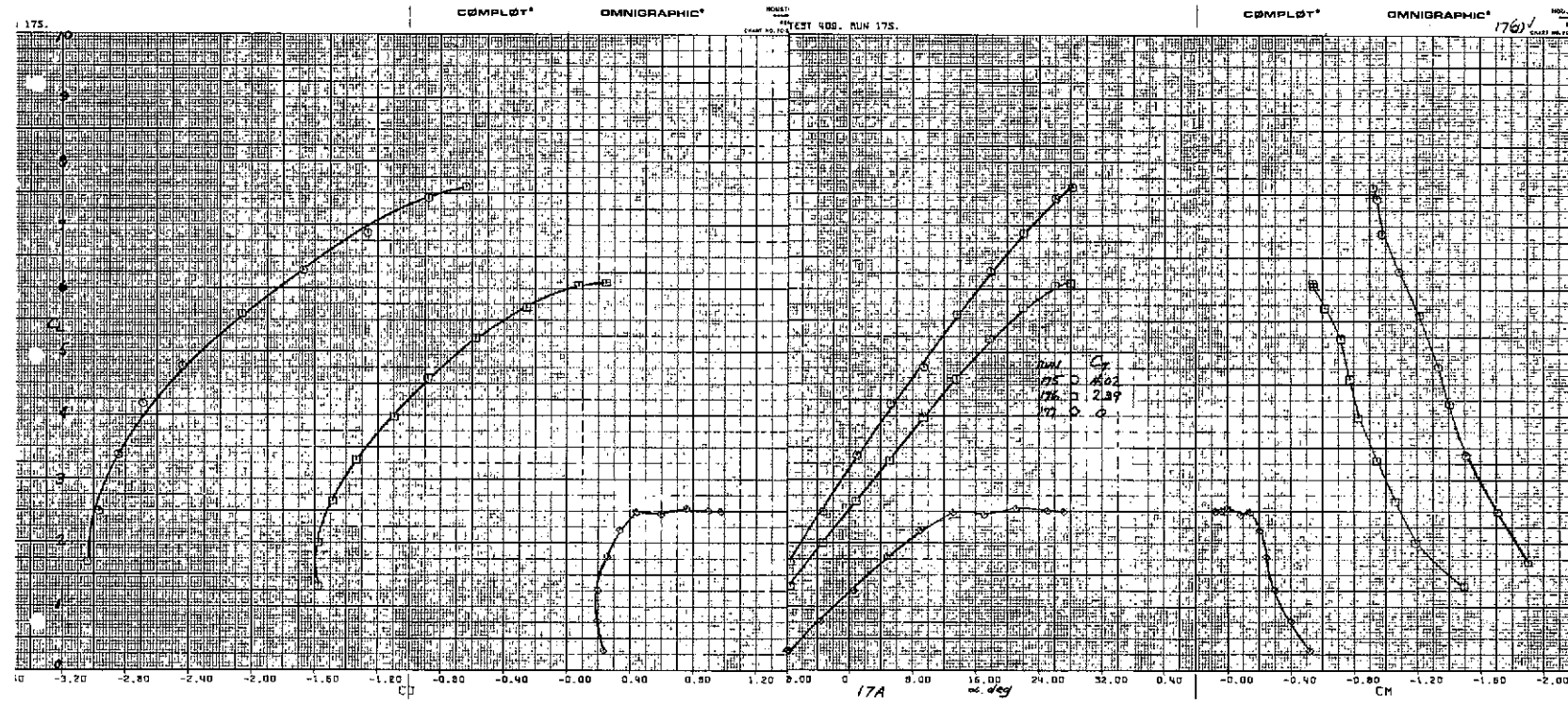
(a) $i_t = 7^\circ$.

Figure 16.—Longitudinal characteristics of the model with full span flaps deflected at two tail incidences; $\delta_{f_1}/\delta_{f_2}/\delta_{f_3} = 15^\circ/35^\circ/55^\circ$, tail on, $\delta_e = -25^\circ$.



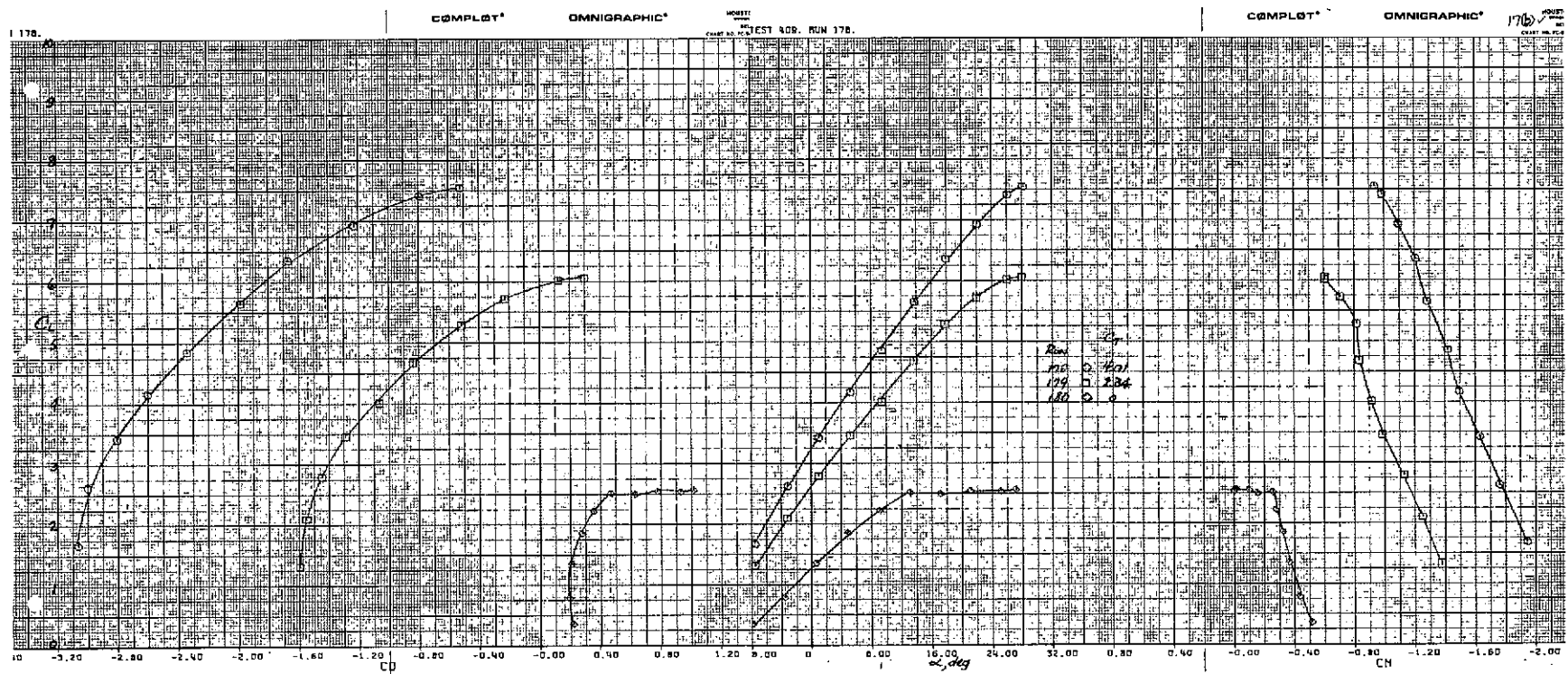
(b) $i_t = -5^\circ$.

Figure 16.—Concluded.



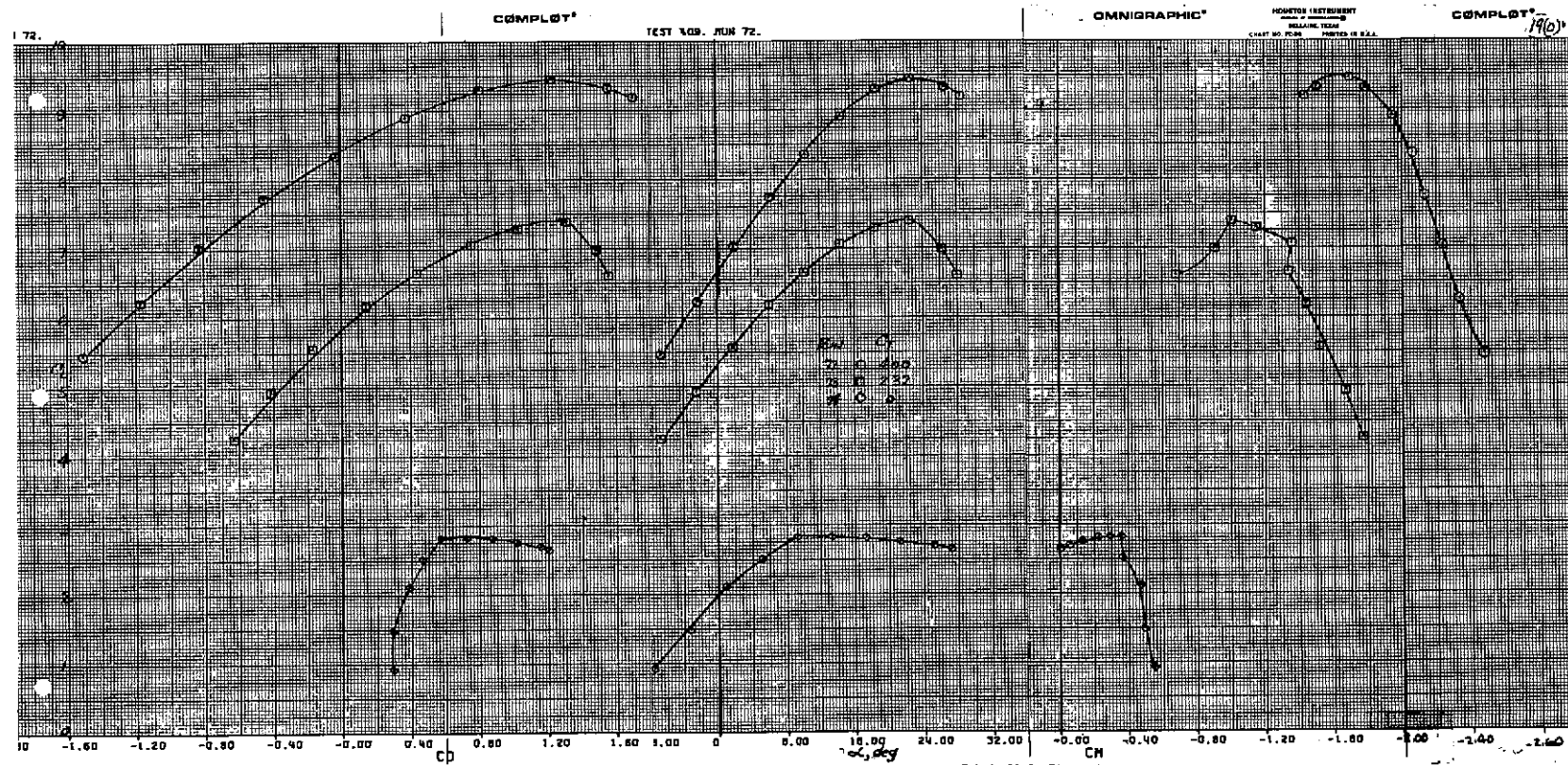
(a) $\delta_{ail} = 5^\circ$.

Figure 17.—Longitudinal characteristics of the model with part span flaps and ailerons symmetrically deflected; $\delta_{f_1}/\delta_{f_2}/\delta_{f_3} = 0^\circ/20^\circ/30^\circ$, tail off.



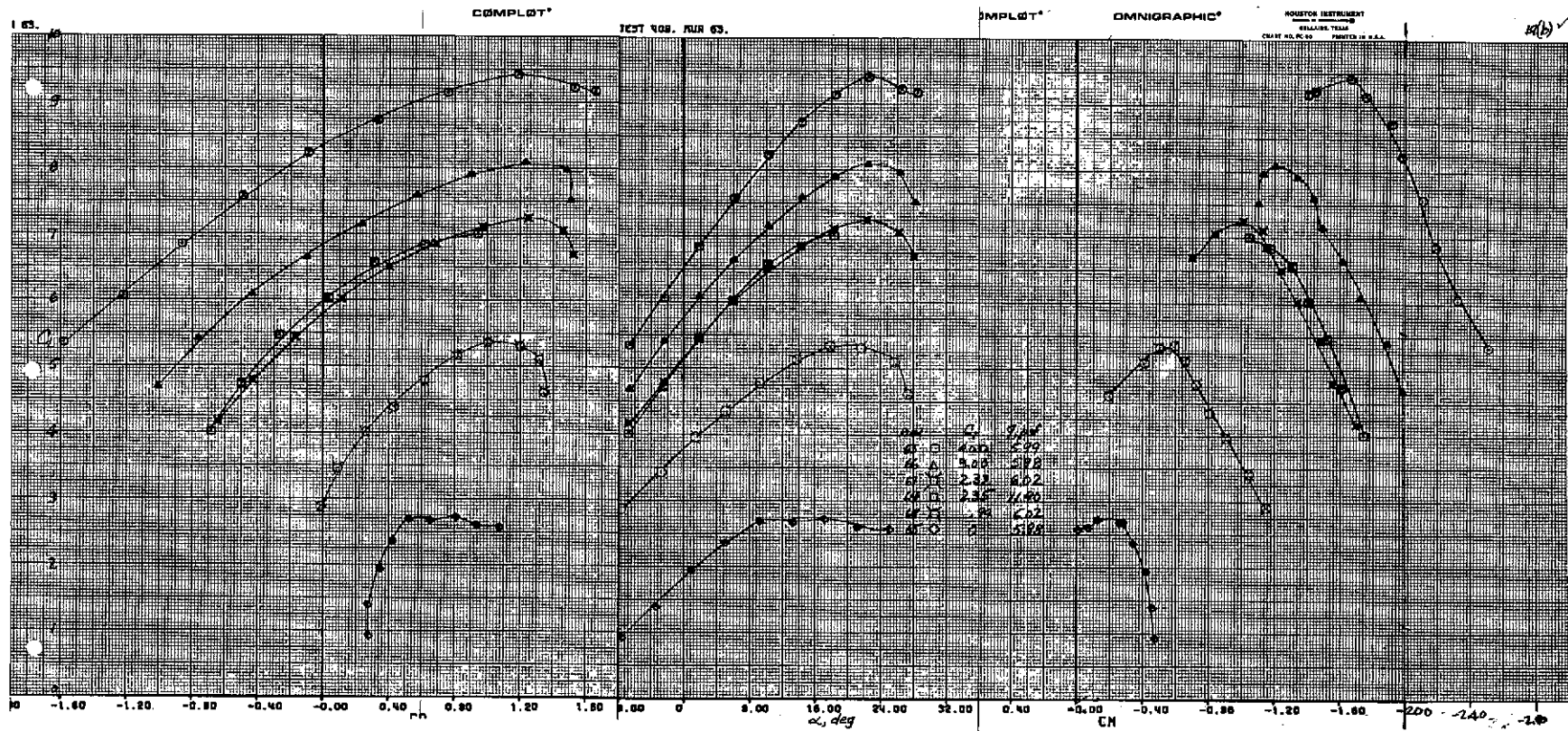
(b) $\delta_{a11} = 20^\circ$.

Figure 17.—Concluded.



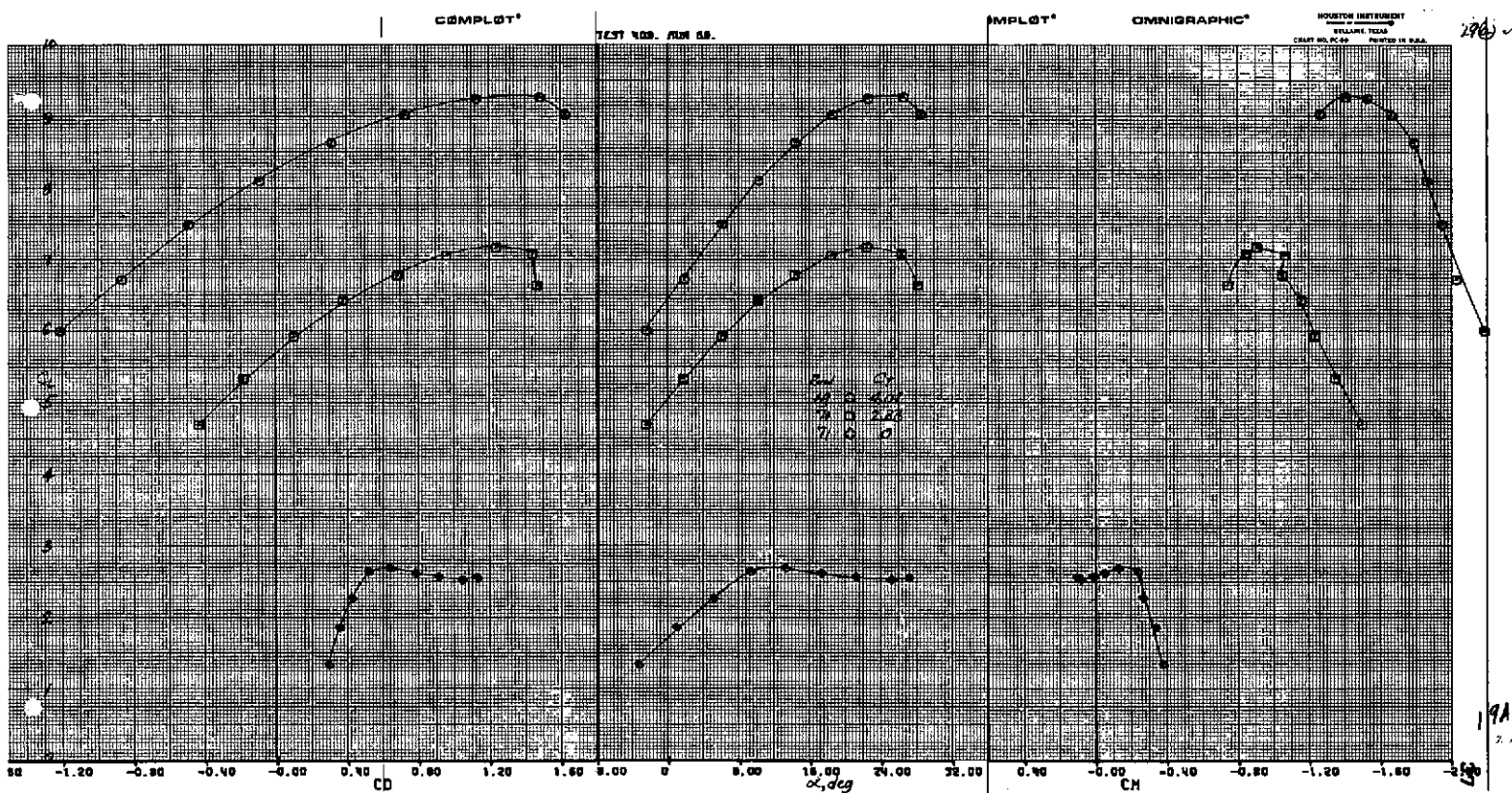
$$(a) \delta_{f_1}/\delta_{f_2}/\delta_{f_3} = 0^\circ/20^\circ/20^\circ.$$

Figure 18.—Longitudinal characteristics of the model with part span flaps and ailerons symmetrically deflected; tail on, $i_t = 0^\circ$, $\delta_e = -25^\circ$, $\delta_{ail} = 5^\circ$.



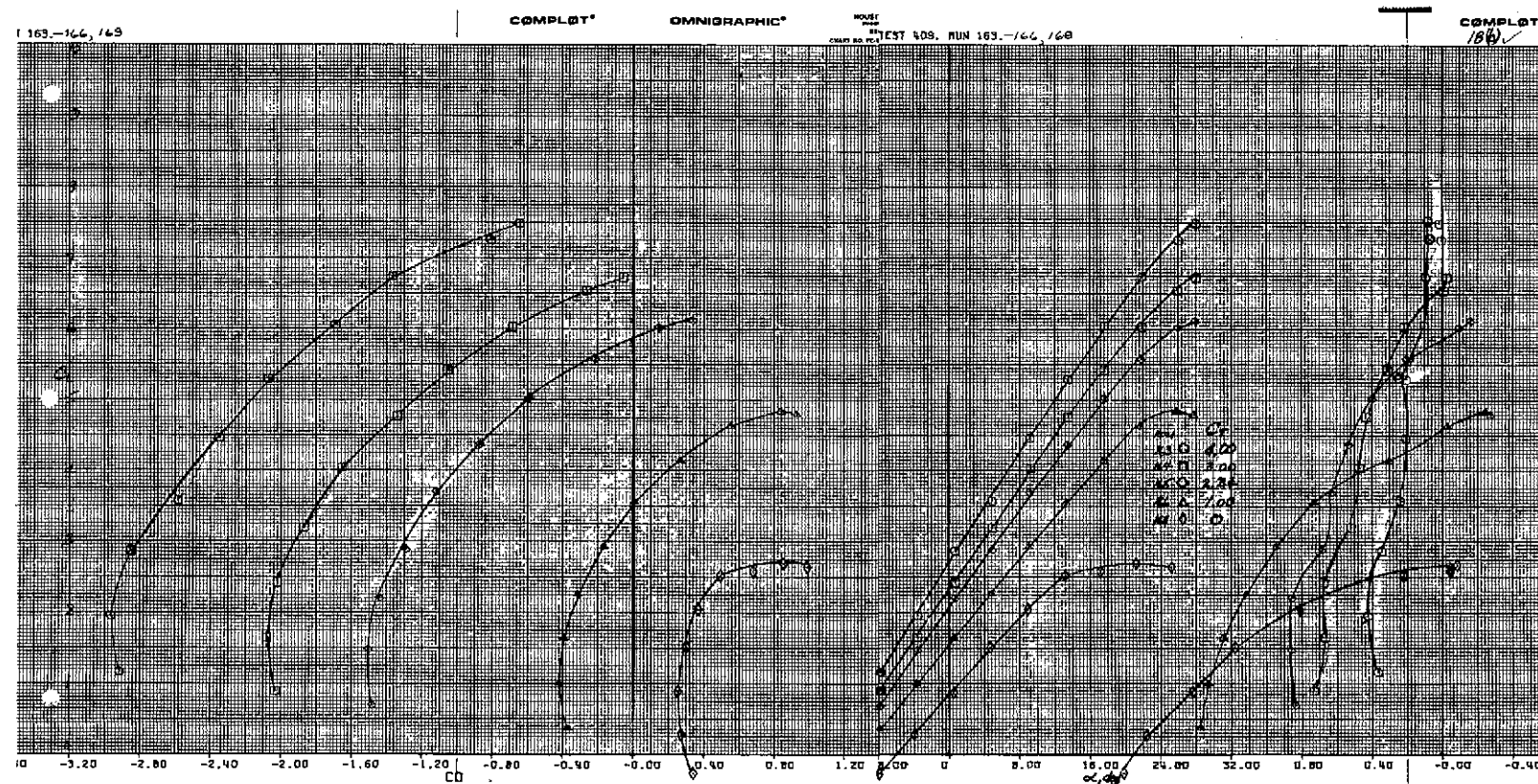
$$(b) \delta_{f_1} / \delta_{f_2} / \delta_{f_3} = 0^\circ / 20^\circ / 30^\circ.$$

Figure 18.—Concluded.



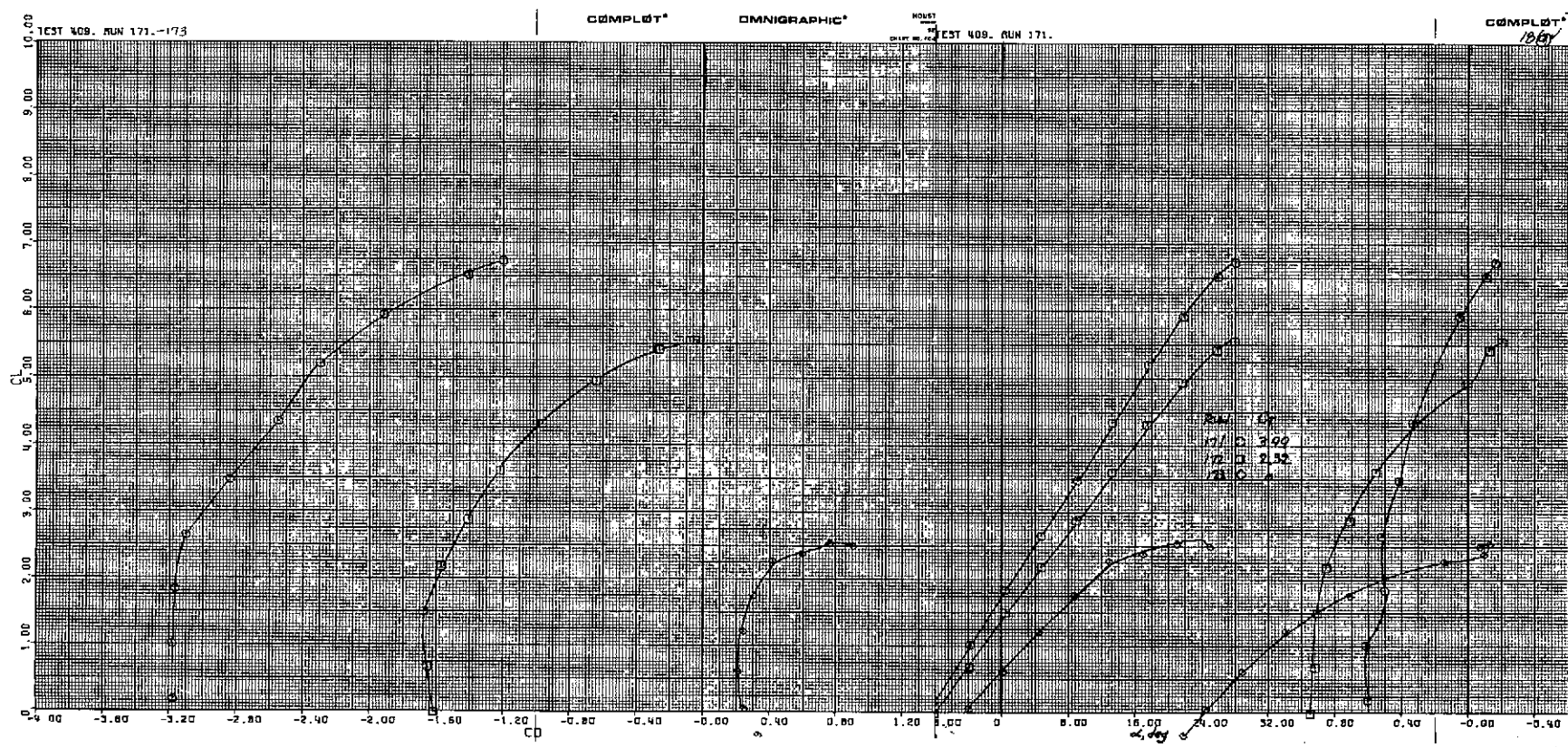
$$(a) \delta_{ail} = 5^\circ.$$

Figure 19.—Longitudinal characteristics of the model with part span flaps and ailerons symmetrically deflected; $\delta_{f_1}/\delta_{f_2}/\delta_{f_3} = 15^\circ/35^\circ/55^\circ$, tail off.



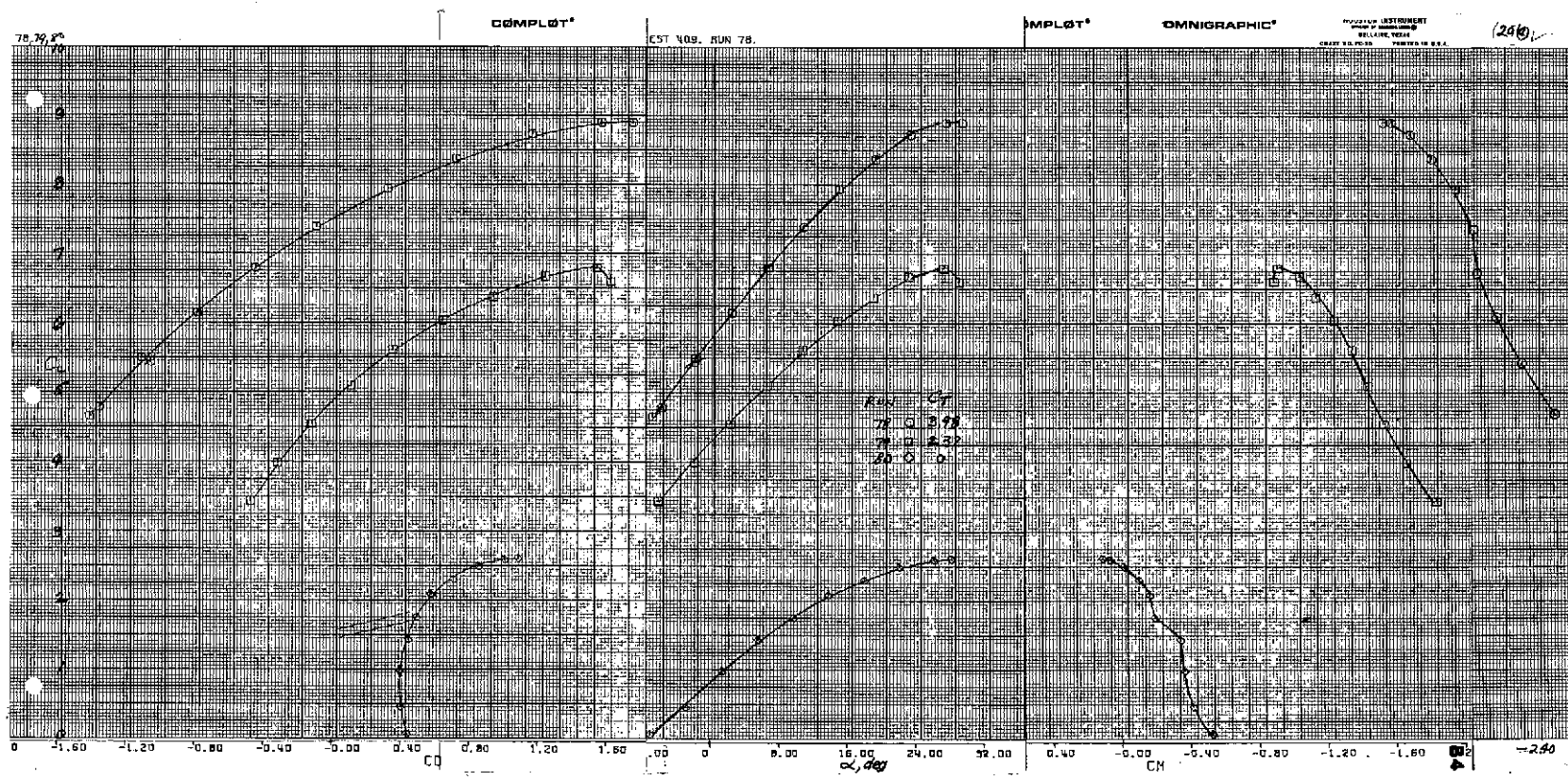
(b) $\delta_{ail} = 20^\circ$.

Figure 19.—Continued.



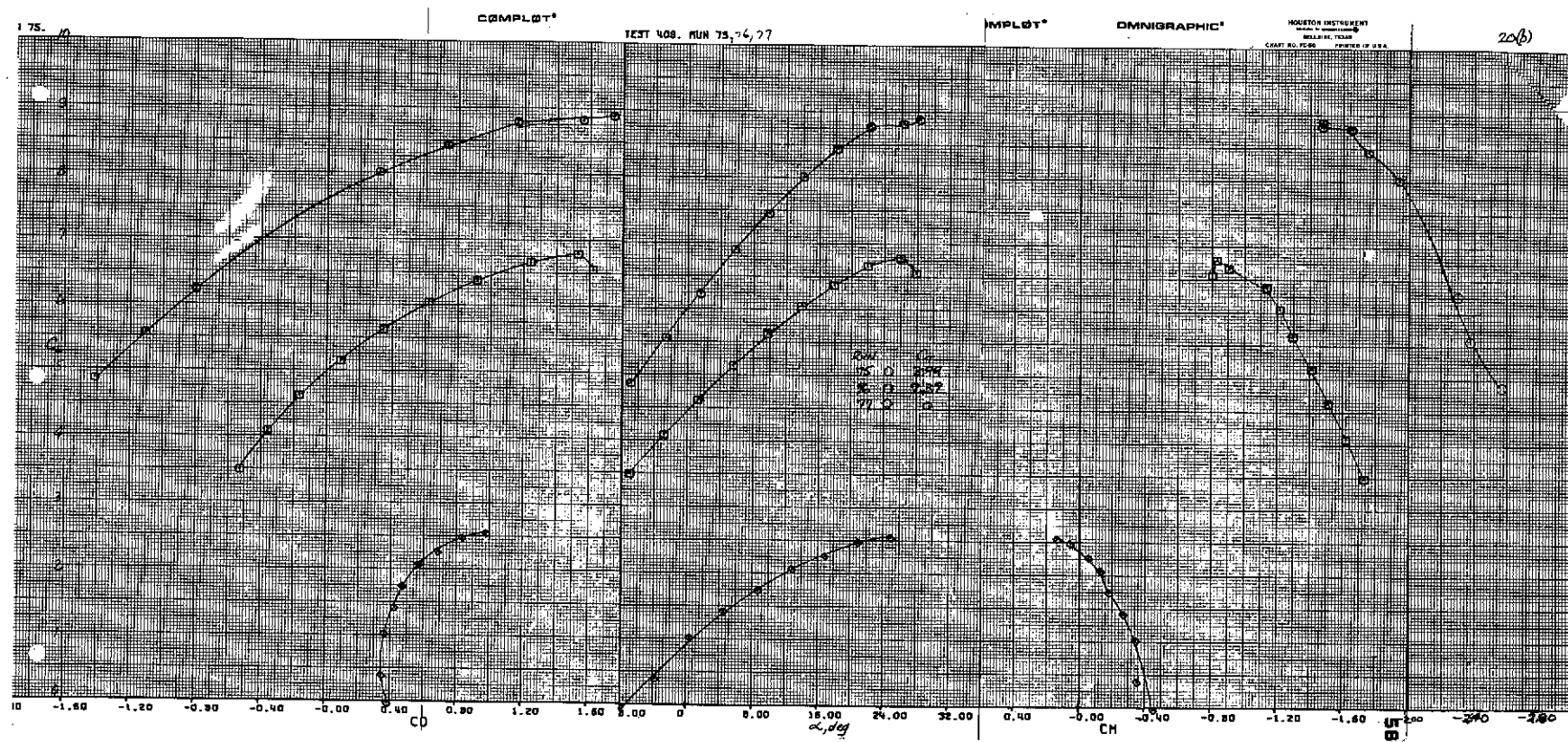
(c) $\delta_{ail} = 35^\circ$.

Figure 19.—Concluded.



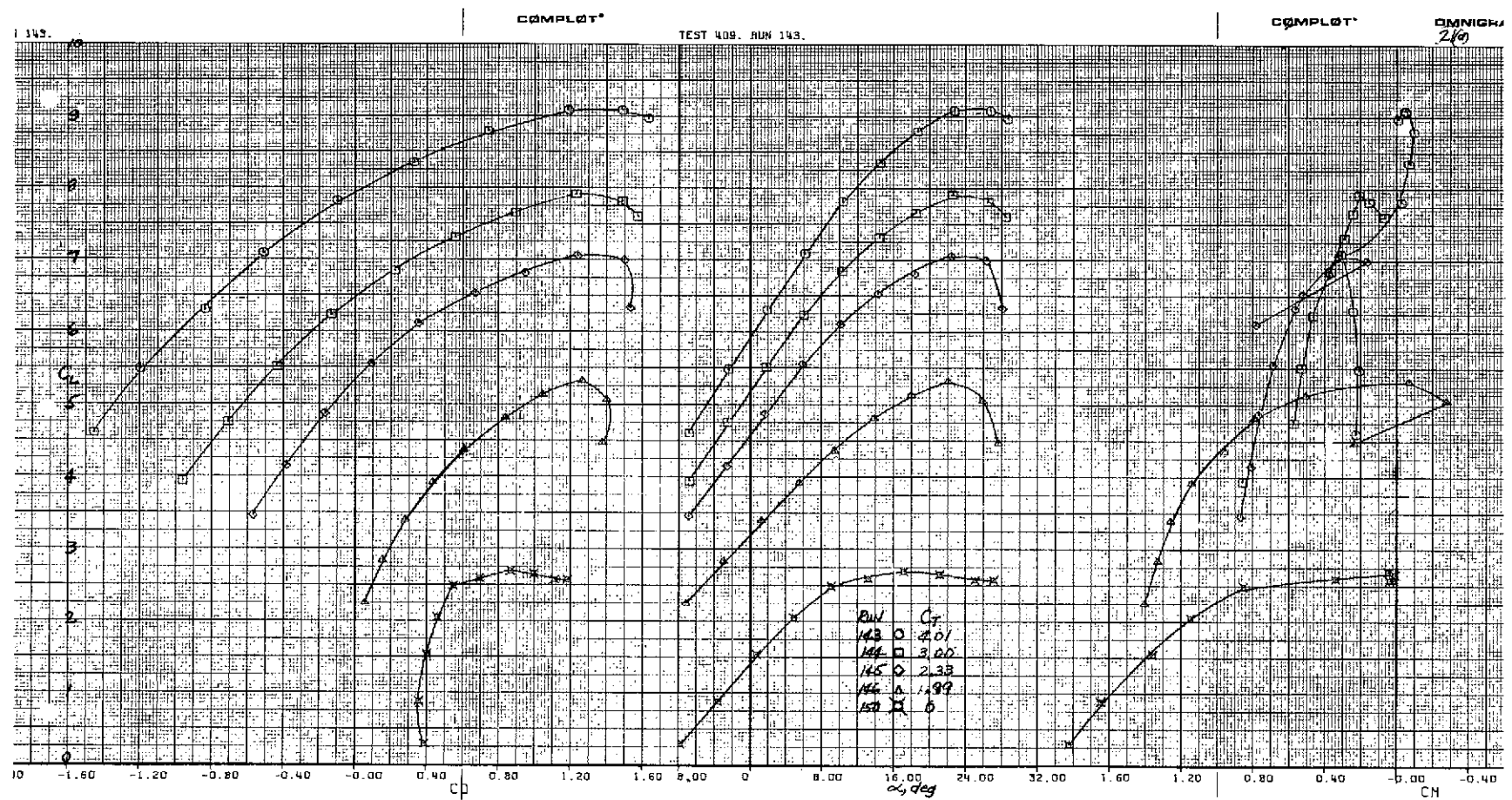
$$(a) \delta_{ail} = 20^\circ.$$

Figure 20.—Longitudinal characteristics of the model with part span flaps and with ailerons and spoilers symmetrically deflected; $\delta_{f_1}/\delta_{f_2}/\delta_{f_3} = 15^\circ/35^\circ/55^\circ$, tail off, $\delta_{sp} = 30^\circ$.



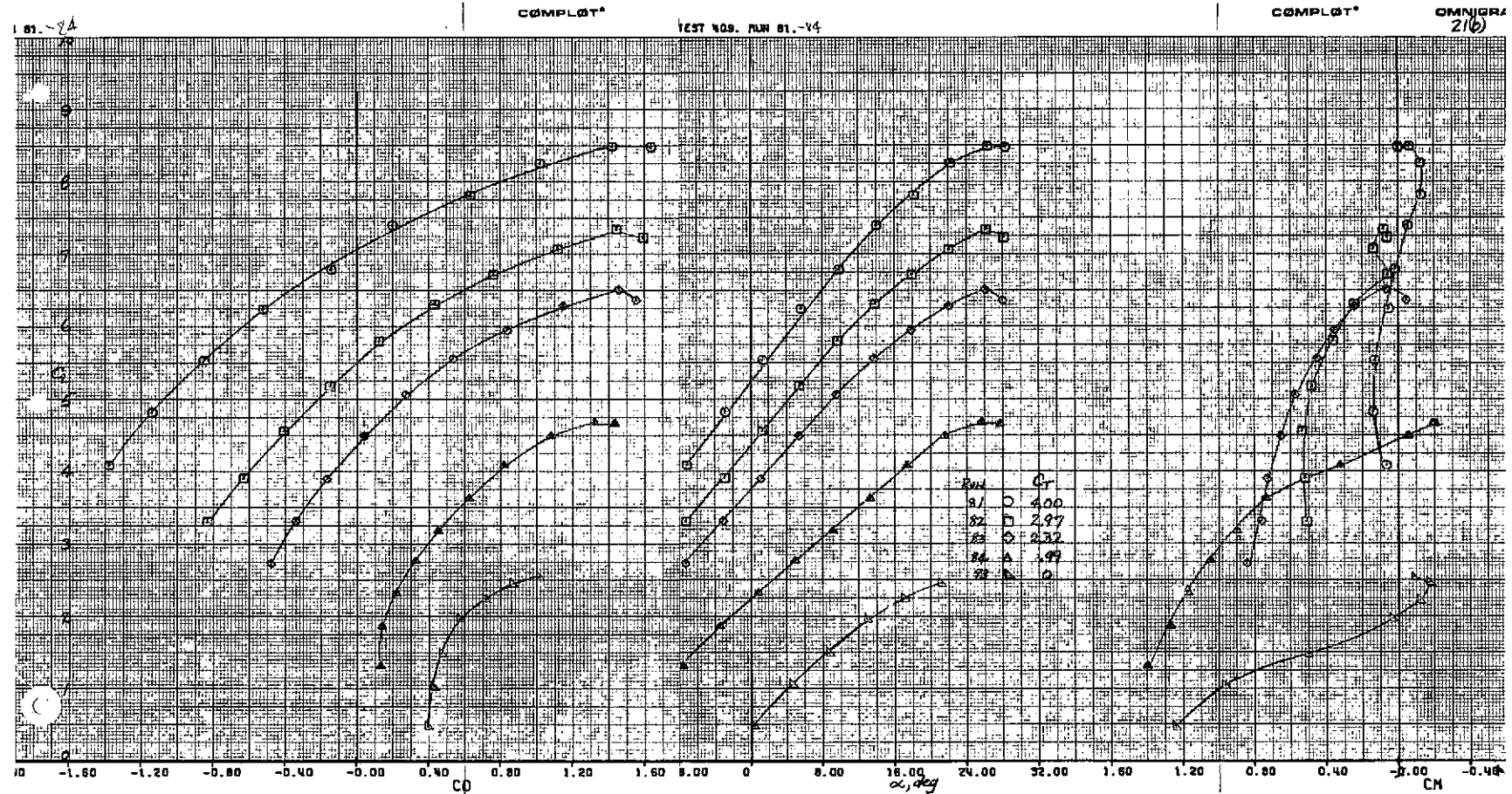
$$(b) \delta_{ail} = 35^\circ.$$

Figure 20.—Concluded.



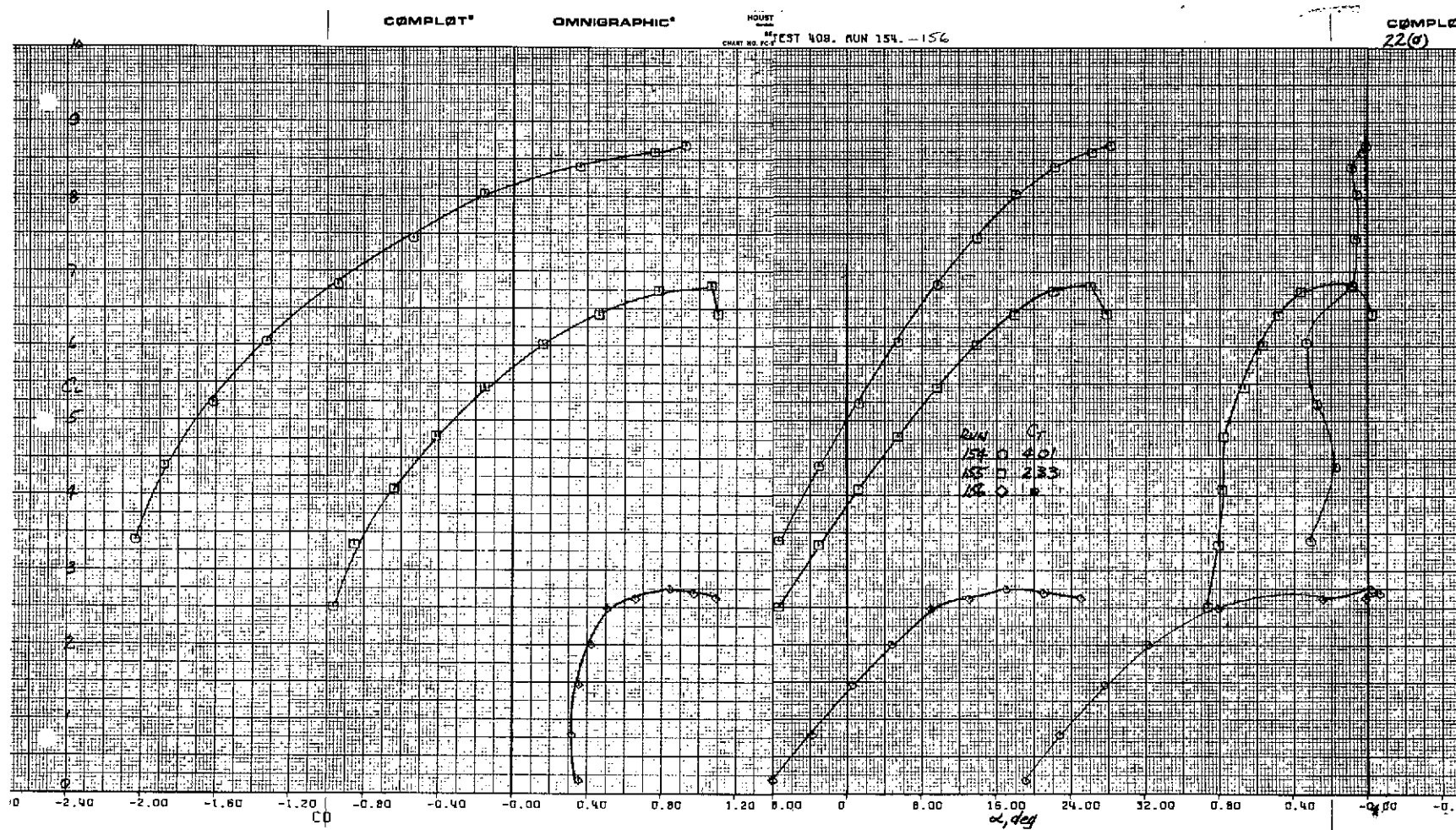
(a) $\delta_{ail} = 23^\circ$, $\delta_{sp} = 0^\circ$.

Figure 21.—Longitudinal characteristics of the model with part span flaps and with ailerons and spoilers symmetrically deflected; $\delta_{f_1}/\delta_{f_2}/\delta_{f_3} = 15^\circ/35^\circ/55^\circ$, tail on, $i_t = 0^\circ$, $\delta_e = -25^\circ$.



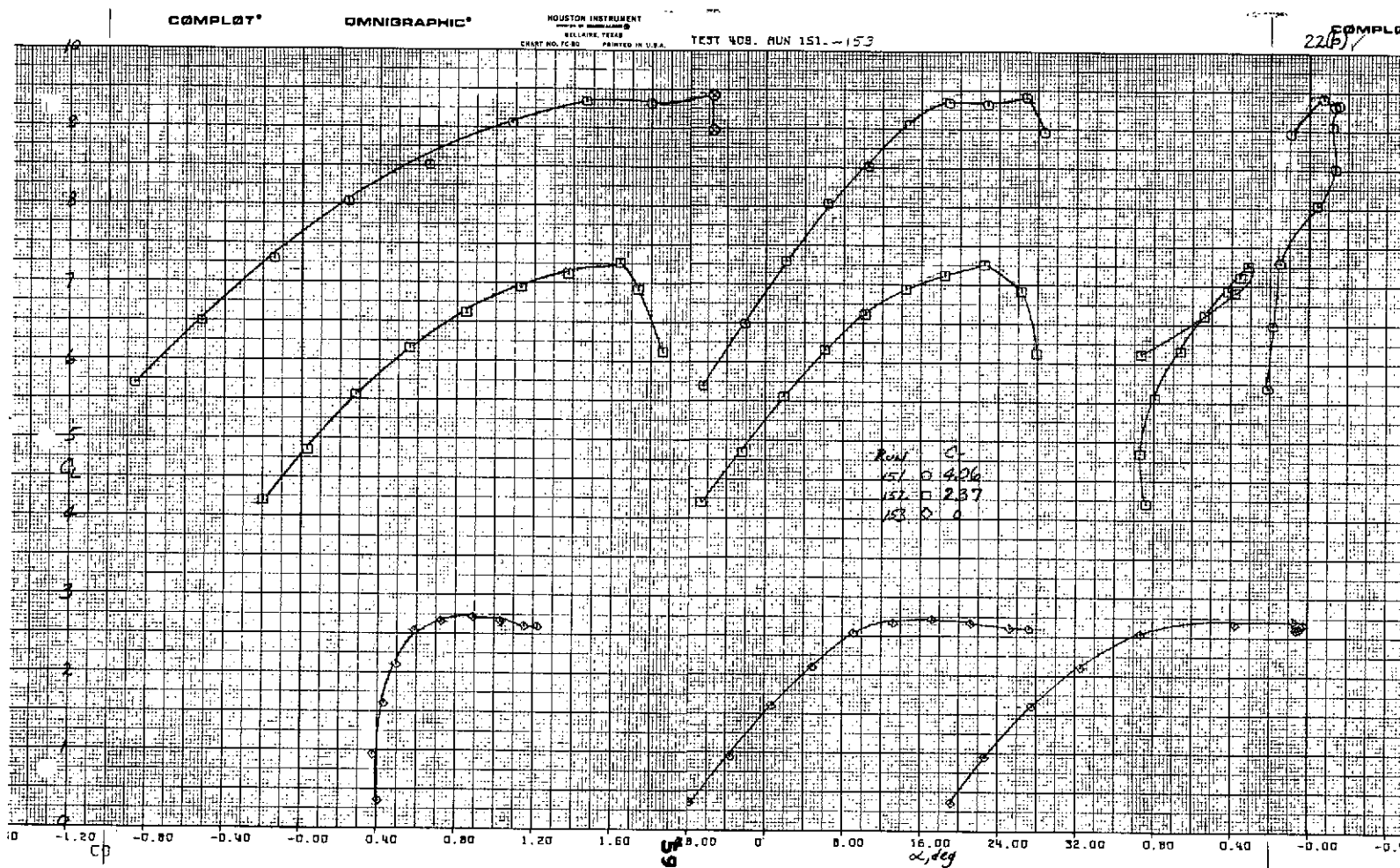
(b) $\delta_{ail} = 20^\circ, \delta_{sp} = 30^\circ$

Figure 21.—Concluded.



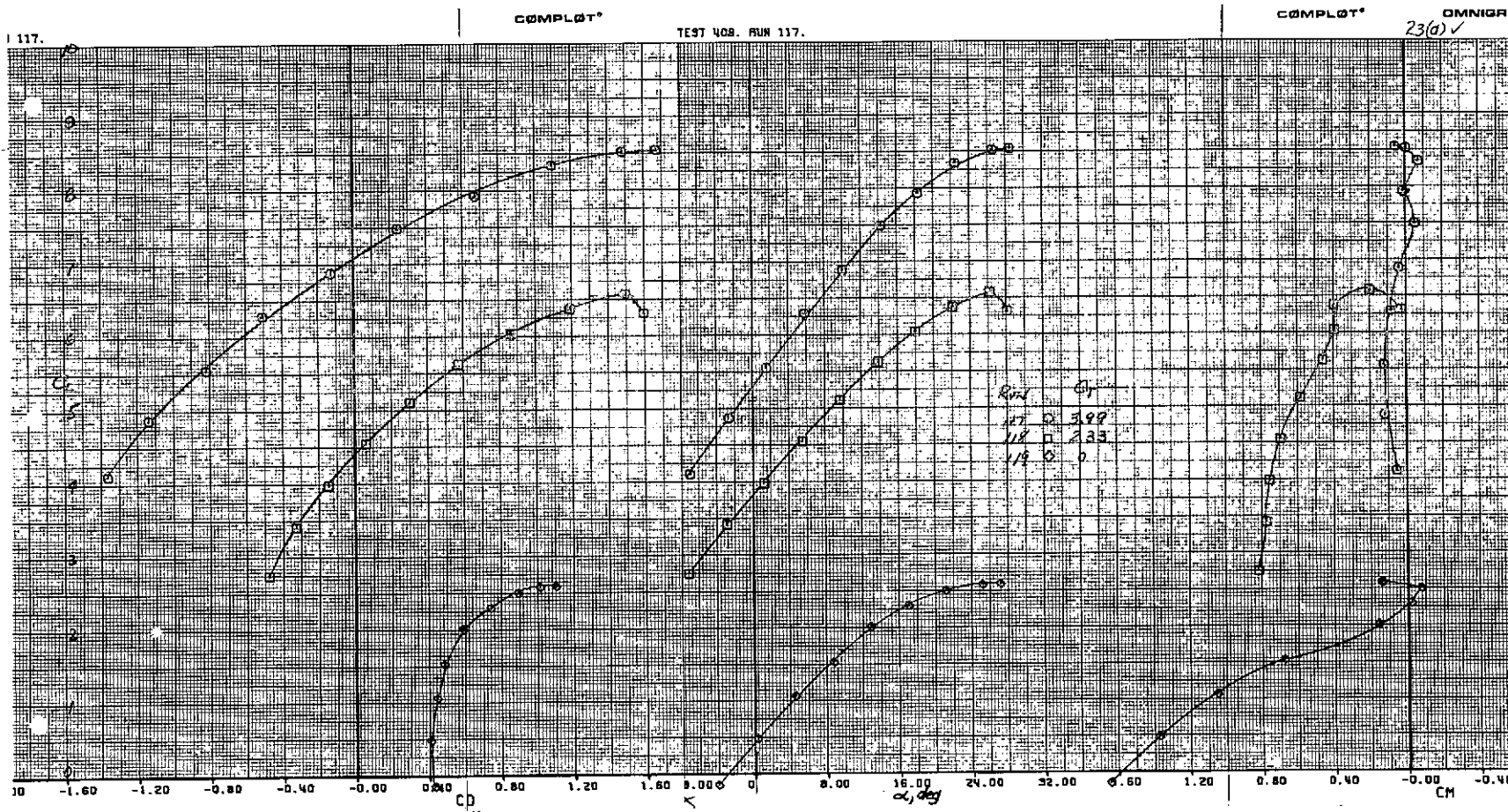
$$(a) \quad \delta_{f_1}/\delta_{f_2}/\delta_{f_3} = 15^\circ/35^\circ/45^\circ.$$

Figure 22.—Longitudinal characteristics of the model with the third flap deflected; part span flaps, tail on, $i_t = 0^\circ$, $\delta_e = -25^\circ$, $\delta_{ail} = 23^\circ$.



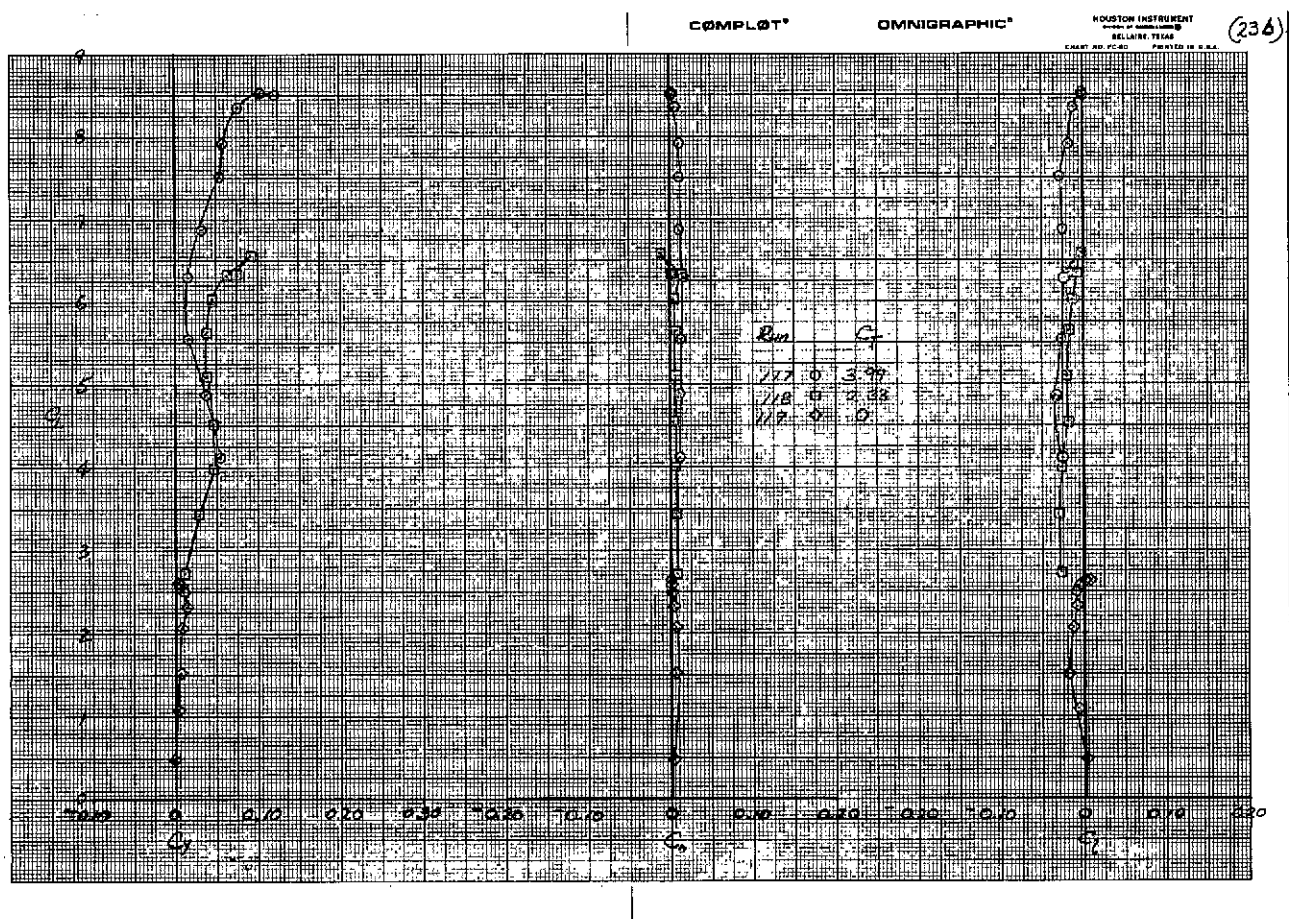
$$(b) \delta_{f_1} / \delta_{f_2} / \delta_{f_3} = 15^\circ / 35^\circ / 65^\circ.$$

Figure 22.—Concluded.



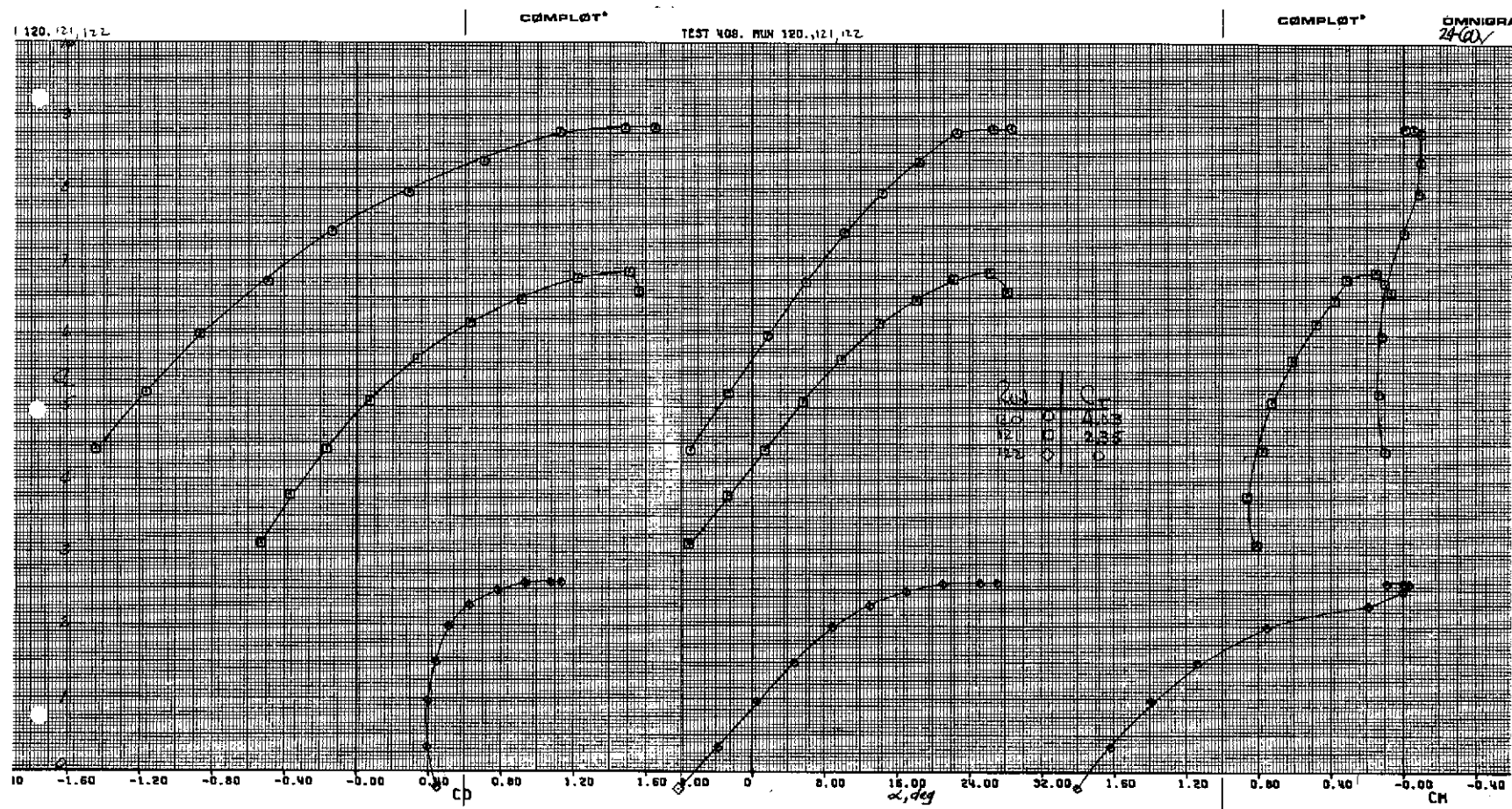
(a) Longitudinal characteristics of the model.

Figure 23.—Aerodynamic characteristics of the model with asymmetric aileron deflections; part span flaps, $\delta_{f_1}/\delta_{f_2}/\delta_{f_3} = 15^\circ/35^\circ/55^\circ$, tail on, $i_t = 0^\circ$, $\delta_e = -25^\circ$, $\delta_{ail} = 20^\circ/35^\circ$.



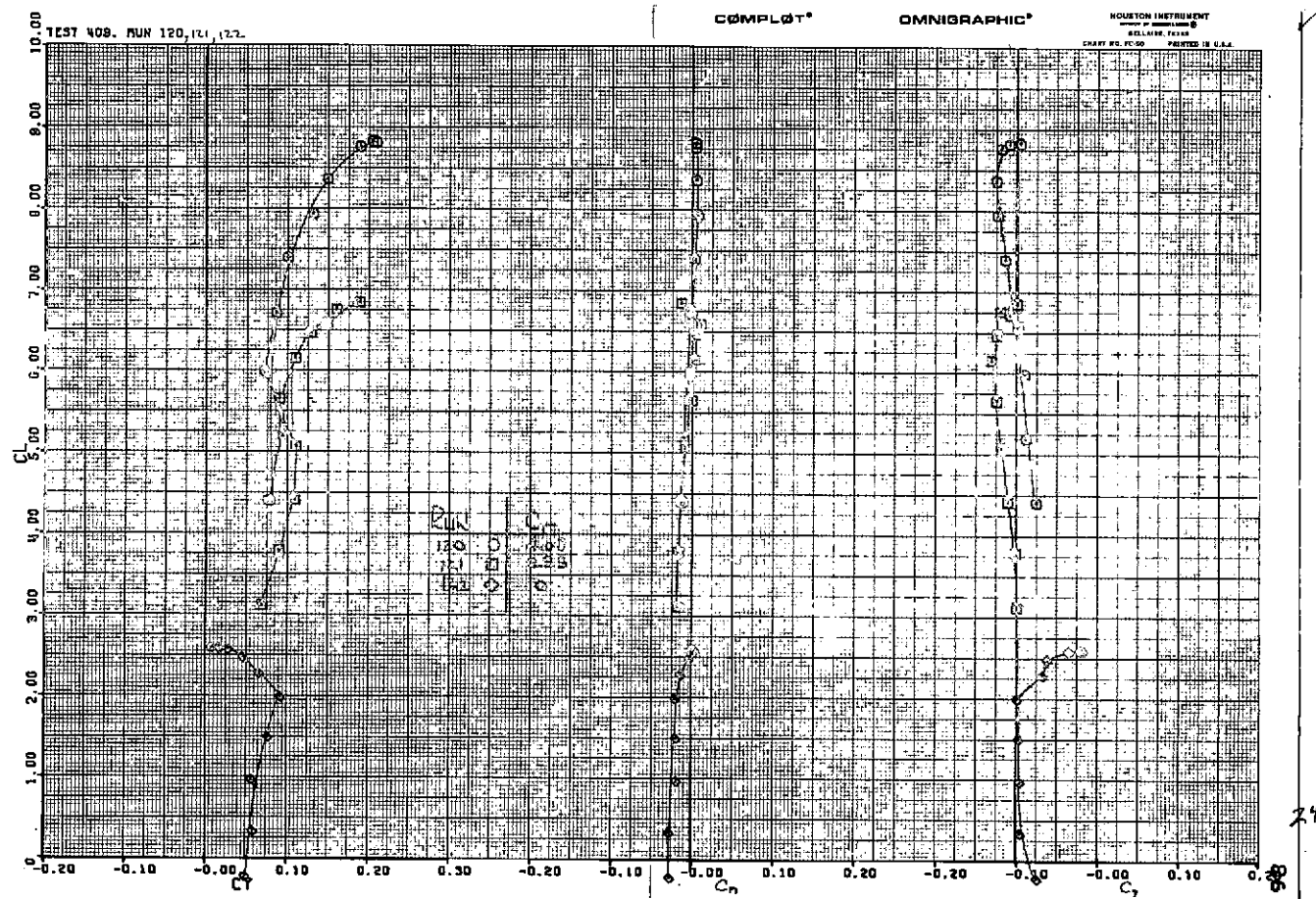
(b) Lateral characteristics of the model.

Figure 23.—Concluded.



(a) Longitudinal characteristics of the model, $\delta_{sp} = 30^\circ/0^\circ$.

Figure 24.—Aerodynamic characteristics of the model with asymmetric spoiler deflections; part span flaps, $\delta_{f_1}/\delta_{f_2}/\delta_{f_3} = 15^\circ/35^\circ/55^\circ$, tail on, $i_t = 0^\circ$, $\delta_e = -25^\circ$.



(b) Lateral characteristics of the model, $\delta_{sp} = 30^\circ/0^\circ$.

Figure 24.—Continued.

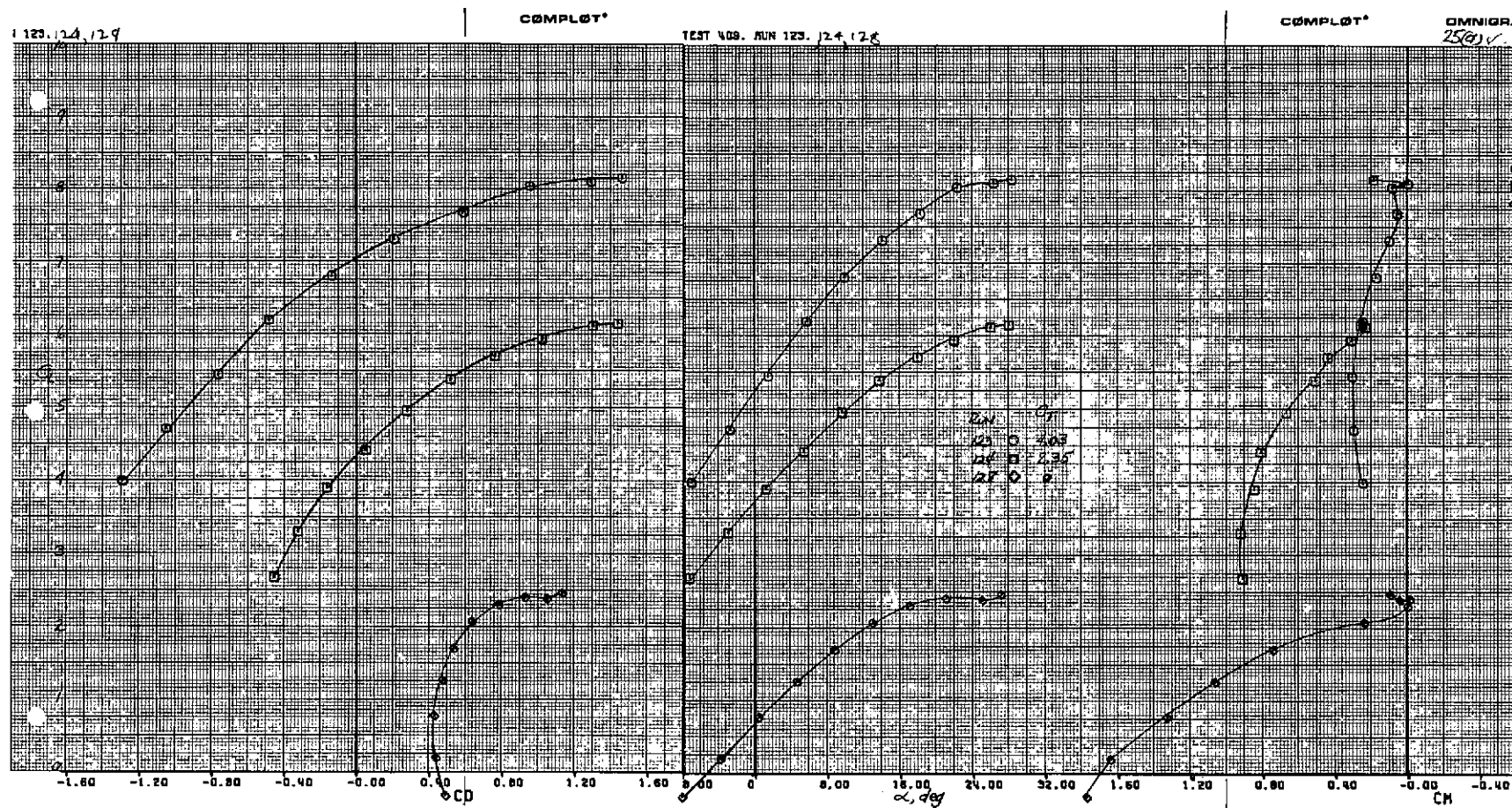


Figure 25.—Aerodynamic characteristics of the model with asymmetric spoiler deflections; part span flaps, $\delta_{f_1}/\delta_{f_2}/\delta_{f_3} = 15^\circ/35^\circ/55^\circ$, tail on, $i_t = 0^\circ$, $\delta_e = -25^\circ$.

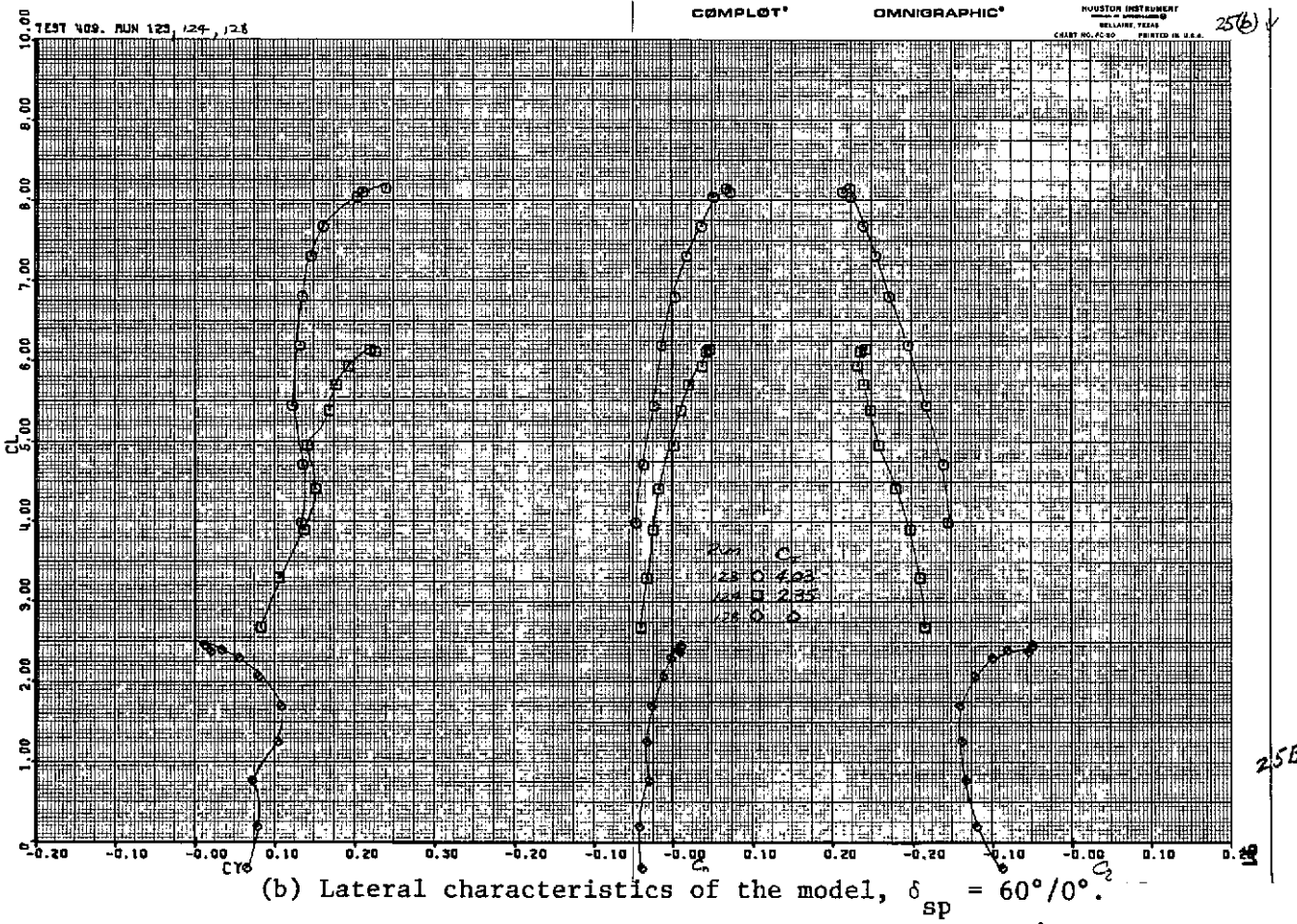
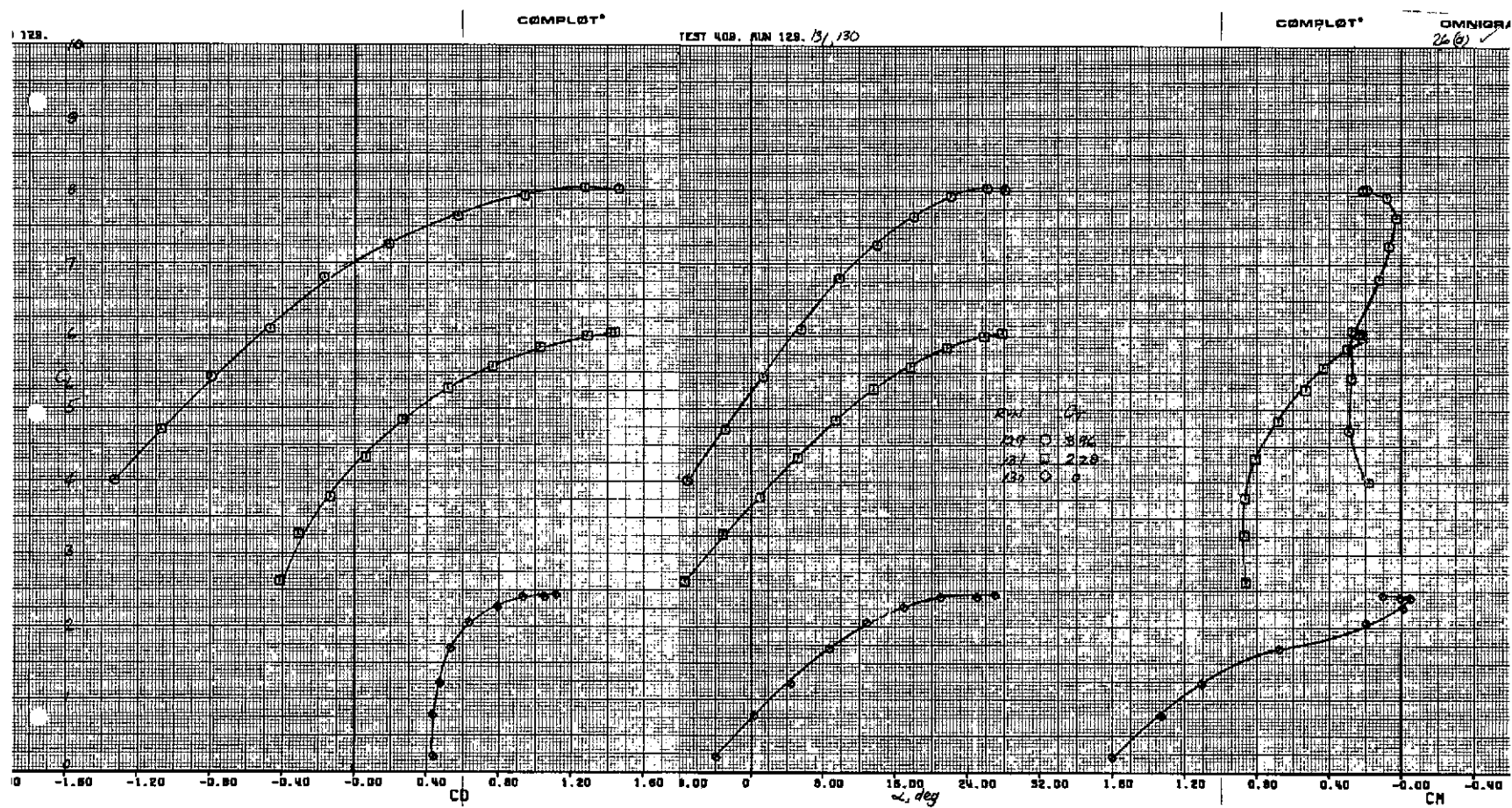
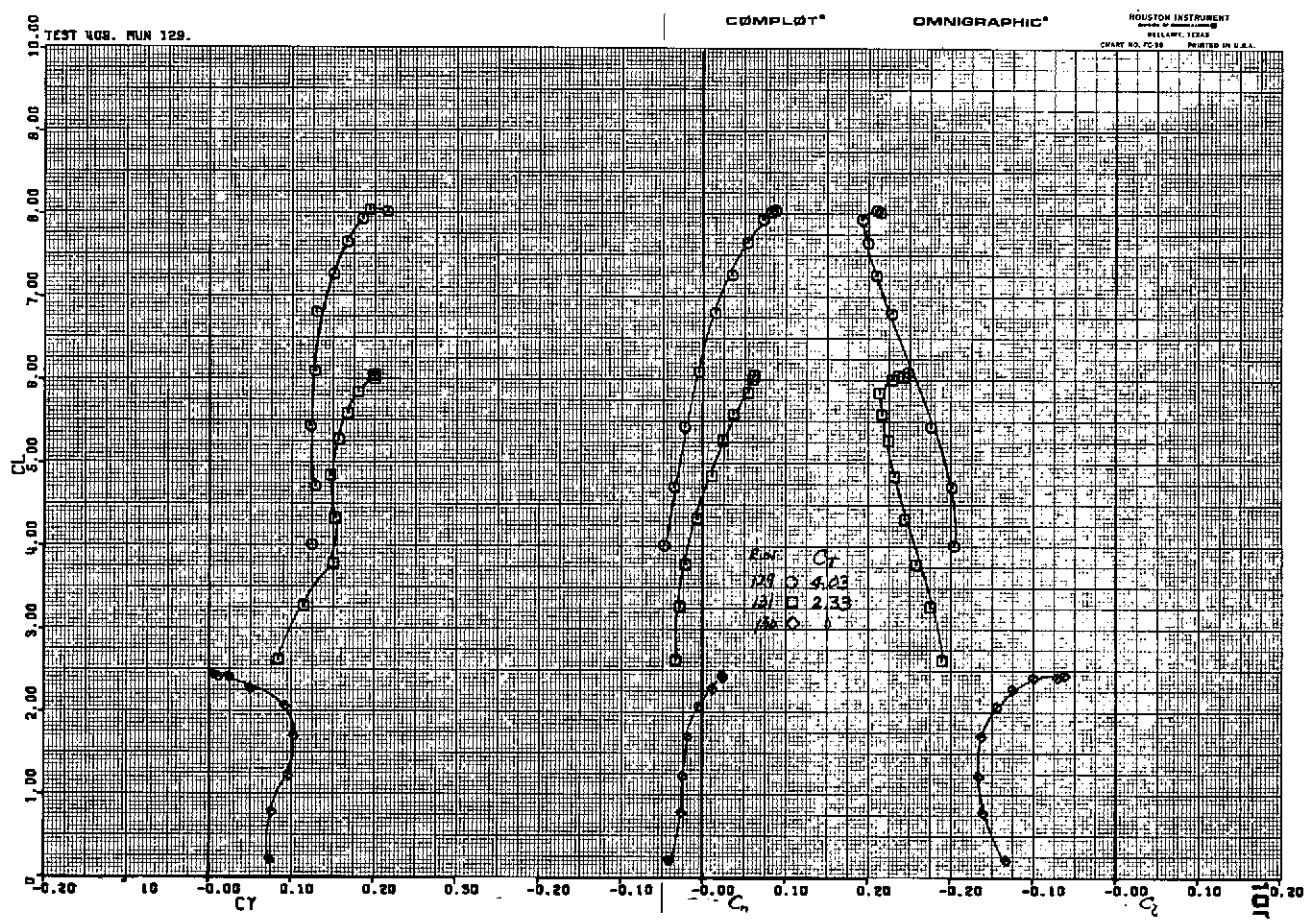


Figure 25.—Concluded.



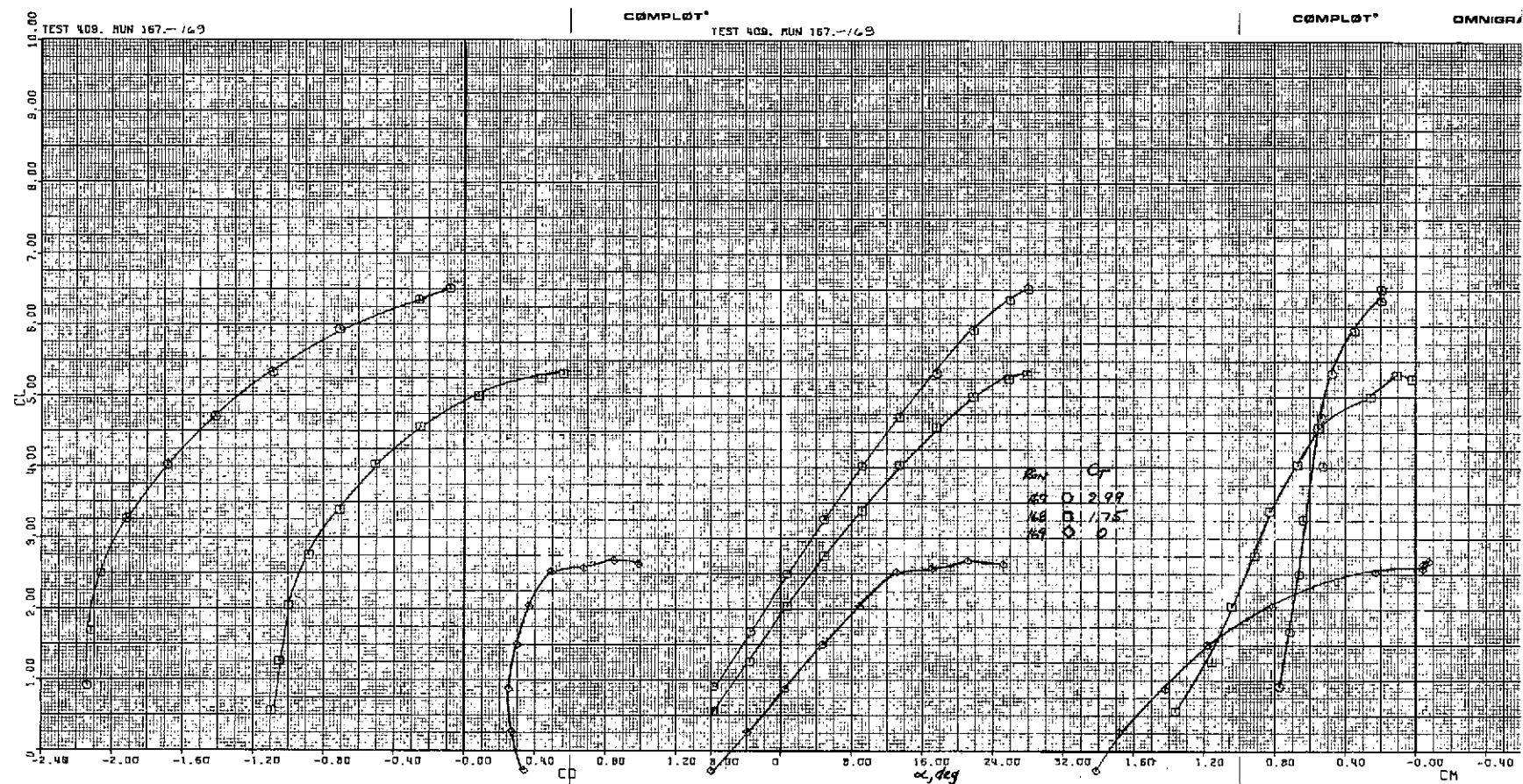
(a) Longitudinal characteristics of the model.

Figure 26.—Aerodynamic characteristics of the model with asymmetric aileron and spoiler deflections; part span flaps, $\delta_{f_1}/\delta_{f_2}/\delta_{f_3} = 15^\circ/35^\circ/55^\circ$, tail on, $i_t = 0^\circ$, $\delta_e = -25^\circ$, $\delta_{ail} = 5^\circ/35^\circ$, $\delta_{sp} = 60^\circ/0^\circ$.



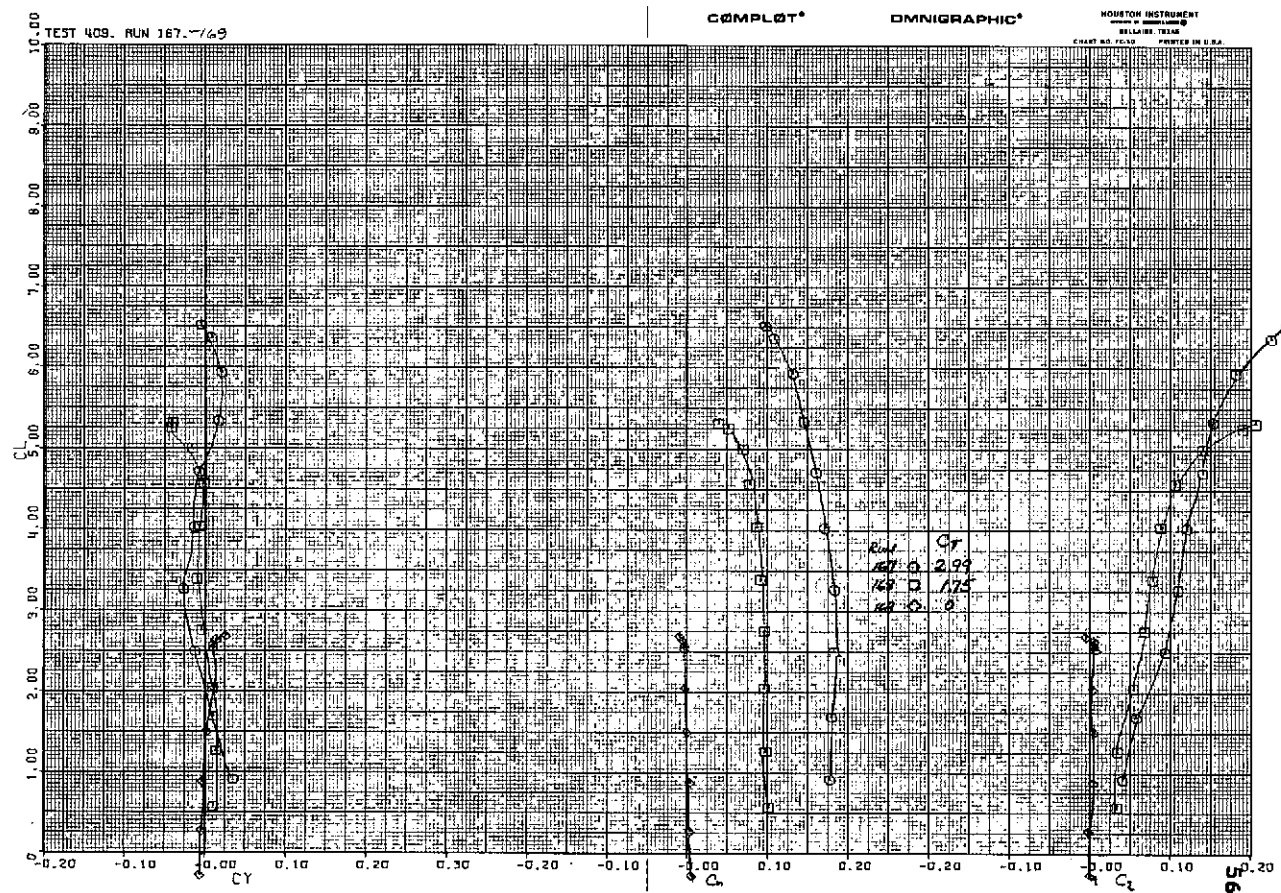
(b) Lateral characteristics of the model.

Figure 26.—Concluded.



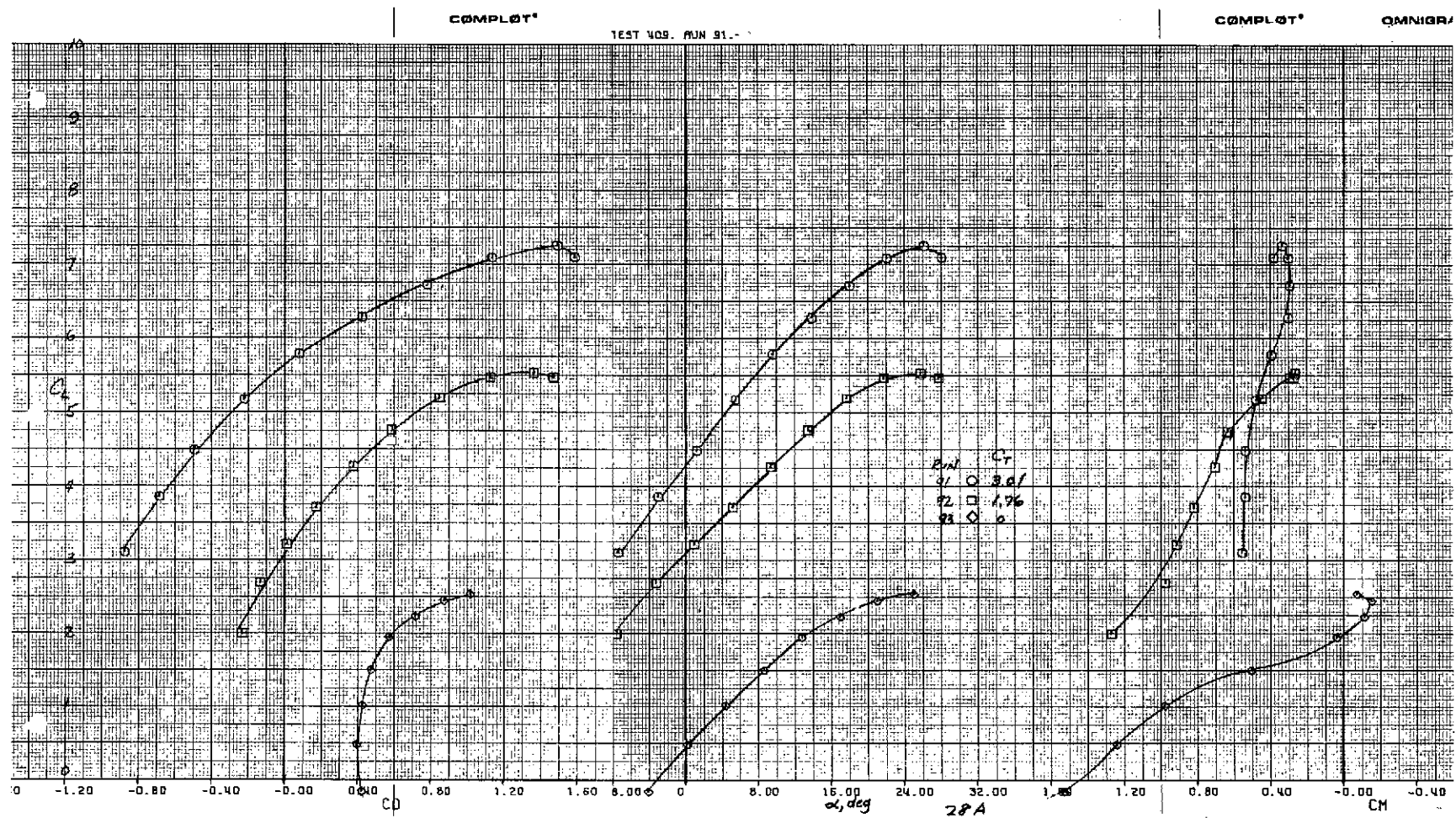
(a) Longitudinal characteristics of the model.

Figure 27.—Aerodynamic characteristics of the model with the right hand outboard engine out, part span slaps, $\delta_{f_1}/\delta_{f_2}/\delta_{f_3} = 0^\circ/20^\circ/30^\circ$, tail on, $i_t = 0^\circ$, $\delta_e = -25^\circ$, $\delta_{ail} = 5^\circ$.



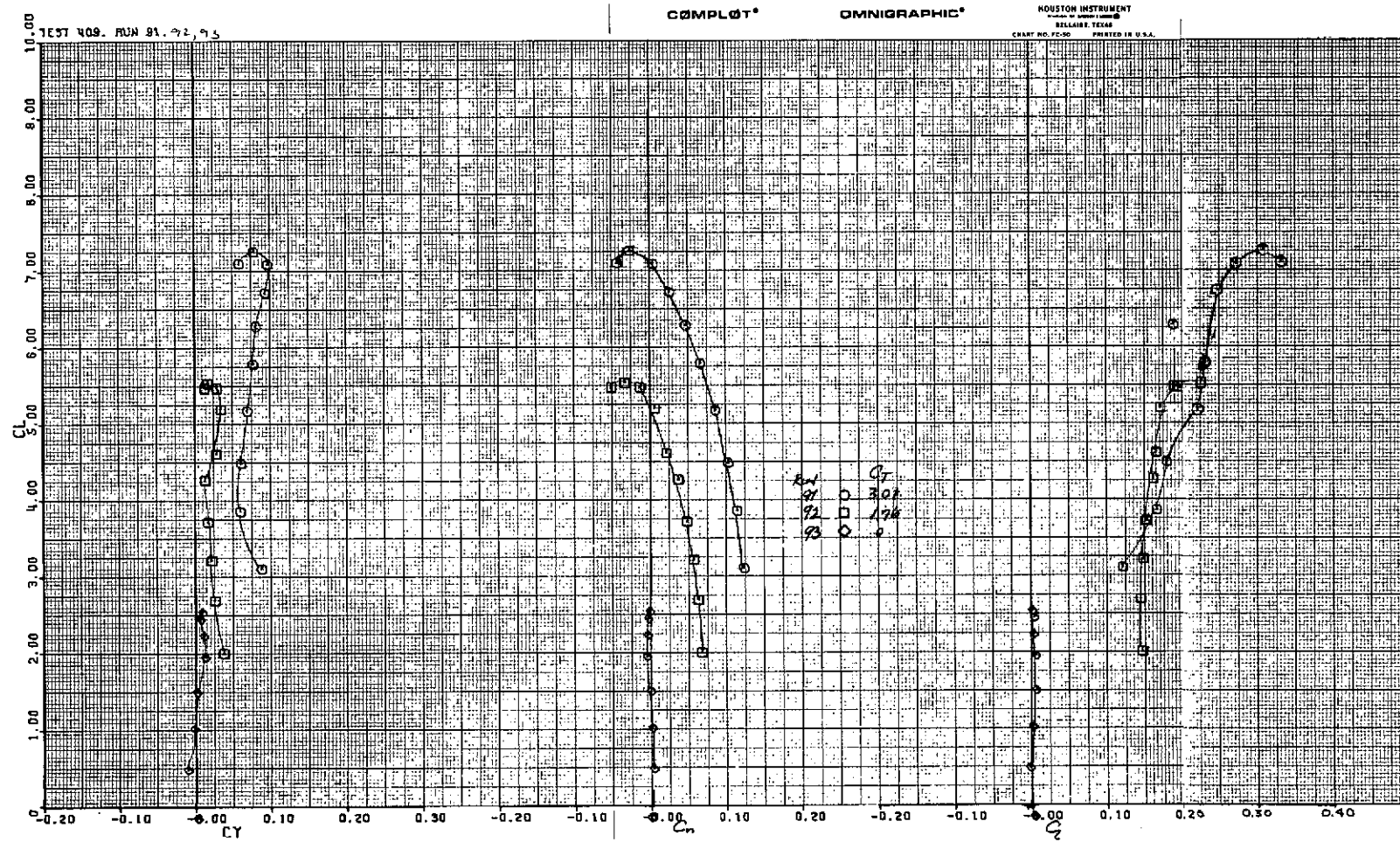
(b) Lateral characteristics of the model.

Figure 27.—Concluded.



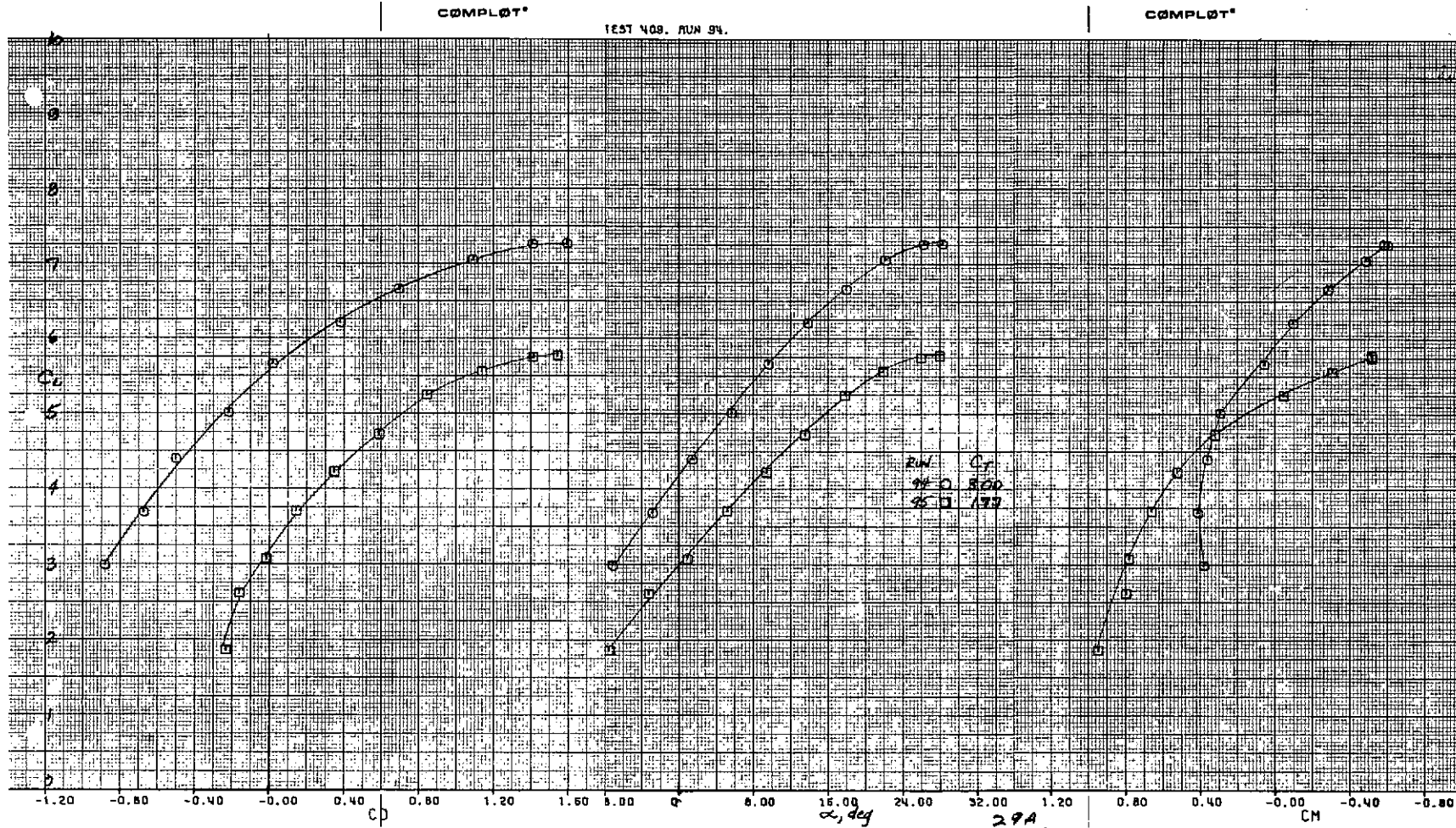
(a) Longitudinal characteristics of the model.

Figure 28.—Aerodynamic characteristics of the model with the right hand outboard engine out;
 part span flaps, $\delta_{f_1}/\delta_{f_2}/\delta_{f_3} = 15^\circ/35^\circ/55^\circ$, tail on, $i_t = 0^\circ$, $\delta_e = -25^\circ$, $\delta_{ail} = 20^\circ$,
 $\delta_{sp} = 30^\circ$.



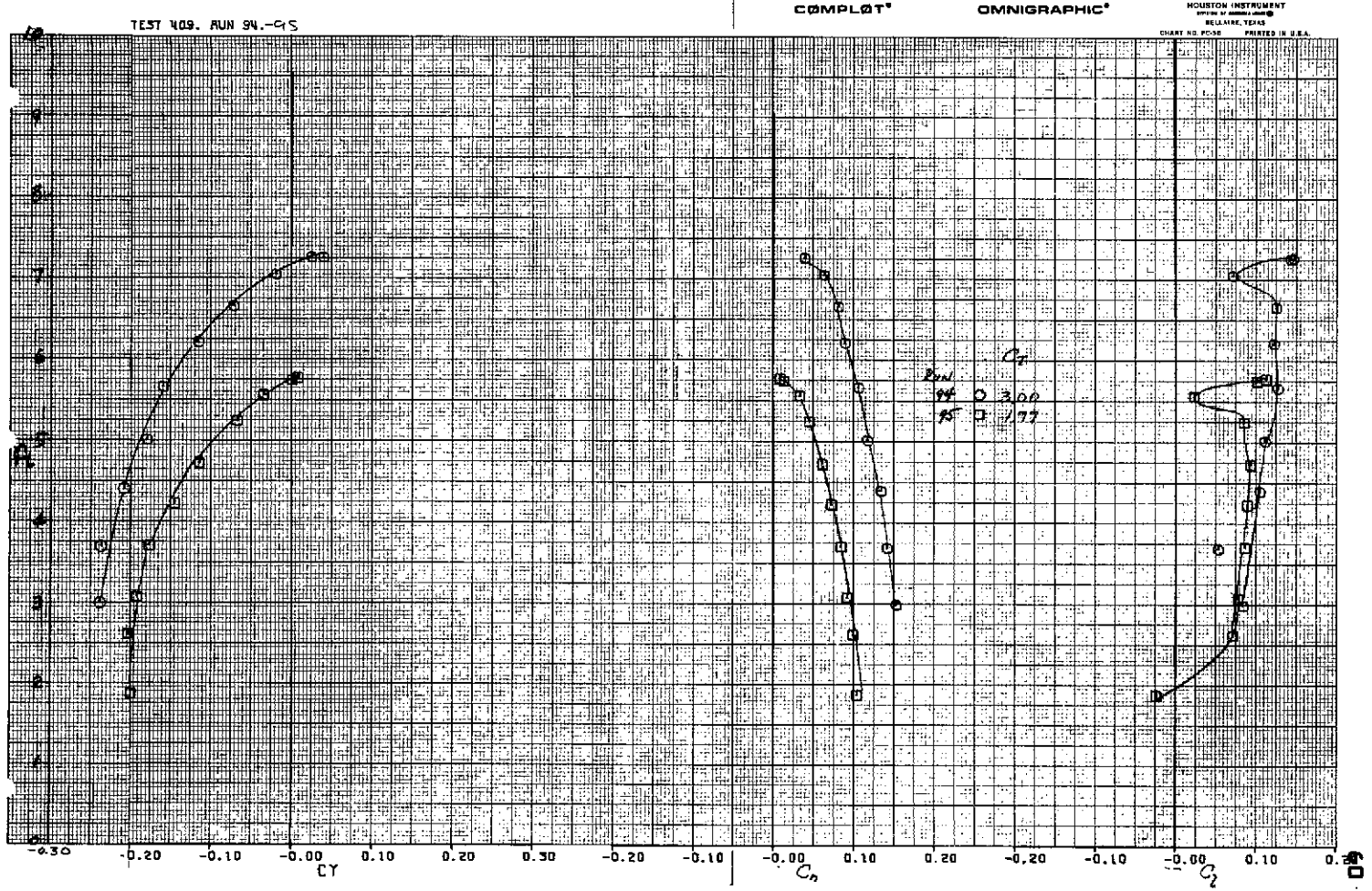
(b) Lateral characteristics of the model.

Figure 28.—Concluded.



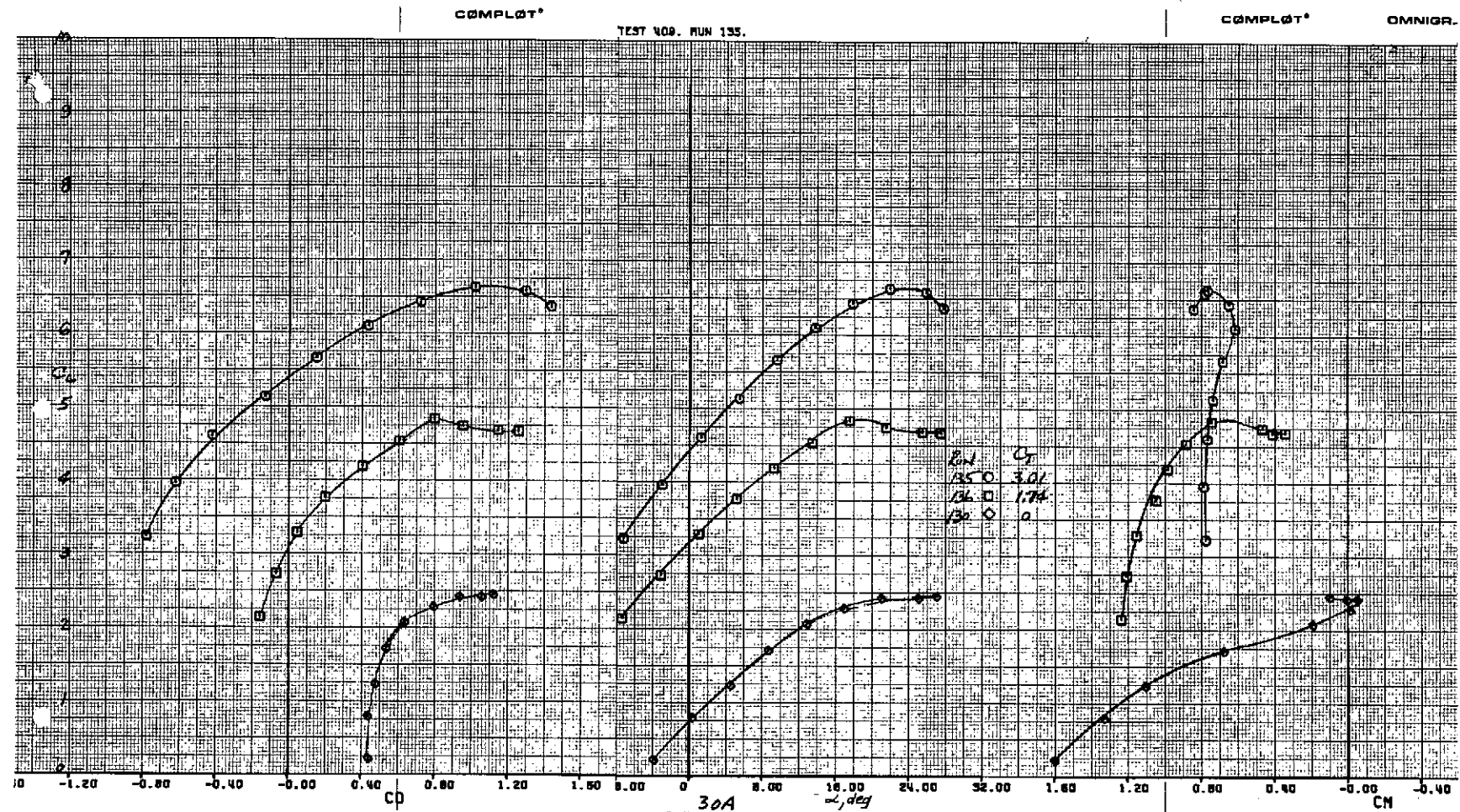
(a) Longitudinal characteristics of the model.

Figure 29.—Aerodynamic characteristics of the model with the right hand inboard engine out; part span flaps, $\delta_{f_1}/\delta_{f_2}/\delta_{f_3} = 15^\circ/35^\circ/55^\circ$, tail on, $i_t = 0^\circ$, $\delta_e = -25^\circ$, $\delta_{ail} = 20^\circ$, $\delta_{sp} = 30^\circ$.



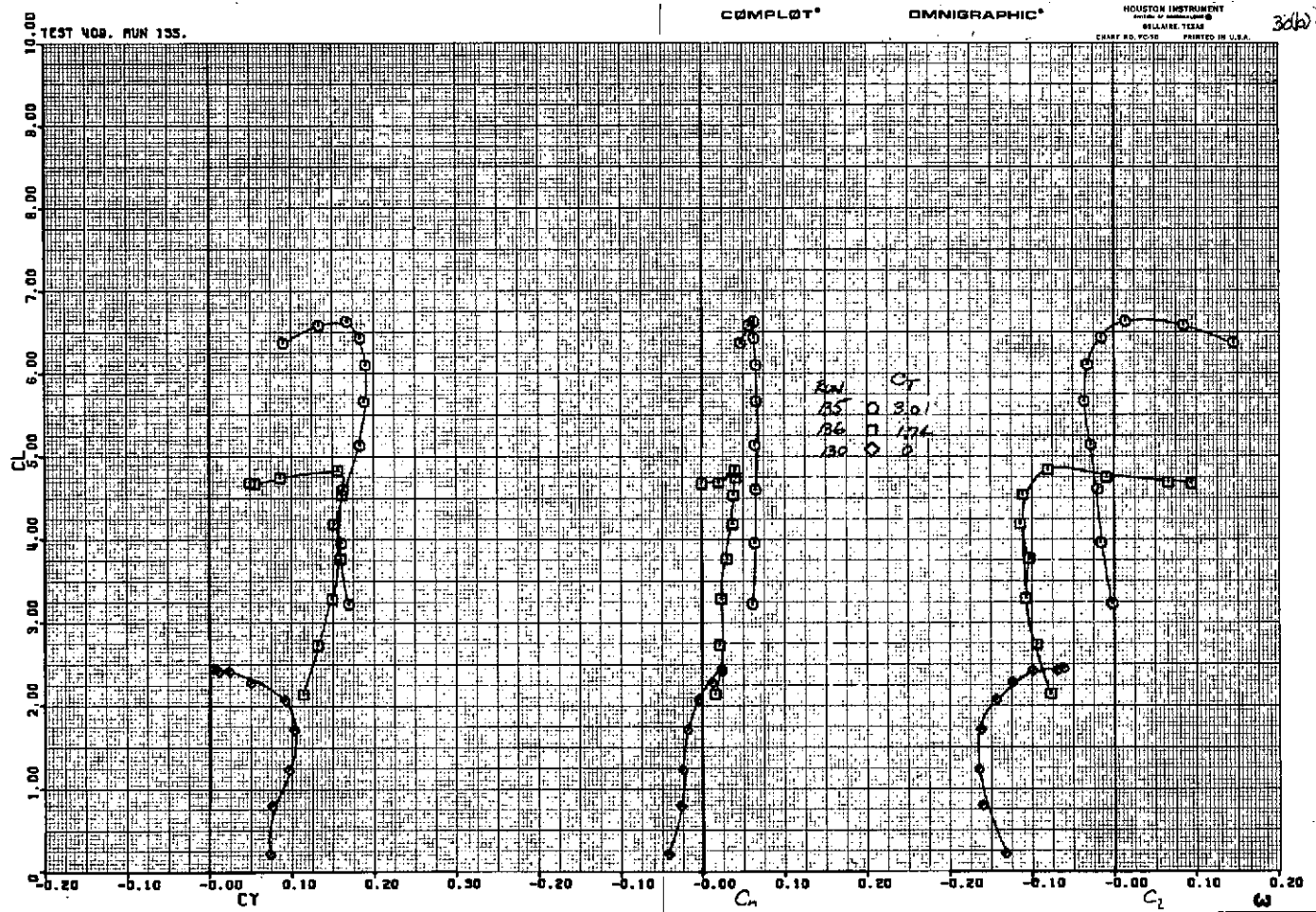
(b) Lateral characteristics of the model.

Figure 29.—Concluded.



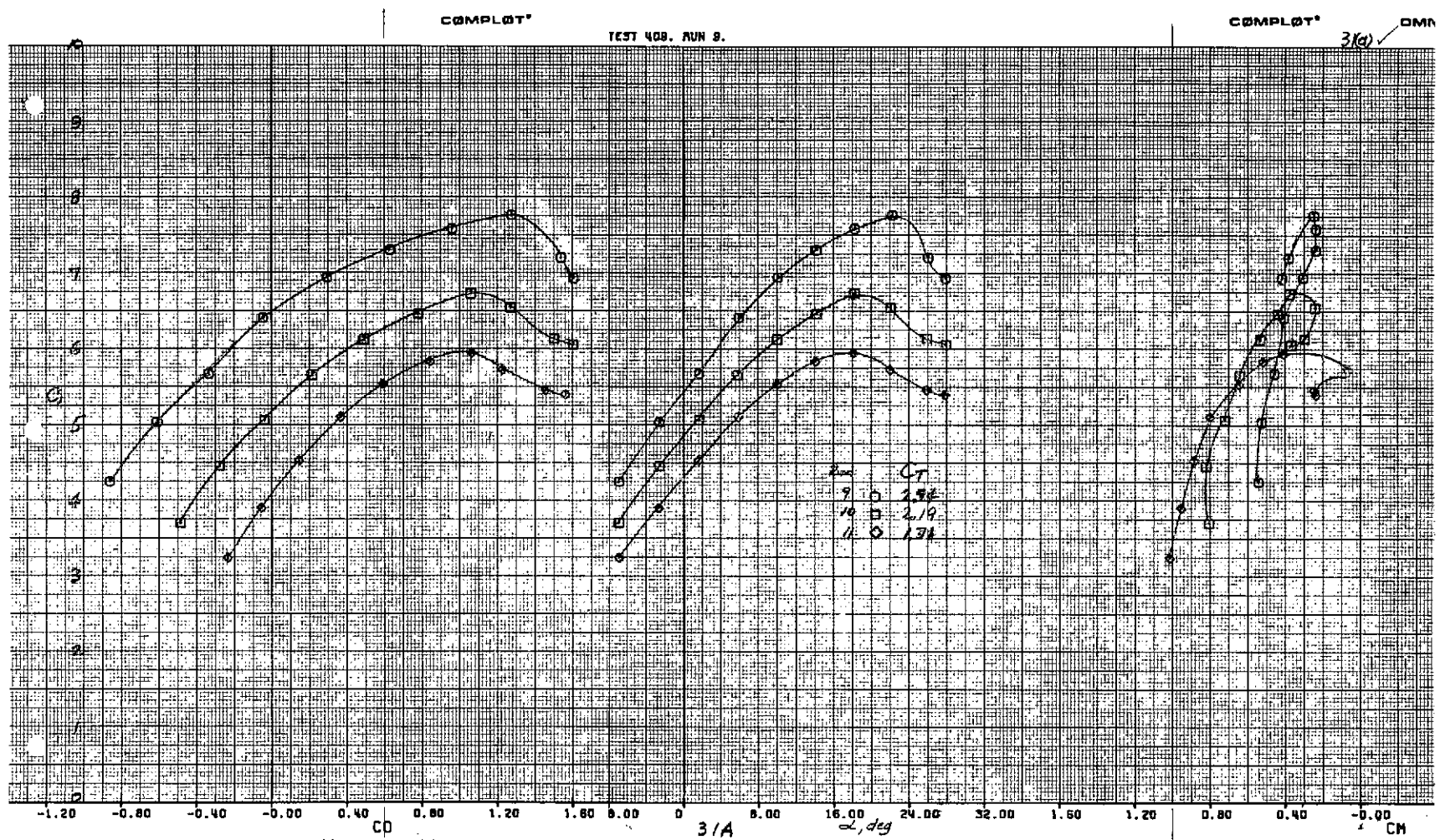
(a) Longitudinal characteristics of the model.

Figure 30.—Aerodynamic characteristics of the model with the right hand outboard engine out and with asymmetric aileron and spoiler deflections; part span flaps, $\delta_{f_1}/\delta_{f_2}/\delta_{f_3} = 15^\circ/35^\circ/55^\circ$, tail on, $i_t = 0^\circ$, $\delta_e = -25^\circ$, $\delta_{ail} = 5^\circ/35^\circ$, $\delta_{sp} = 60^\circ/0^\circ$.



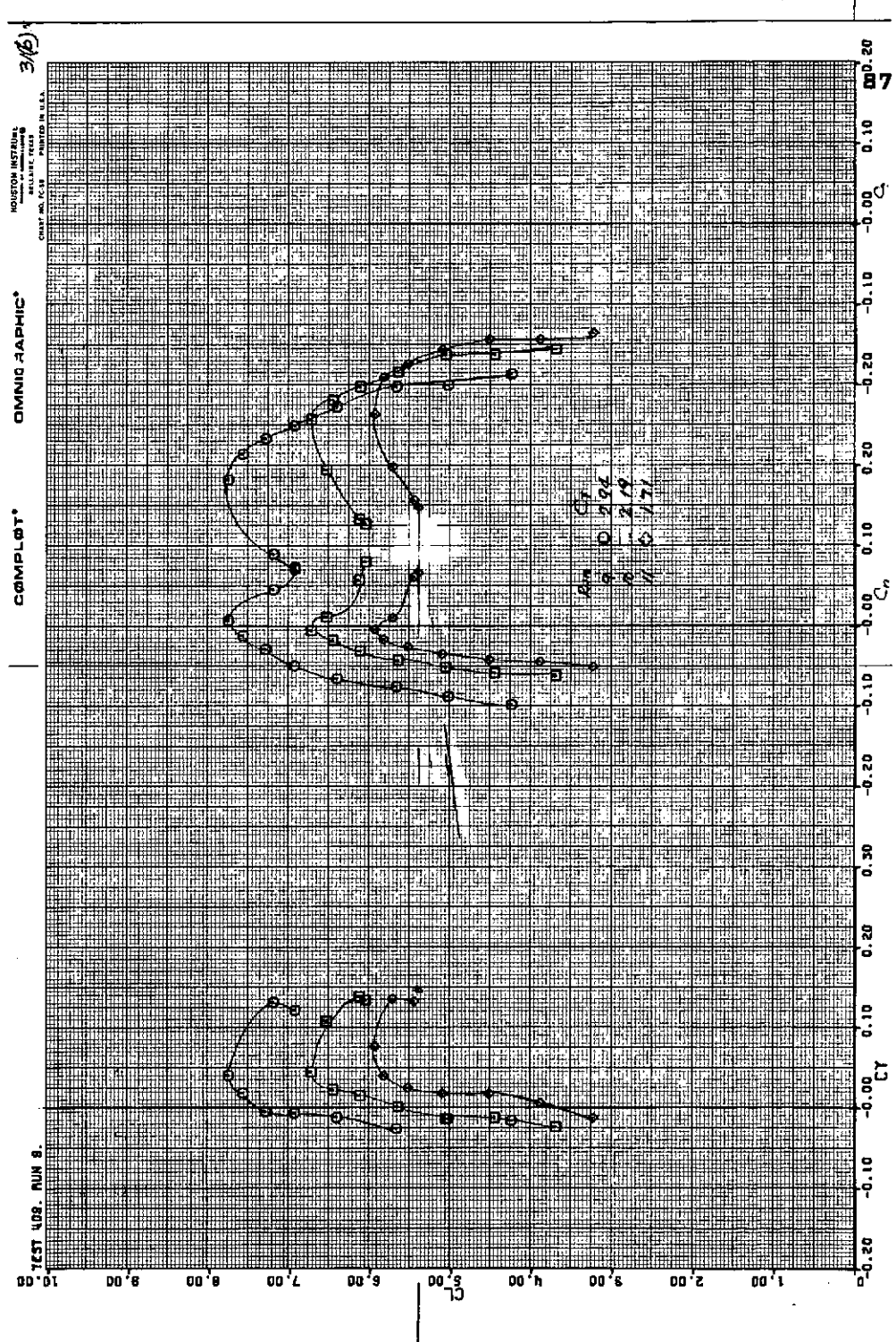
(b) Lateral characteristics of the model.

Figure 30.—Concluded.



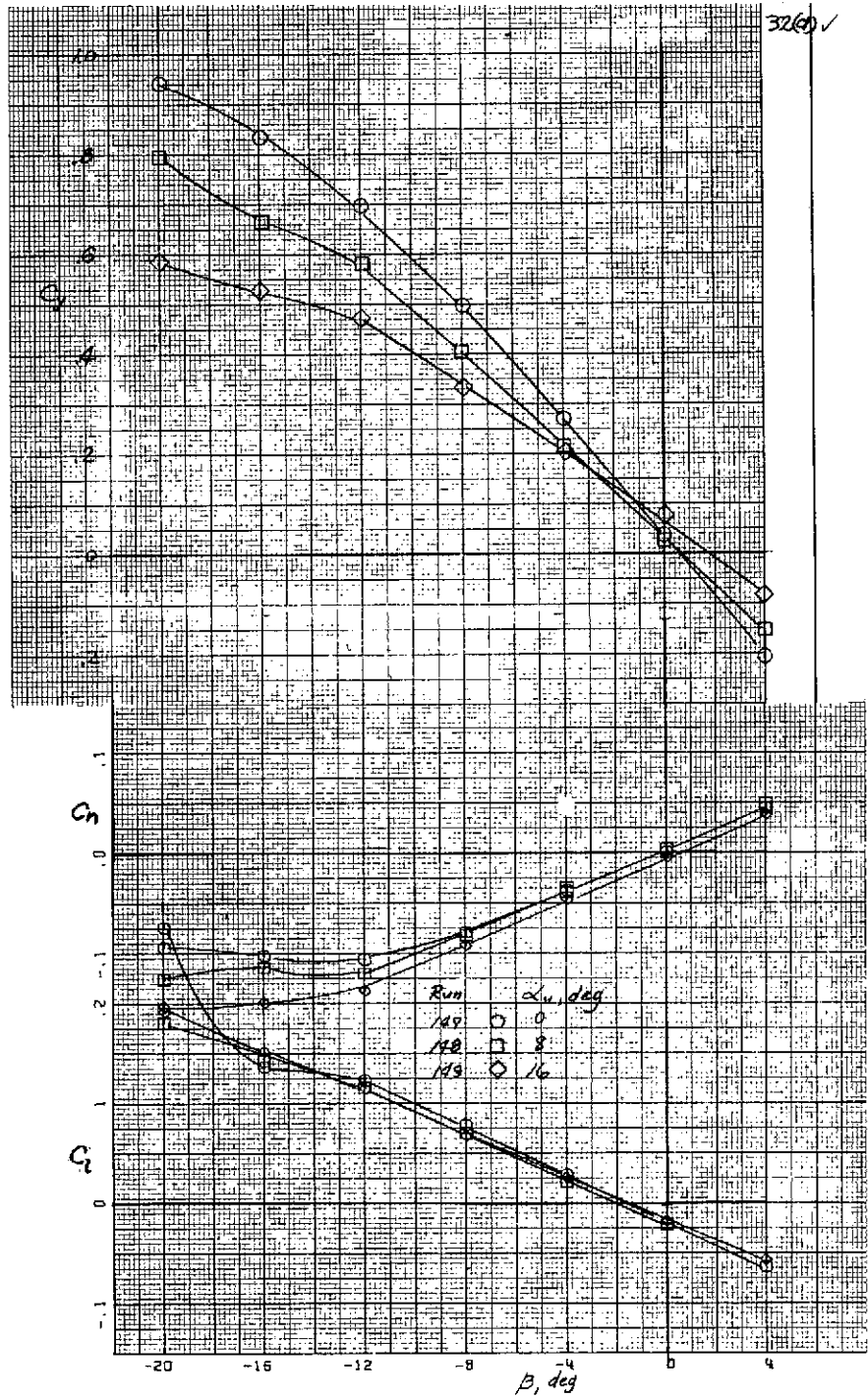
(a) Longitudinal characteristics of the model.

Figure 31.—Aerodynamic characteristics of the model with the left hand outboard engine out; full span flaps, $\delta_{f_1}/\delta_{f_2}/\delta_{f_3} = 15^\circ/35^\circ/55^\circ$, tail on, $i_t = 0^\circ$, $\delta_e = -25^\circ$.



(b) Lateral characteristics of the model.

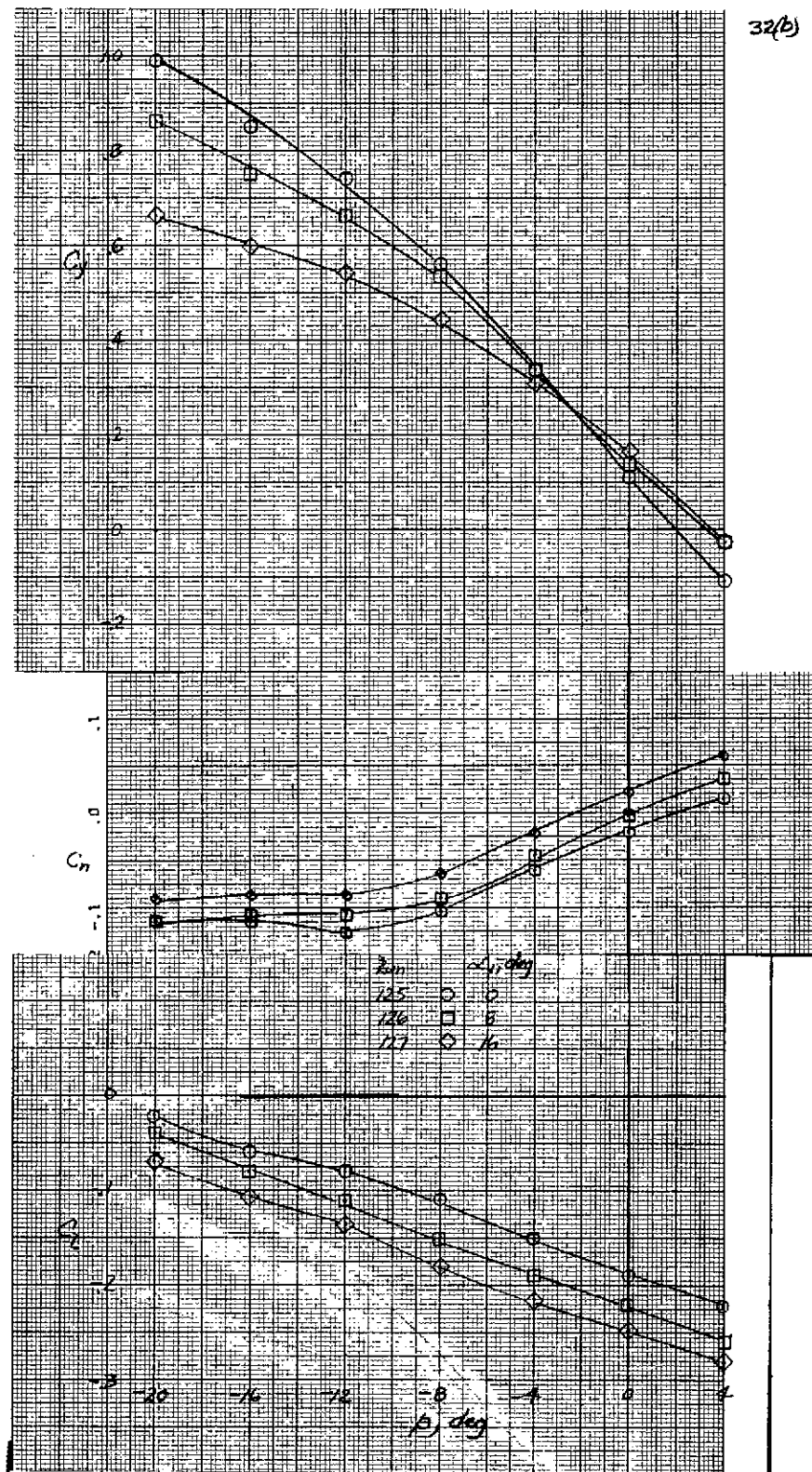
Figure 31.—Concluded.



(a) $\delta_{sp} = 0^\circ/0^\circ$.

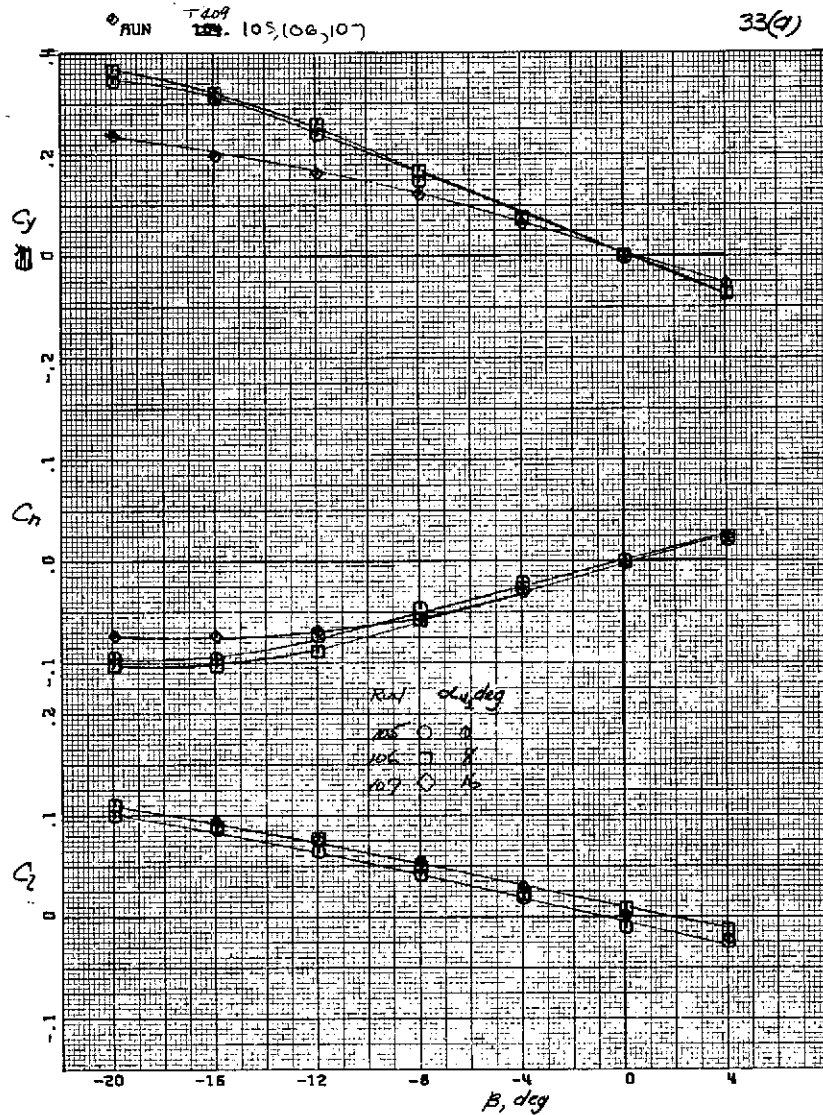
Figure 32.—Variation of side force, yawing-moment, and rolling-moment coefficients with sideslip; $\delta_{f_1}/\delta_{f_2}/\delta_{f_3} = 15^\circ/35^\circ/55^\circ$, $i_t = 0^\circ$, $\delta_e = -25^\circ$, $\delta_{ail} = 23^\circ/23^\circ$, $C_T = 2.34$.

32(b)



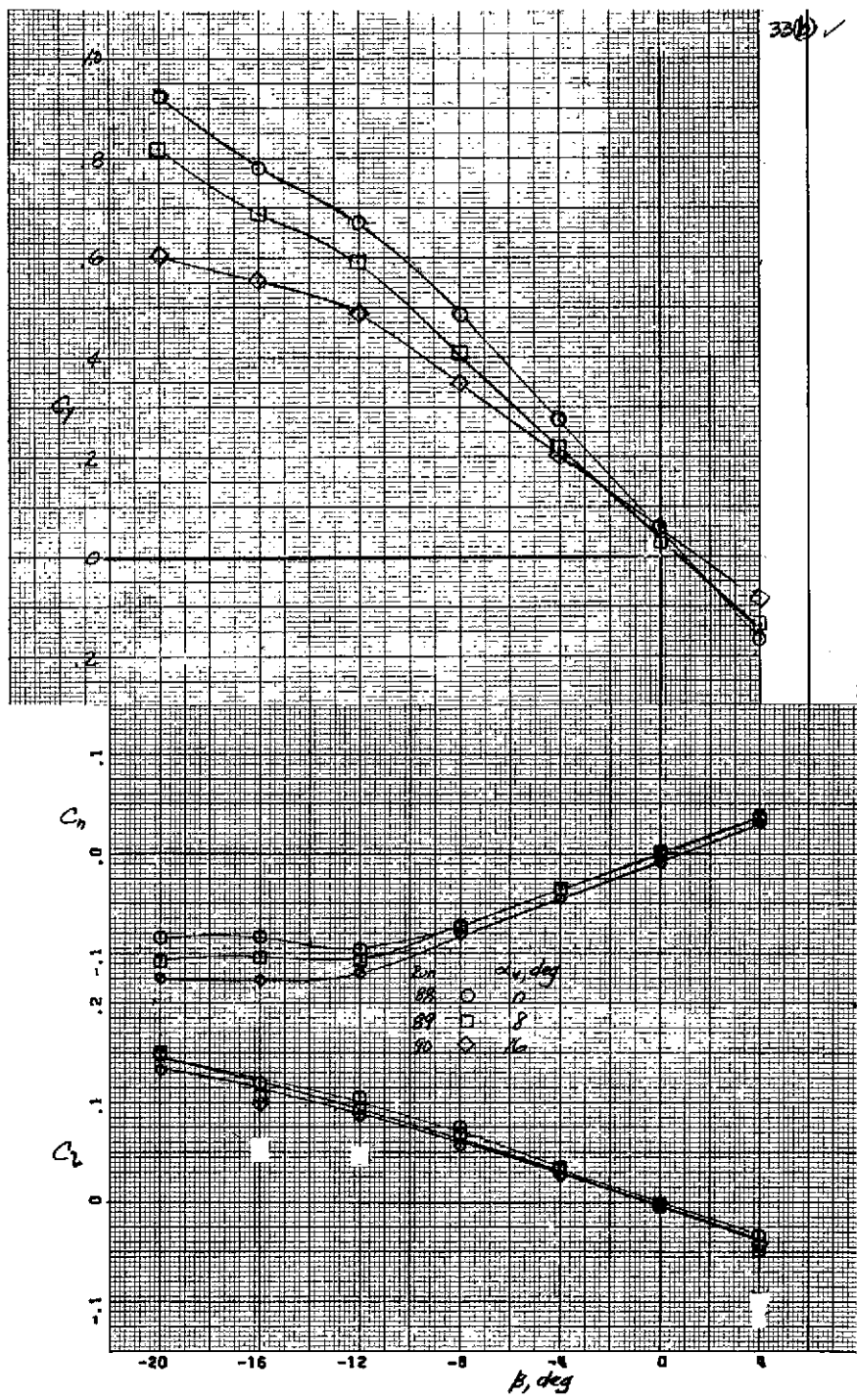
(b) $\delta_{sp} = 60^\circ/0^\circ$.

Figure 32.—Concluded.



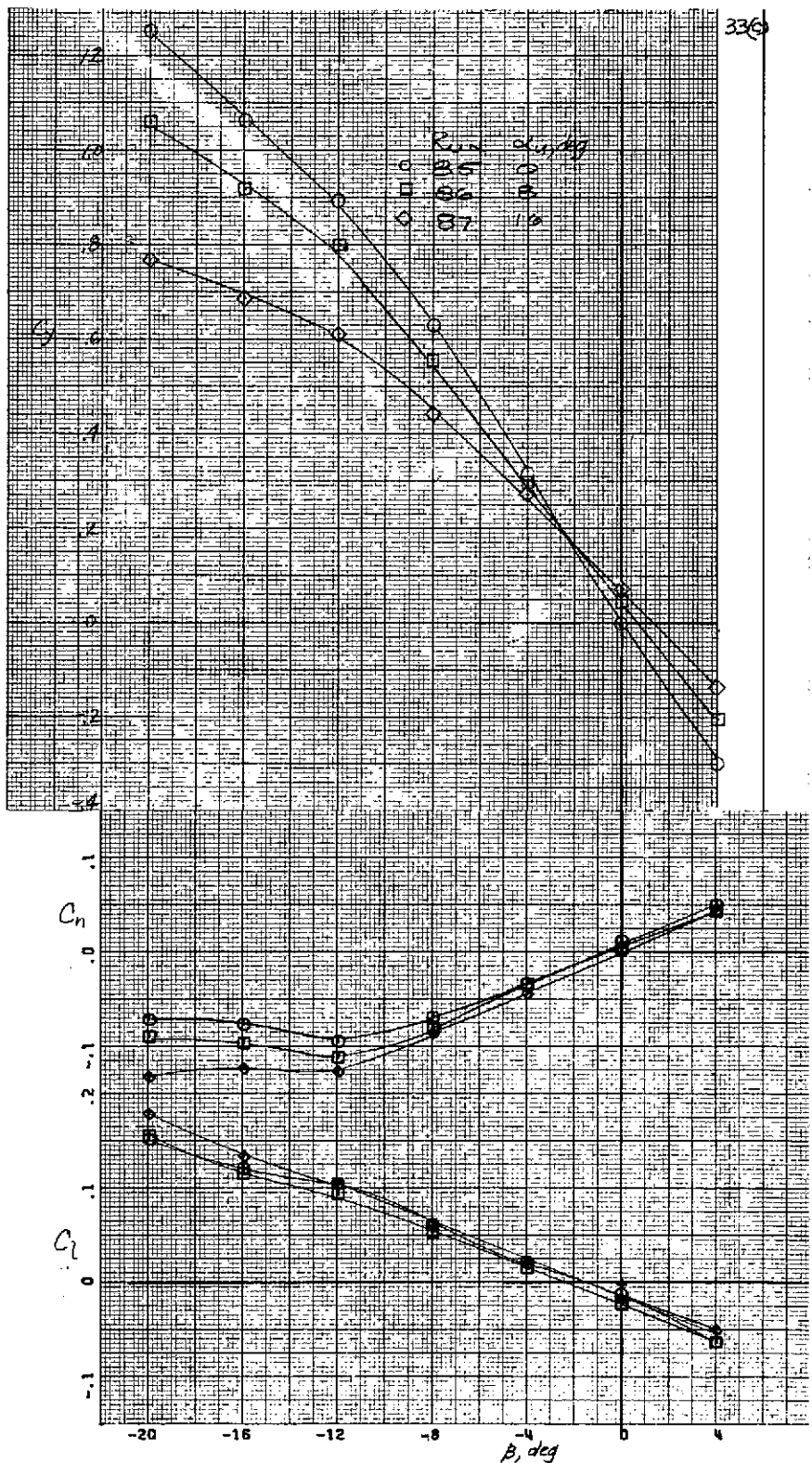
(a) $C_T = 0.$

Figure 33.—Variation of side force, yawing-moment, and rolling-moment coefficients with sideslip; $\delta_{f_1}/\delta_{f_2}/\delta_{f_3} = 15^\circ/35^\circ/55^\circ$, $i_t = 0^\circ$; $\delta_e = -25^\circ$, $\delta_{ail} = 20^\circ/20^\circ$, $\delta_{sp} = 20^\circ/20^\circ$.



(b) $C_T = 2.34$.

Figure 33.—Continued.



(c) $C_T = 4.00$

Figure 33.—Concluded.

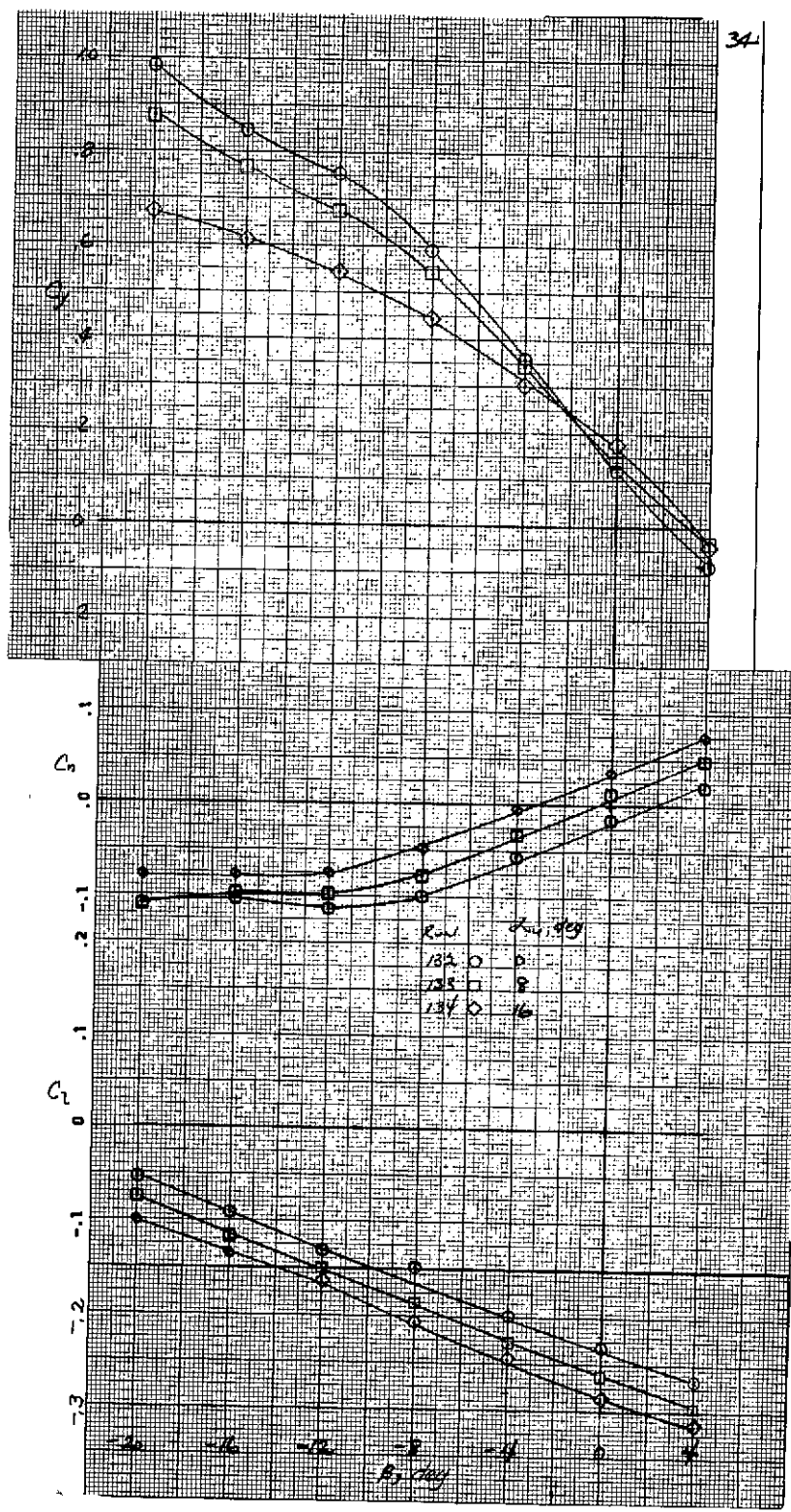
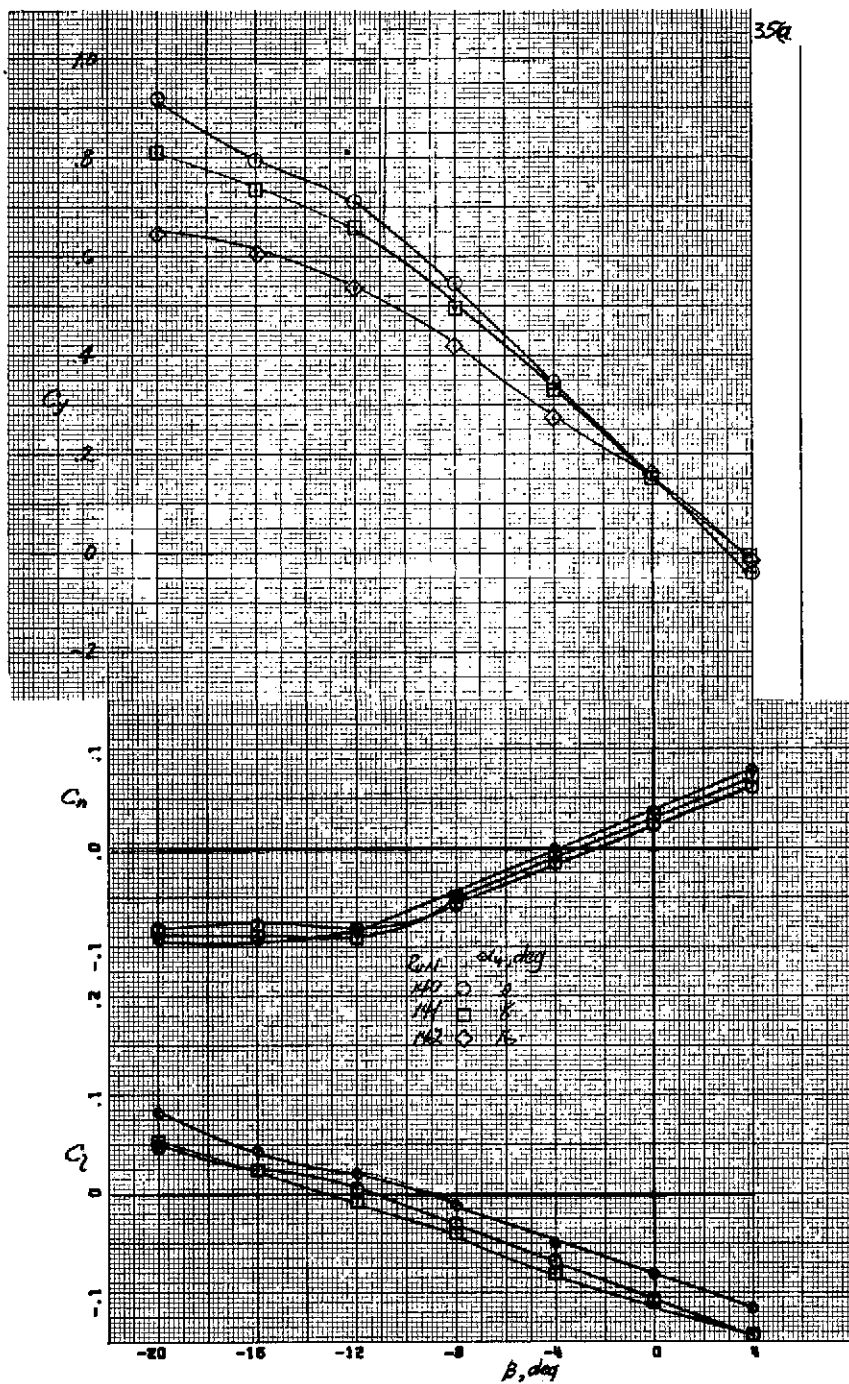
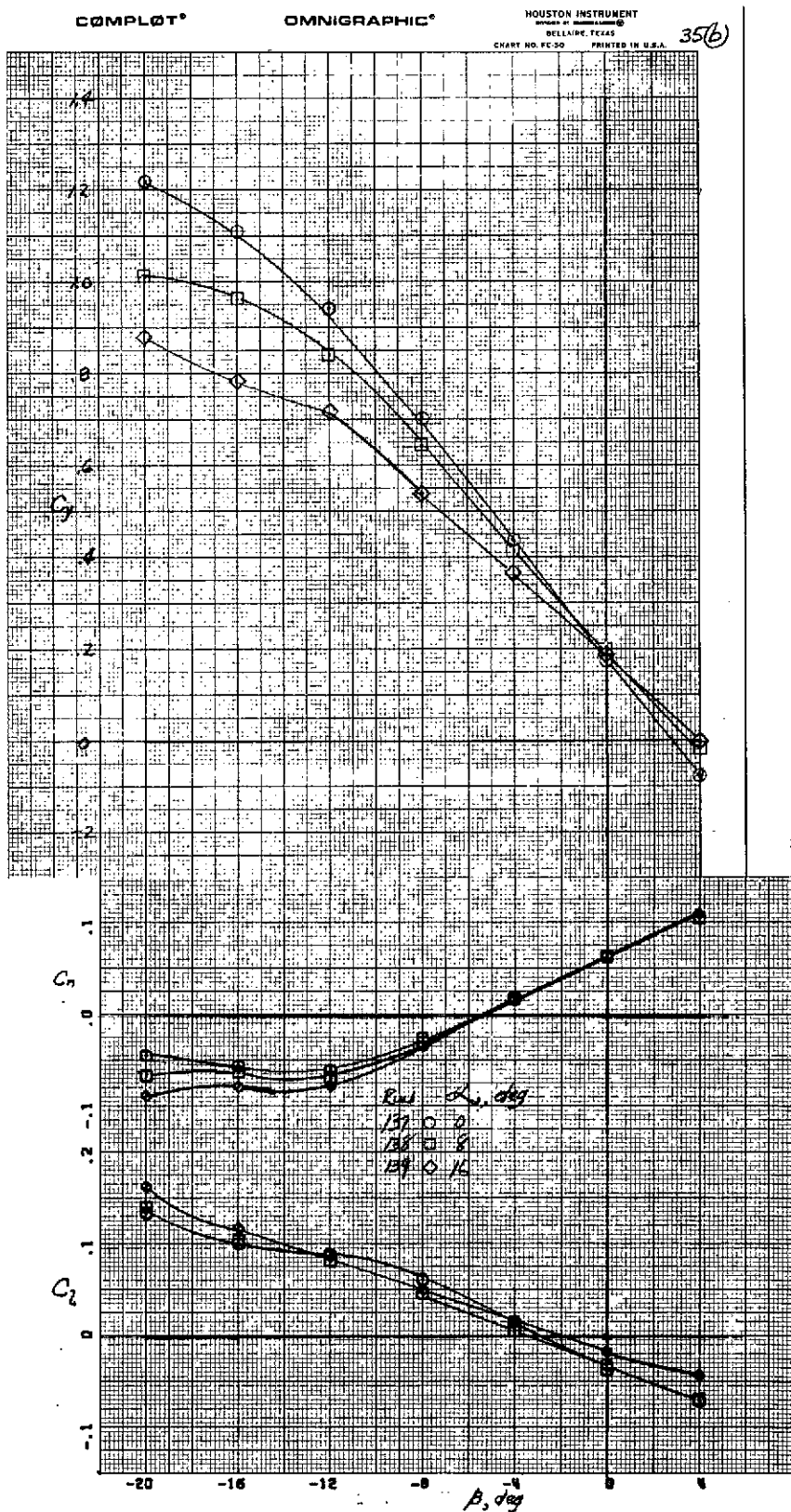


Figure 34.—Variation of side force, yawing-moment, and rolling-moment coefficients with sideslip and with 4 engine operation; $\delta_{f_1}/\delta_{f_2}/\delta_{f_3} = 15^\circ/35^\circ/55^\circ$, $i_t = 0^\circ$, $\delta_e = -25^\circ$, $\delta_{ail} = 5^\circ/35^\circ$, $\delta_{sp} = 60^\circ/0^\circ$, $C_T = 2.33$.



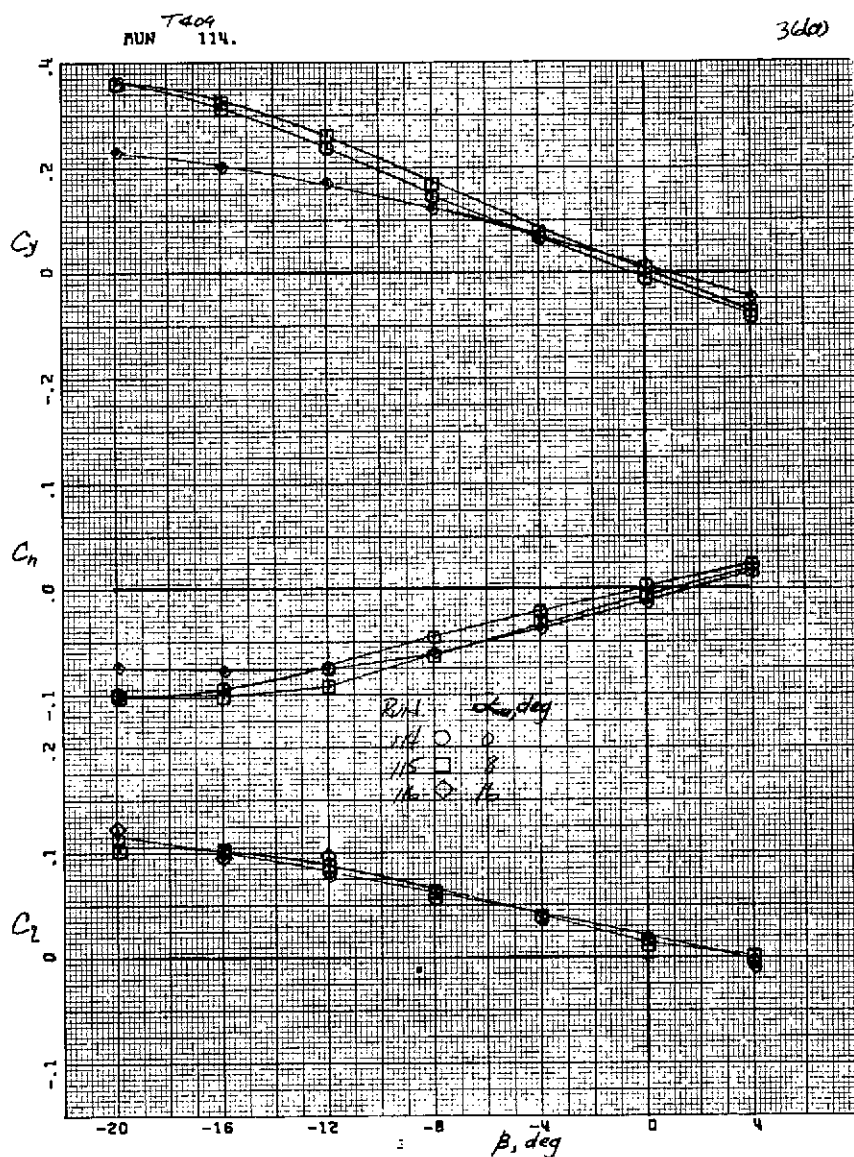
(a) $C_T = 1.74$.

Figure 35.—Variation of side force, yawing-moment, rolling-moment coefficients with sideslip and with the right hand outboard engine out;
 $\delta_{f_1}/\delta_{f_2}/\delta_{f_3} = 15^\circ/35^\circ/55^\circ$, $i_t = 0^\circ$, $\delta_e = -25^\circ$, $\delta_{ail} = 5^\circ/35^\circ$,
 $\delta_{sp} = 60^\circ/0^\circ$.



(b) $C_T = 2.99$.

Figure 35.—Concluded.



(a) $C_T = 0.$

Figure 36.—Variation of side force, yawing-moment, and rolling-moment coefficients with sideslip; $\delta_{f_1}/\delta_{f_2}/\delta_{f_3} = 15^\circ/35^\circ/55^\circ$, $i_t = 0^\circ$, $\delta_e = -25^\circ$, $\delta_{ail} = 20^\circ/5^\circ$, $\delta_{sp} = 30^\circ/30^\circ$

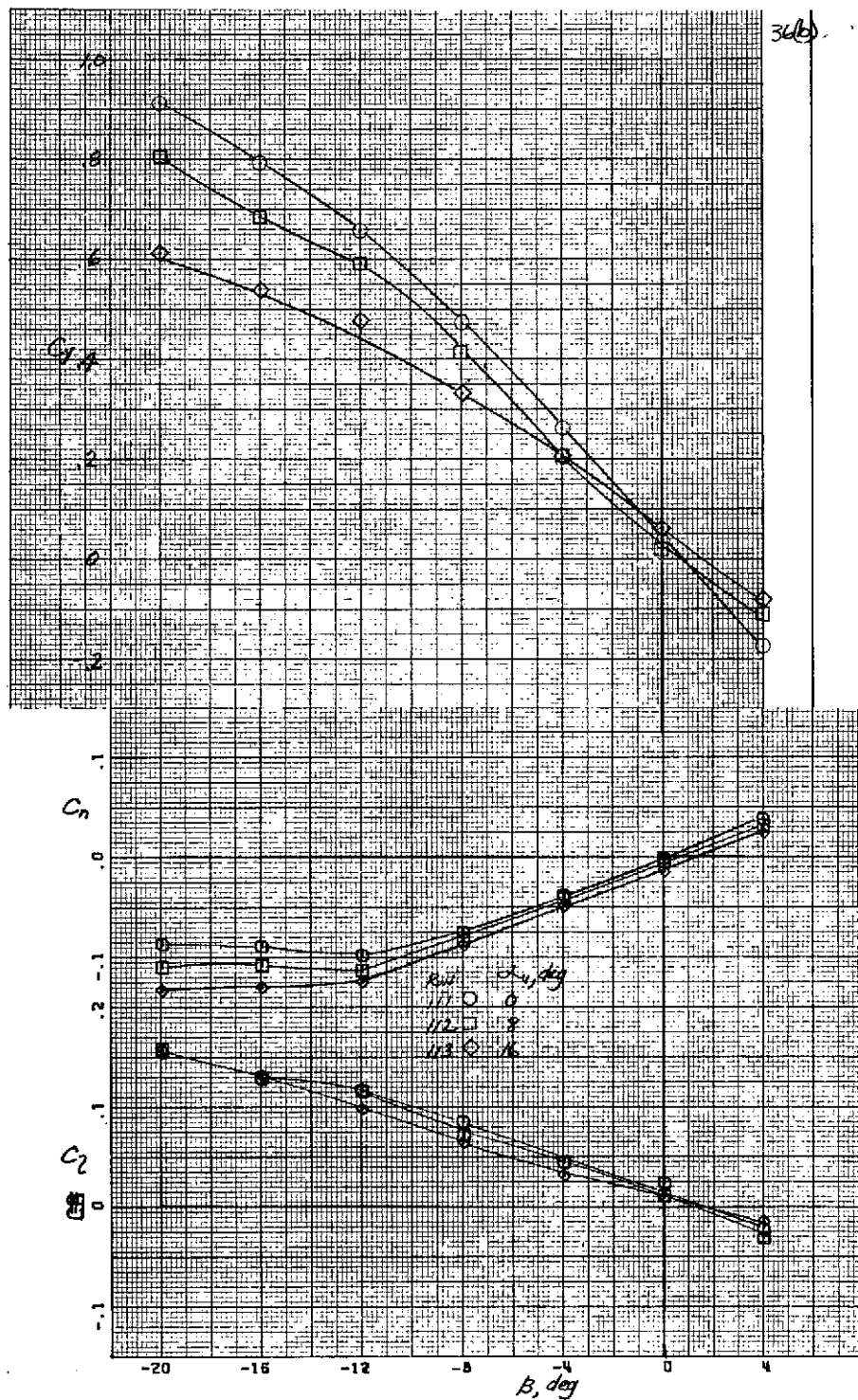
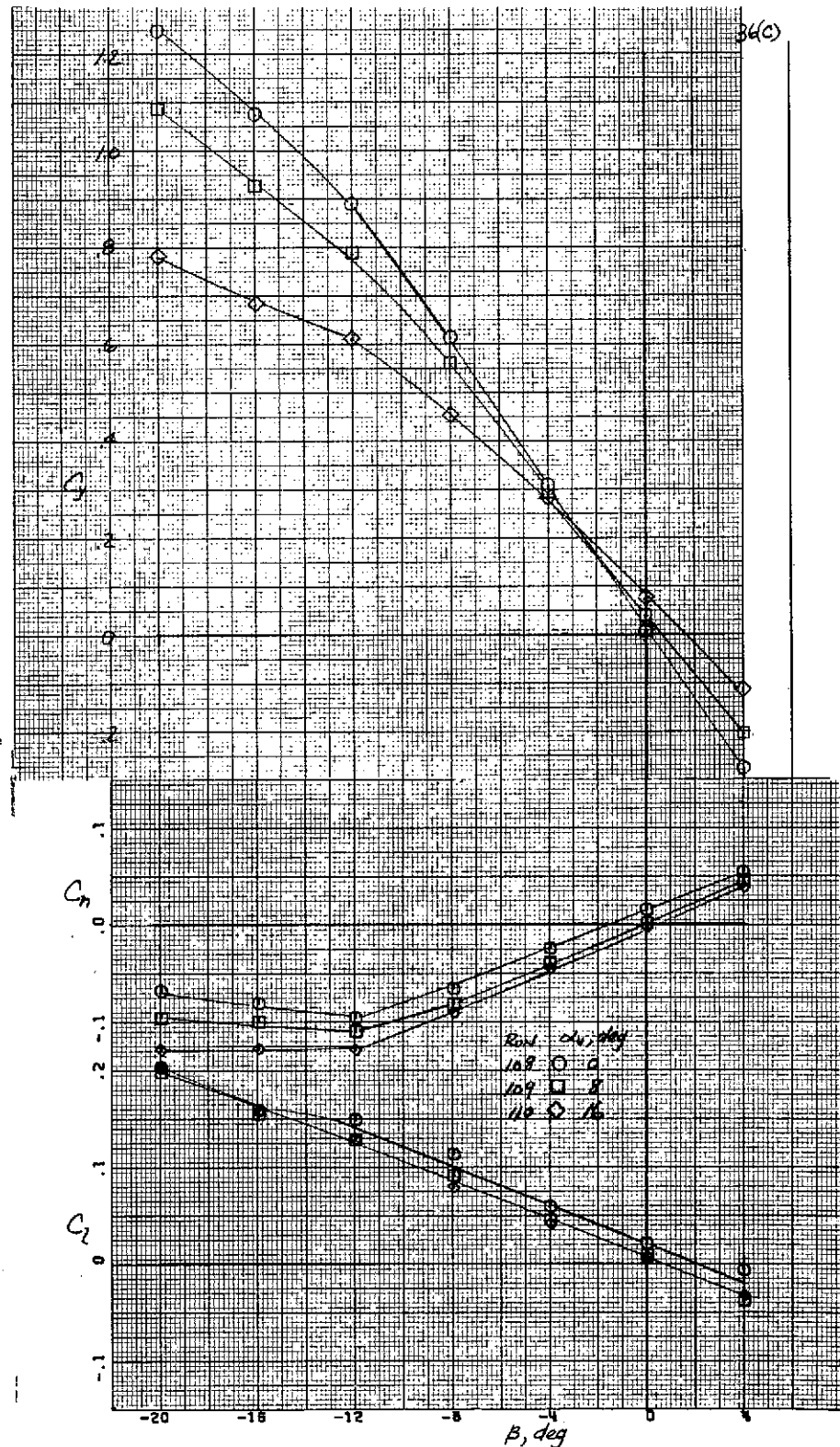
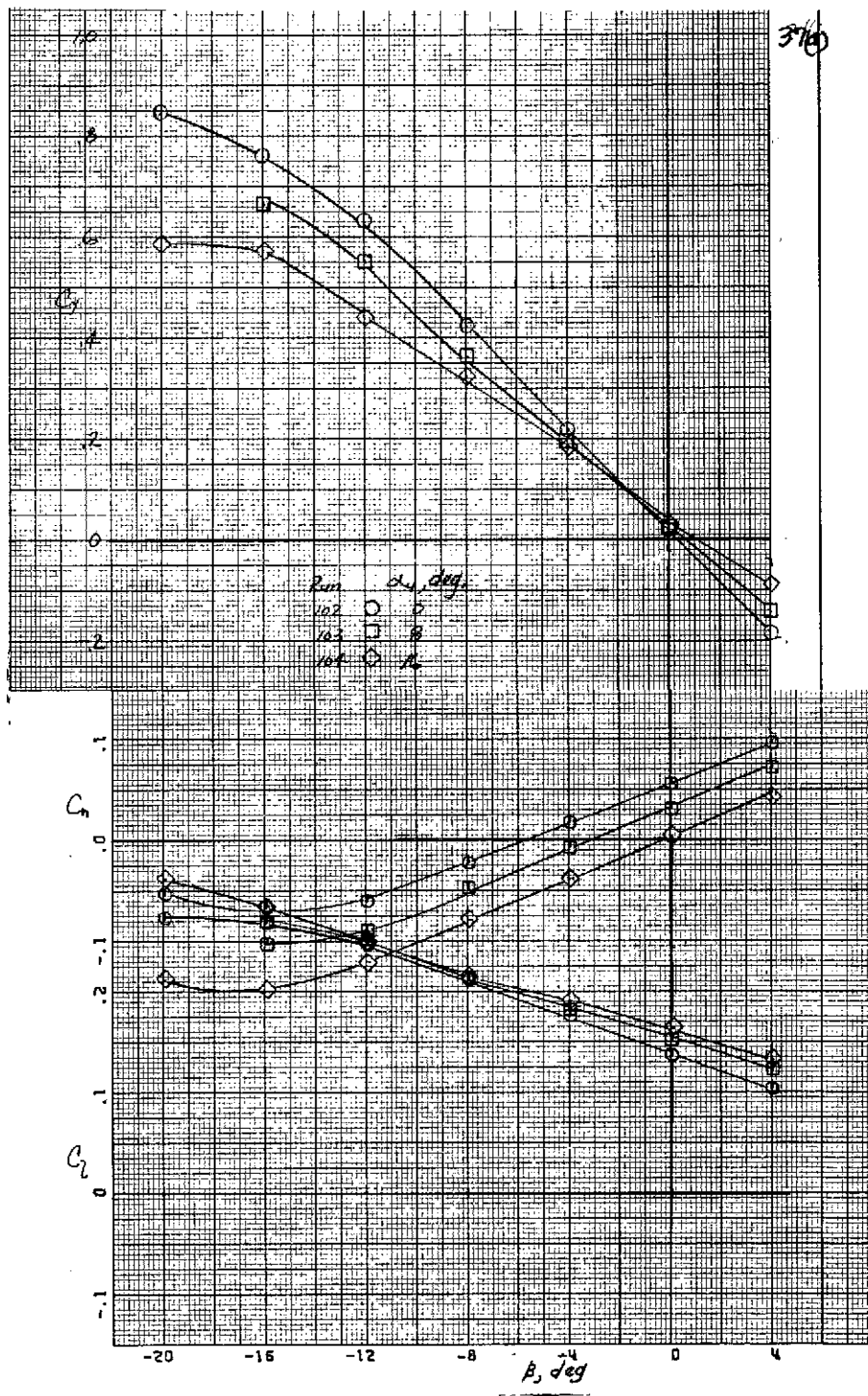


Figure 36.—Continued.



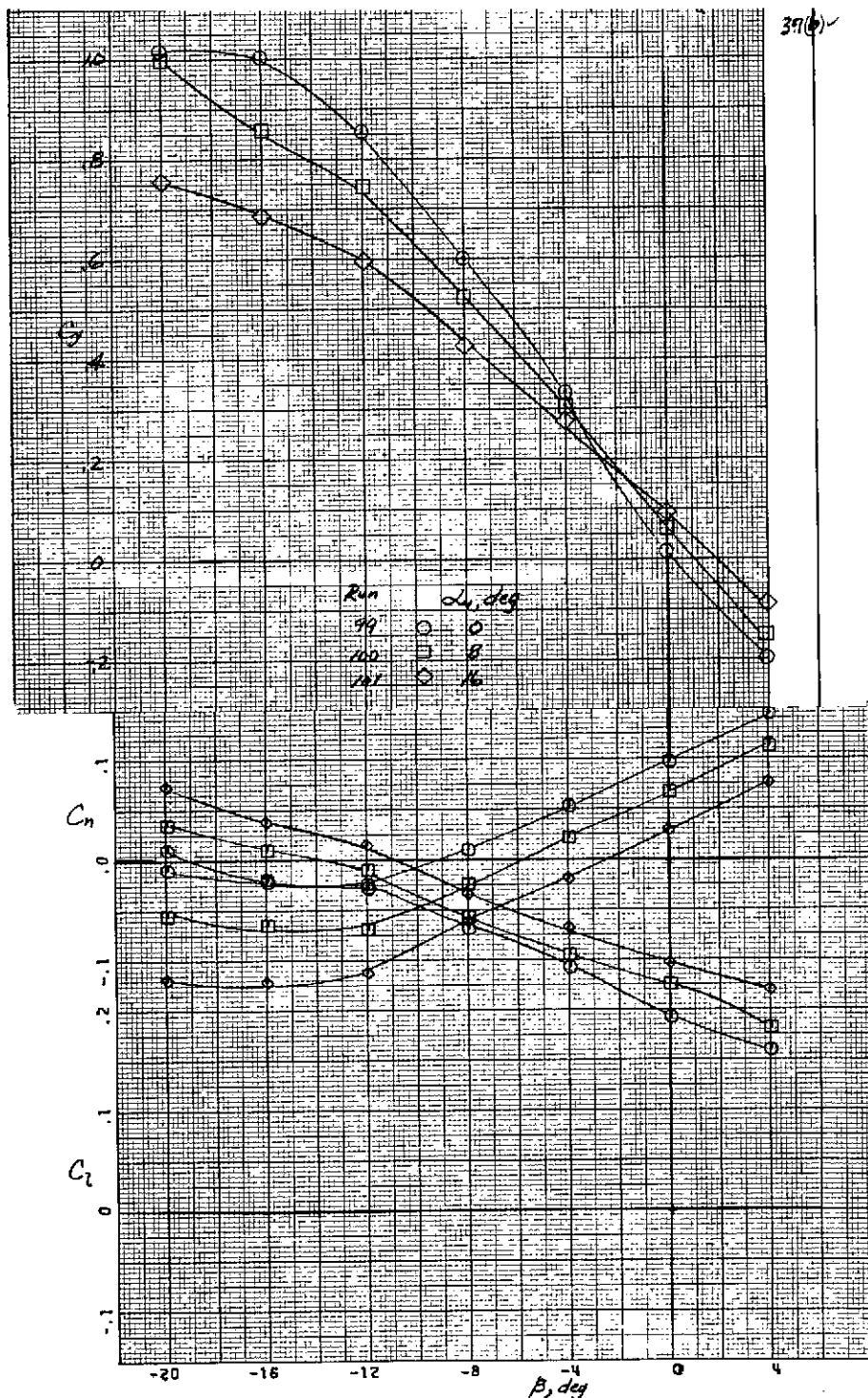
(c) $C_T = 3.99.$

Figure 36.—Concluded.



(a) $C_T = 1.74$.

Figure 37.—Variation of side force, yawing-moment, and rolling-moment coefficients with sideslip and with the right hand outboard engine out;
 $\delta_{f_1}/\delta_{f_2}/\delta_{f_3} = 15^\circ/35^\circ/55^\circ$, $i_t = 0^\circ$, $\delta_e = -25^\circ$, $\delta_{ail} = 20^\circ/20^\circ$,
 $\delta_{sp} = 30^\circ/30^\circ$.



(b) $C_T = 2.99.$

Figure 37.—Concluded.

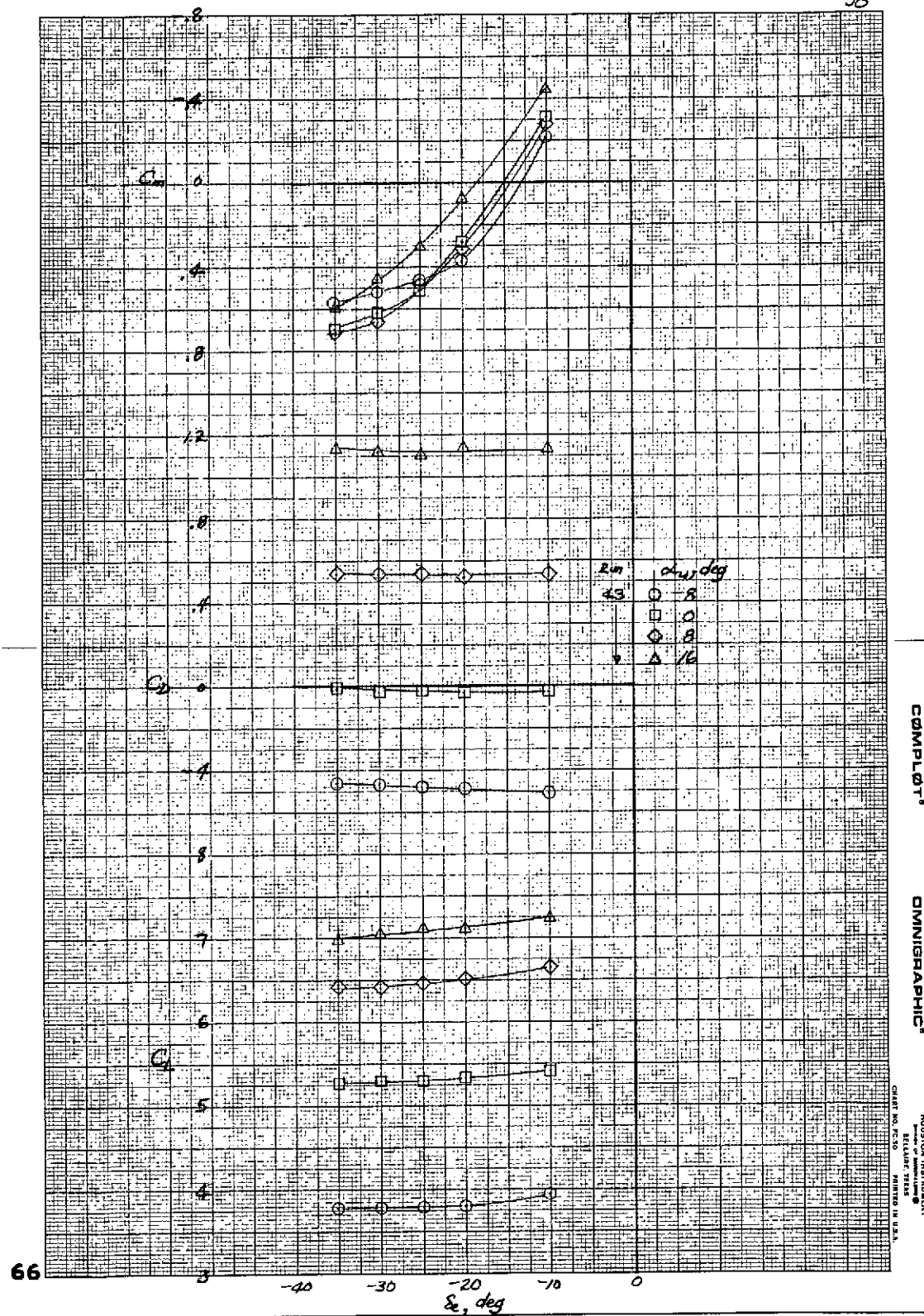


Figure 38.—Elevator effectiveness; $\delta_{f_1}/\delta_{f_2}/\delta_{f_3} = 15^\circ/35^\circ/55^\circ$, $i_t = 0^\circ$
 $C_T = 2.32$.